PATHOLOGICAL CRYSTALLIZATION FROM MIXED AQUEOUS — ORGANIC SOLVENTS

A Dissertation

Presented to

The Faculty of the Department of Chemical & Biomolecular Engineering

University of Houston

In Partial Fulfillment

Of the Requirements for the Degree of

Doctor of Philosophy

by

Megan Ann Ketchum

December 2016

PATHOLOGICAL CRYSTALLIZATION FROM MIXED AQUEOUS — ORGANIC SOLVENTS

Megan Ann Ketchum

Approved:

Co-Chair of the Committee
Jeffrey D. Rimer, Ph.D.
Ernest J. and Barbara M. Henley Associate Professor
Chemical & Biomolecular Engineering

Co-Chair of the Committee
Peter G. Vekilov, Ph.D.
John and Rebecca Moores Professor
Chemical & Biomolecular Engineering and Chemistry

Committee Members:

Richard C. Willson, Ph.D.
Huffington-Woestemeyer Professor
Chemical & Biomolecular Engineering

Navin Varadarajan, Ph.D.
Associate Professor
Chemical & Biomolecular Engineering

Arnold Guloy, Ph.D.
John and Rebecca Moores Professor
Chemistry

Frank J. Claydon, Ph.D.
Professor
Electrical & Computer Engineering

Suresh K. Khator, Ph.D.
Associate Dean
Cullen College of Engineering

Michael P. Harold, Ph.D.
Chair
Chemical & Biomolecular Engineering

ACKNOWLEDGEMENTS:

The process of obtaining my doctorate began years ago before I even knew where I truly wanted the direction of my life to go. There are many people to express my sincere gratitude and heartfelt thanks. Without everyone's help and support, I may not have made it to where I am now.

First, I would like to thank both of my advisors, Dr. Jeffrey D. Rimer and Dr. Peter G. Vekilov. Both of you have molded me into a better researcher and given me confidence to assert myself. When I joined both of your lab groups, I know there was only one spot available for the hematin project yet you chose to accept two students; thank you for taking that leap of faith and giving us the opportunity to shine. The work presented in this dissertation is the fruition of our teamwork together on these projects.

Thank you to my committee members, Dr. Richard Willson, Dr. Navin Varadarajan, and Dr. Arnold Guloy, for taking their time to serve on my committee and providing pensive brainstorming ideas.

To Dr. Fritz Claydon, I owe you so much for the part you've played in my life. Thank you for taking a chance on a KU girl who turned in her REU application very close to the deadline. You gave me the opportunity to experience research and see the prospects of obtaining a higher education. The funding you have provided me through the GK-12 program has enabled me to continue my research while pursuing my passion of improving engineering education at all stages.

To my partner in crime for the hematin project, Katy Olafson, you have been such an inspiration to work alongside. You have provided thoughtful discussion throughout the entire process and a calming presence at all times. Without you, the project may have

stuck in a rut at the very beginning and I may have lost my sanity along the way. I could not have wished for anyone better to share my graduate school experience with me.

During the course of my graduate school career, there have been several individuals who have been extremely helpful to my projects. I would like to thank Andrea Lee for working for three summers in the lab and basically doing whatever I tell her without complaint. I never knew how much you cleaned glassware for me until after you left. To Zachery Baker, thank you for helping me start the cholesterol project and endlessly make batch after batch of crystals. I need to thank Thomas Bessy for performing the night shifts during the beginning development of the assays. To both of my lab groups, thank you for all of your support and assistance along the way, specifically Wei Qin for performing XRD experiments and Mohammad Safari for turning off my water baths late at night.

Graduate school can be a rough journey that takes a toll on you mentally. I need to express my thanks to all my friends who have supported and encouraged me, ensuring that while I obtain my degree, I enjoy my life and take time for me. I need to say thank you for being a colleague, Mike Byington. You will never be referred to as more per request.

Last, but not least, I must thank my family. To my brother and sister, Steve and Lisa, thank you for providing examples for me as I was growing up. While I may not have enjoyed every minute of our childhood, you made me tougher and able to handle any situation. To my parents, William and Jan, thank you for your encouragement at all stages of my life and never telling me I could not achieve something. You enabled your children at a young age to test ideas by blowing up bottles in the driveway with chemical

reactions or burning things in the microwave. You taught me how to use resources and offered to burn projects in the fireplace that ended poorly. I truly hope that I have made you proud.

PATHOLOGICAL CRYSTALLIZATION FROM MIXED AQUEOUS — ORGANIC SOLVENTS

An Abstract

of a

Dissertation

Presented to

The Faculty of the Department of Chemical & Biomolecular Engineering

University of Houston

In Partial Fulfillment

Of the Requirements for the Degree of

Doctor of Philosophy

by

Megan Ann Ketchum

December 2016

ABSTRACT:

Crystallization occurs under a variety of conditions including inside the human body. Many of these processes are undesirable diseases, which require pharmaceuticals or surgical procedures as treatment. Hematin, a toxic compound, crystallizes in malaria parasites to prevent eradication from the body while cholesterol crystallizes in the gallbladder and arteries creating blockages of vital fluids. In malaria, the parasite mutates to become resistant to current antimalarials while atherosclerosis exhibits no signs until heart attack, stroke or death. For these diseases, new pharmaceuticals are imperative as preventative medicine. However, knowledge of these phase changes is limited as no one has performed systematic studies to fundamentally understand crystallization or inhibition in physiologically relevant environments. With this knowledge, a platform for the design of potential drug compounds could be implemented.

For malaria, gallstones, and atherosclerosis, both lipid and aqueous media are present where crystallization transpires. For this study, the solution properties (solubilities in aqueous, organic and mixed aqueous-organic solvents) governing each pathological disease's crystallization were scrutinized to elucidate the growth environment.

For malaria, current approaches to identify lead candidates rely on combinatorial screening methods employing whole-parasite assays, which are incapable of elucidating the effect(s) of inhibitors on hematin crystallization. In this study, a physiologically-relevant growth medium (mixed aqueous-organic solution) was used to develop a facile, robust method of screening compounds that inhibit hematin crystal growth. As benchmarks, antimalarials and antibiotics that are commonly used in combination

therapies were selected. This assay possesses the capability to be used as a high-throughput platform to screen libraries of compounds as a more streamlined approach to identify inhibitors of pathological crystallization.

For atherosclerosis, the studies attempted to discern the crystal growth mechanism using *in situ* atomic force microscopy (AFM) in a mixed solvent. The surface features and polydispersity of cholesterol crystals are facilitated by the growth conditions (supersaturation, rate of cooling, etc.); therefore, bulk crystallization of cholesterol in the absence and presence of bile salts was performed to illustrate how natural compounds affect crystallization.

Table of Contents:

List of Figures:

List of Tables:

Chapter 1: Introduction

Crystallization is a natural phenomenon occurring in a variety of environments ranging from the atmosphere to the core of the earth to inside the human body. The environment in which a crystal develops is important for its structure, growth rate, mechanism of formation, and morphology. The understanding of how environments affect crystallization is imperative in pathological diseases where crystallization is an integral process, such as kidney stones,[1,2] gallstones,[3,4] atherosclerosis,[5,6] and malaria.[7,8] For all of these maladies, crystallization is an undesired activity where pharmaceuticals or surgical techniques are required to eliminate the condition. When attempting to discover or design new pharmaceuticals for these diseases, it is essential to comprehend how the crystallization processes transpire and the effect of the growth environment.

1.1 Mechanisms of Crystal Growth

When crystals grow from solution, there are a variety of different pathways by which this can occur as seen in Figure 1.[9] All of these can be categorized into two broad classifications: classical and nonclassical.

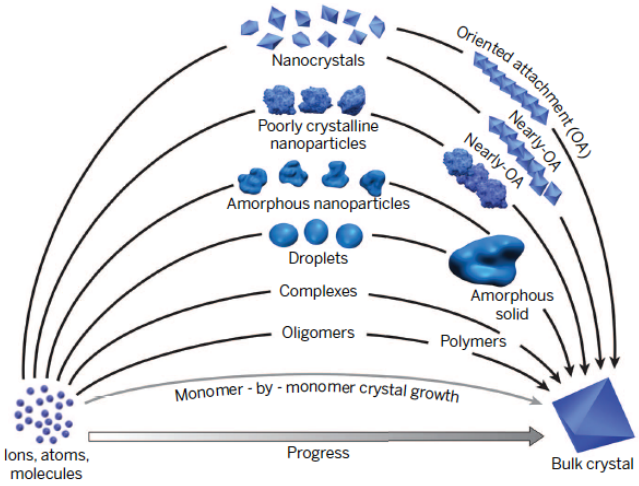

Figure 1: Illustration of the numerous routes for crystallization to proceed from simple building blocks to a bulk crystal.[9]

1.1.1 Classical Crystallization

In classical crystallization, growth occurs by monomer-by-monomer addition from the solution to the crystal surface.[10] A Kossel crystal is the general shape of a basic cubic crystal represented as stacked blocks. The surface of a Kossel crystal (Figure 2) has specific features where monomer attachment occurs: terraces, steps, and kinks.[11] Terraces are the flat surface areas between step edges; steps are the separate layers of monomers propagating across the surface; kinks form where the step edge is unfinished with half of the neighboring bond sites empty.

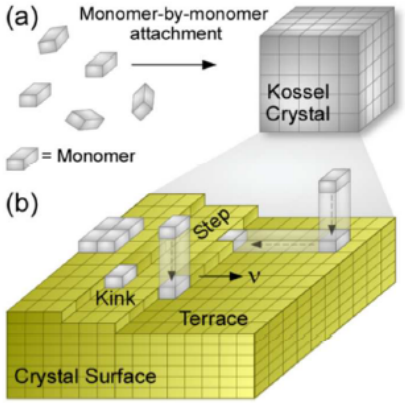

Figure 2: Schematic of Kossel crystal specifically illustrating the surface features of terraces, steps and kinks where solute attachment ensues.[12]

On the surface of the crystal, there are five important sites where monomers will attach as shown in Figure 3: (1) vacancy in a terrace/face, (2) hole in a step, (3) kink, (4) step edge, and (5) directly to terrace or face. Monomer incorporation is more energetically favorable based on the number of bonds between the crystal and solute. If there is a vacancy or hole in a terrace or an edge, monomer addition would leave the least number of dangling bonds at one or two. However, the likelihood of a monomer attaching directly into those specific sites is low. The most likely sites for attachment are kinks. For kink sites, three monomer-crystal bonds are produced and the surface free energy of the crystal is unaltered as the kink site is regenerated. The degree of supersaturation

surrounding the crystal interface is the driving force behind monomer addition. The rate of growth is proportional to the supersaturation. The slowest growing faces of a crystal determine the bulk crystal habit. Overall, both kinetic and thermodynamic driving forces govern the final crystal habit and size, which are influenced by growth conditions: solvent, supersaturation, time, temperature, modifiers, etc.[13]

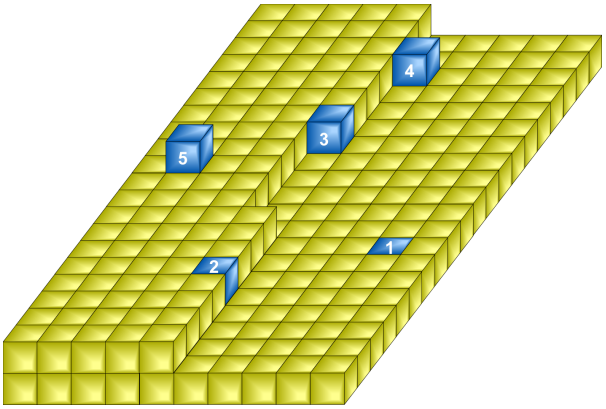

Figure 3: Five sites for monomer attachment in classical crystallization.

When a monomer attaches to a surface, there are two modes (Figure 4) by which it can transpire: direct incorporation and surface diffusion. In direct incorporation, a molecule in solution binds to a kink, step or terrace. Alternatively for surface diffusion, attachment to a kink, step or terrace occurs after the molecule first absorbs to the crystal surface and diffuses to a growth site for further integration.[14]

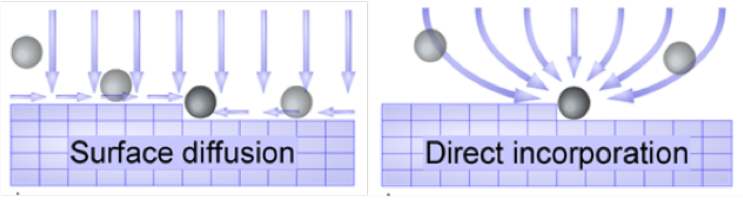

Figure 4: Methods of monomer addition to a crystal surface – surface diffusion and direct incorporation.

Classical crystal growth typically occurs by either a 2-dimensional (2D) layered mechanism or from a dislocation.[15] In 2D growth, new layers nucleate from 2D nuclei and propagate across the surface by addition of monomers illustrated by the schematic in

Figure 5.[16] During the crystallization of water into ice,[17] new layers nucleate as islands as shown in Figure 6a.

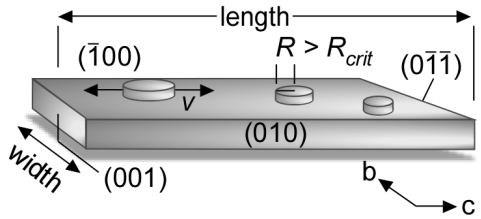

Figure 5: Diagram of two-dimensional nucleation and layer propagation on a crystal surface.[16]

The more common method for classical crystal growth is the formation of hillocks emanating from a dislocation source[18] (Figure 7[19]) or a combination of both 2D and dislocation.[15] A partial shifting of planes causes a linear defect resulting in an edge or screw dislocation. In Figure 6b-e,[15,20-23] a variety of crystals growing from a dislocation source can be observed.

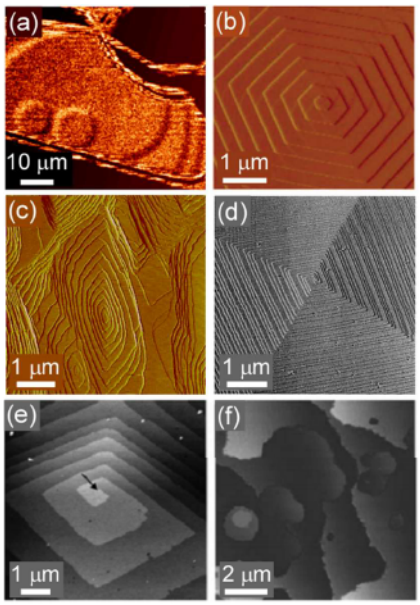

Figure 6: Examples of crystals with 2D or screw dislocation growth mechanisms. (a) 2D nucleation of ice crystals,[17] screw dislocations on (b) L-cysteine crystal,[20] (c) calcium oxalate monohydrate crystal, (d) calcite crystal,[21] (e) insulin crystal,[22] and (f) ferritin crystal with 2D nucleation.[15]

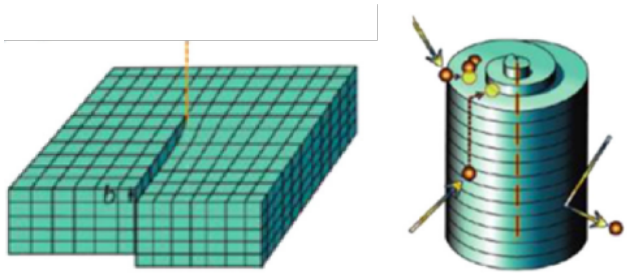

Figure 7: Schematics of a screw dislocation and how the unit cell orients for this configuration.[19]

1.1.2 Nonclassical Crystallization

For nonclassical crystal growth, monomers form higher order oligomers, amorphous or nanocrystalline particles in solution and attach to the surface furthering crystallization. These oligomers, amorphous or crystalline particles serving as growth units are termed precursors. Precursors vary with respect to microstructure, size, shape and state of matter.[24-26] For oligomers, it follows a similar pathway of crystal growth as classical crystallization for monomers as shown in Figure 8.[12]

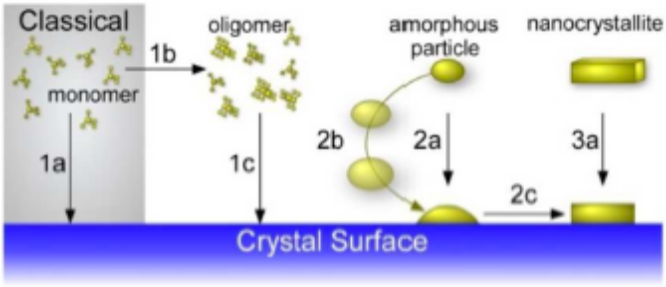

Figure 8: Pathways for classical crystallization and nonclassical crystallization demonstrating how precursors are developed in solution before addition to the surface.[12]

Gels or liquid-like aggregates can form when monomers or oligomers are loosely connected.[9] If monomers or oligomers bond covalently, they materialize into amorphous particles or bulk solid aggregates. After attachment, precursors undergo a transition from disordered to ordered.[27] This transition is necessary for the particles to fully rearrange and integrate into the crystal lattice structure. A few examples of crystals, which grow by nonclassical crystallization, are shown in Figure 9.[12,27-29]

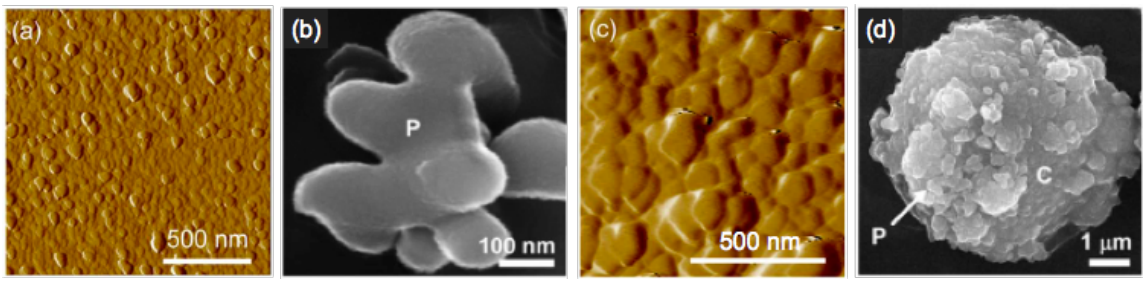

Figure 9: Examples of nonclassical crystallization in zeolites: (a) silicalite-1,[27] (b) LTL,[28] and (c-d) SSZ-13 or CHA.[12,29]

1.2 Modifiers in Solution

Modifiers are regulators of crystallization capable of changing the crystal morphology, size, suppressing or promoting growth.[30,31] They can range from ions to macromolecules, such as polymers or proteins. Both classical and nonclassical crystallization pathways are affected by the presence of modifiers, possessing different mechanisms.[32-34]

1.2.1 Classical Modes of Growth Inhibition

In classical crystallization, the effect of modifiers can be explained by type of species attachment and the location on the crystal surface. There are three proposed mechanisms for types of inhibition based on the type of species attachment (Figure 10): (i) the solute could form a complex with the inhibitor and block crystal growth by binding to the surface; (ii) a solute/inhibitor complex does not bind the crystal surface, altering the degree of supersaturation slowing growth; and (iii) the inhibitor could bind directly to the crystal surface causing inhibition.[35]

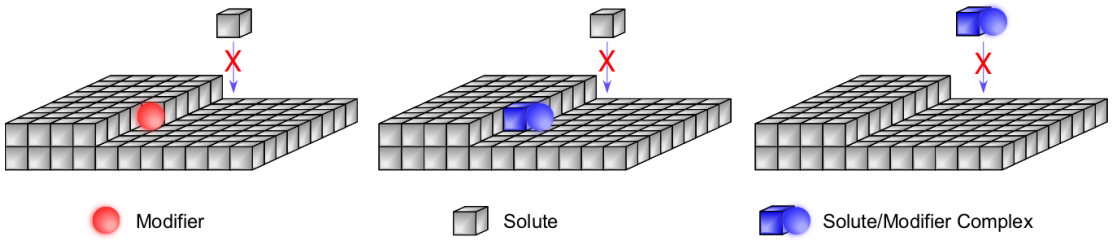

Figure 10: Three proposed mechanisms of inhibition based on type of species attachment.

On the crystal surface, modifiers can bind to kinks, steps and terraces. In the step pinning mechanism, modifiers attach to crystal terraces and impede further propagation of steps.[36] As steps advance and chance upon a modifier on a terrace, the step velocity decreases due to strain imposed. If two or more modifiers are spaced on a terrace close enough, the step propagation will be fully arrested as seen in Figure 11a.[12]

For kink blocking mechanism, modifiers bind to kink sites on the crystal surface shown in Figure 11b.[12] This attachment decreases step velocity due to blocking the most energetically favorable site for monomer addition.[13] Depending on the concentration of modifier attachment to kinks, step advancement can be fully suppressed or significantly reduced.

Larger modifiers can cause macro-step induction or bridging. In this case, the modifier binds to a step edge and the terrace above the step. This causes macro-steps to form and step velocity to decline.[37]

Another mechanism, shown in Figure 11c-d,[12] behaves similar to the kink blocking mechanism, but can cause dissolution of crystal surfaces under certain conditions by inducing localized strain.[21] This mode of action is not fully resolved yet and only works for specific range of concentrations; if the concentration is too low or high, it will revert to kink blocking or competitive attachment/detachment of monomers leading to non-uniform attachment and disappearance of distinct layers, respectively.

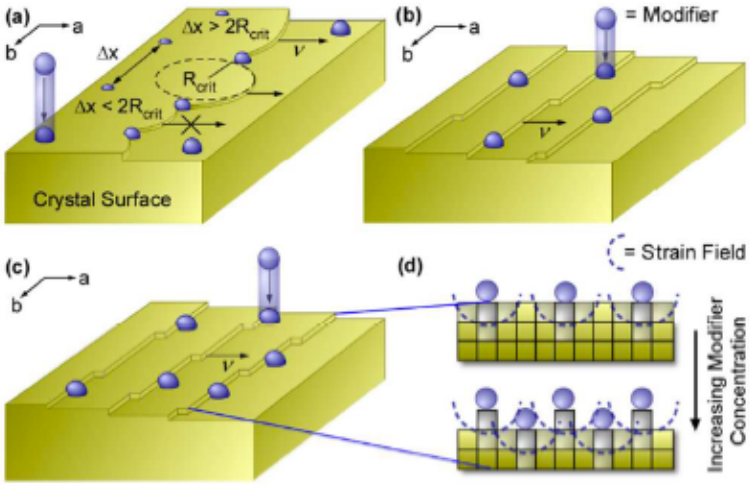

Figure 11: Modes of inhibition for classical crystallization: (a) step pinning, (b) kink blocking, and (c-d) strain induced dissolution.[12]

1.2.2 Inhibition of Nonclassical Crystallization

In nonclassical crystallization, there are no specific crystal surface binding sites for modifier attachment.[9] However, modifiers can alter monomer, oligomer or precursor attachment, speciation reactions, self-assembly of amorphous particles and structural evolution of precursors. On the surface, the transition from disordered to ordered can also be hindered. The modifier can complex with oligomers in solution or stabilize precursors to prevent aggregation and attachment to crystal surfaces. Overall for nonclassical crystallization, there are a plethora of pathways for inhibition.[27,29,38]

1.3 Crystallization of Hematin

Malaria is a mosquito-borne parasitic infectious disease caused by five species of parasites of the genus Plasmodium (*falciparum*, *vivax*, *malariae*, *knowlesi*, and *ovale*).[39] While significant public health efforts have eradicated malaria from North America, Europe, and other well-developed regions of the world, the disease is endemic in the equatorial regions of Africa, South America, Southeast Asia, and Oceania as seen in

Figure 12 with approximately 40% of the global population is at risk for transmission, 200 million episodes occurring annually and 600,000 episodes resulting in deaths.[40]

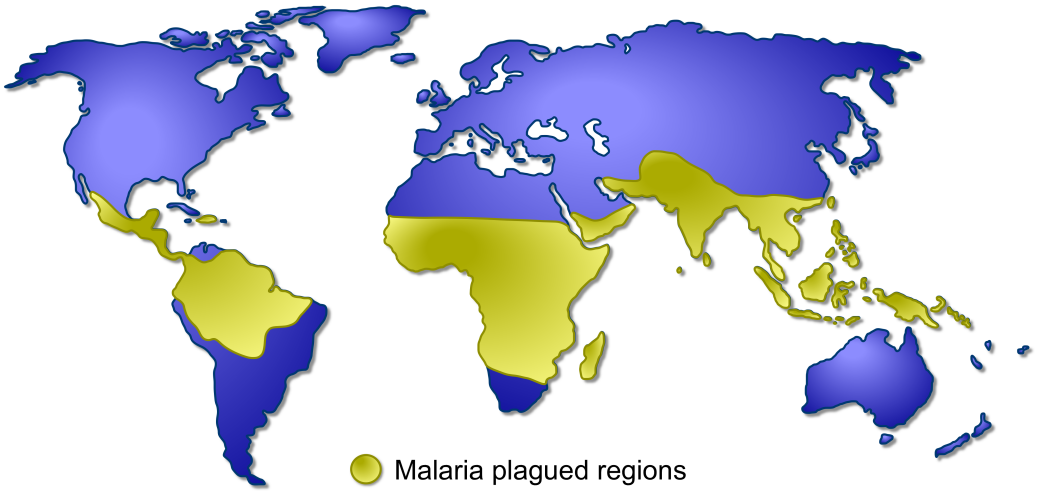

Figure 12: World map illustrating areas where malaria is prevalent.[40]

The pathophysiology of malaria is complex, but relies on crystallization for the survival of parasites. The life cycle of the malaria parasite in the human body consists of multiples stages shown in Figure 13.[41] When a human is infected with the parasite via a mosquito bite, the parasite travels to the liver where it reproduces asexually, creating merozoites.[42] The merozoites then relocate to the circulatory system where they infect erythrocytes.[43] At this stage, merozoites can either reproduce asexually (transforming into trophozoites and subsequently schizonts) or develop into immature gametocytes. When a mosquito bites a human, it withdraws blood and gametocytes, repeating the cycle again.[44] While in the bloodstream, parasites infiltrate red blood cells and catabolize hemoglobin, releasing heme that is oxidized to toxic hematin. The latter is sequestered into innocuous crystals called *hemozoin*. Many antimalarial drugs inhibit the sequestration of heme (i.e., hemozoin crystallization), thereby eradicating the parasite from the body due to the cytotoxicity of hematin. The full process is illustrated in Figure 14.

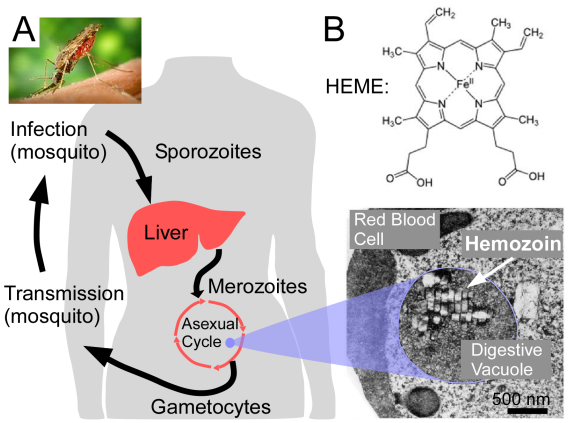

Figure 13: Schematic demonstrating the life cycle of Plasmodium parasites. (A) Mosquito infects the human host where it is circulated throughout the body to reproduce in various stages. (B) Heme molecule resulting from catabolization of hemoglobin.

Heme detoxification occurs within the parasite's digestive vacuole (DV), which is a complex environment for crystallization comprised of membrane interfaces, an acidic aqueous solution with pH 4.8 – 5.5, and a collection of various neutral lipids.[7] The latter are mostly mono- and di-glycerides that result from the degradation of the transport vesicle membranes that carry hemoglobin into the DV. The lipid nanospheres in the digestive vacuole are composed of five different lipids: monopalmitoyl glycerol, monostearoyl glycerol, dipalmitoyl glycerol, dioleoyl glycerol, and dilinoleoyl glycerol in a ratio of 2:4:1:1:1.[45]

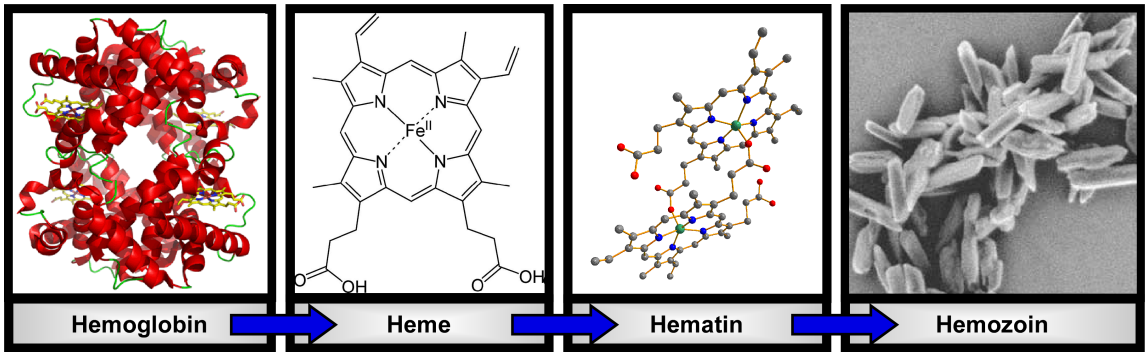

Figure 14: Diagram of hemoglobin catabolization process in the parasite. Hemoglobin is broken down into heme, which is unstable, and immediately oxidizes to toxic hematin. Hematin is sequestered into innocuous crystals called hemozoin.

The traditional Western treatment for malaria, quinine, and its synthetic homologues (i.e., chloroquine, mefloquine, and others) putatively work by blocking hematin crystallization.[46] Available evidence suggests that artemisinin, another antimalarial drug, binds to heme.[47] Currently, combination therapies are the suggested method for malaria treatment by the World Health Organization. In combination therapies, two or more drugs with different modes of action and biochemical targets are utilized simultaneously to produce a highly effective treatment.[48] For example, an antibiotic, such as doxycycline which causes abnormal cell division, and an antimalarial, such as quinine which inhibits crystallization of hematin, are administered together to eliminate malaria from the body.

Very disturbingly, a resurgence of the disease throughout the world has occurred since the 1960s and 1970s due to the emergence and spread of Plasmodium parasites resistant to chloroquine combination treatments.[49,50] Delayed parasite clearance has been recorded even for the most recent artemisinin-based therapies.[51] These processes weaken responses to the common antimalarial drugs underscoring the urgent need for research into the main processes of the malaria pathophysiology. Thus, improved understanding of the mechanism of hematin crystallization is crucial for new drug development.[52,53]

To start to comprehend the entire process of crystallization, the project was divided into four areas (Figure 15): solution properties, mechanism of crystallization, inhibition, and bulk assay. With all of this potential knowledge combined, a platform for designing and screening prospective new compounds as antimalarials can be established. This work concentrated on the solution properties and bulk assay while others in the group, simultaneously, focused on the mechanism of crystallization and inhibition.

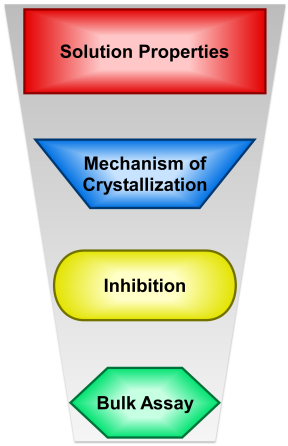

Figure 15: Overview of project areas for experimentation.

Currently, there is a dispute as to the location of crystallization inside the DV of the parasite. The possible locations of hemozoin formation in the bulk of the two phases in the parasite's DV (aqueous and lipid) and three interfaces (aqueous/lipid, aqueous/membrane, and lipid/membrane) are marked in Figure 16: 1—in the bulk of aqueous phase, 2—in the bulk of the lipid nanospheres, 3—at lipid/aqueous interface, 4—at the DV membrane in the lipid phase, and 5—at the DV membrane in the aqueous phase.[54] The driving force behind crystallization is the solubility of the solute molecule.[10] To ascertain the potential effectiveness of a solvent as a growth solution, the solution properties need to be determined.

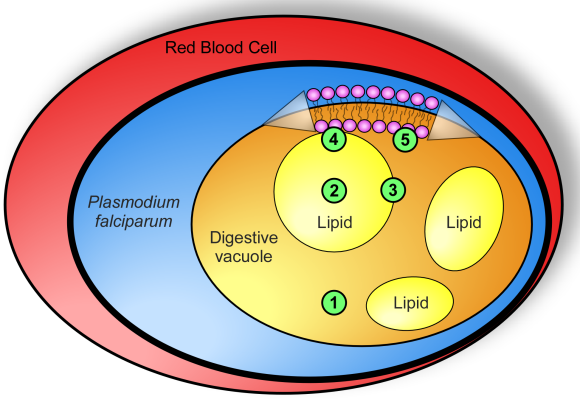

Figure 16: Schematic illustration of P. falciparum infecting a red blood cell. Spherical agglomerations of neutral lipids that are several hundred nanometers in size, referred to as nanospheres, are present in the digestive vacuole.

Using the solution properties, the most probable growth environment of hematin crystallization can be elucidated after attempts to grow crystals in various conditions of each solvent. With this knowledge, another colleague determined the mechanism of crystal growth utilizing in situ atomic force microscopy (AFM). In conjunction, she introduced a number of current antimalarial drugs to observe their inhibition effects on hematin crystallization.

Assays play an integral role in the discovery of new pharmaceutical drugs for diseases.[55] With high-throughput assays, companies test libraries of drugs containing thousands of compounds to determine their applicability. Current methods for discovery of new antimalarials are parasite-based assays, which do not indicate the functionality of the compounds whether they act by corrupting the reproductive cycle of the parasite, inhibiting crystallization or some other means. To aid in this endeavor, a new biomimetic assay was designed to determine the efficacy and potency of antimalarials for hematin crystallization. To enhance its utility, it must be adaptable to high-throughput. Such an assay will help streamline the process for detection of compounds that should be studied further utilizing more extensive methods, such as AFM.

In Chapter 2, the detailed background of malaria and hematin crystallization including initial understanding of the disease, previous methods of crystallization, current treatments, resistance of parasites, etc. will be reviewed.

In Chapter 3, the determination of the solution properties of hematin, current antimalarials and antibiotics will be examined. The growth environment will be debated and the discovered mechanism of hematin crystallization and inhibition will be described.

In Chapter 4, the biomimetic assay of hematin crystallization designed to quantify efficacy and potency of antimalarials will be explained. The adaptation to a high-throughput configuration will be elaborated.

In Chapter 5, the work on the hematin project and the valuable information gleaned from our systematic approach to fundamentally understanding hematin crystallization will be summarized.

1.4 Cholesterol Crystallization

The gallbladder stores and releases bile made by the liver into the small intestines to help digest fats. Gallstones form in the gallbladder when the bile is supersaturated with cholesterol or bilirubin.[56,57] These are similar to tiny rocks or stones, which can become lodged in the ducts transporting bile from the gallbladder as shown in Figure 17. This creates blockages resulting in inflammation of the gallbladder, liver and pancreas. In the developed world, between 10-15% of the population have gallstones with 1-4% developing symptoms annually.[58,59]

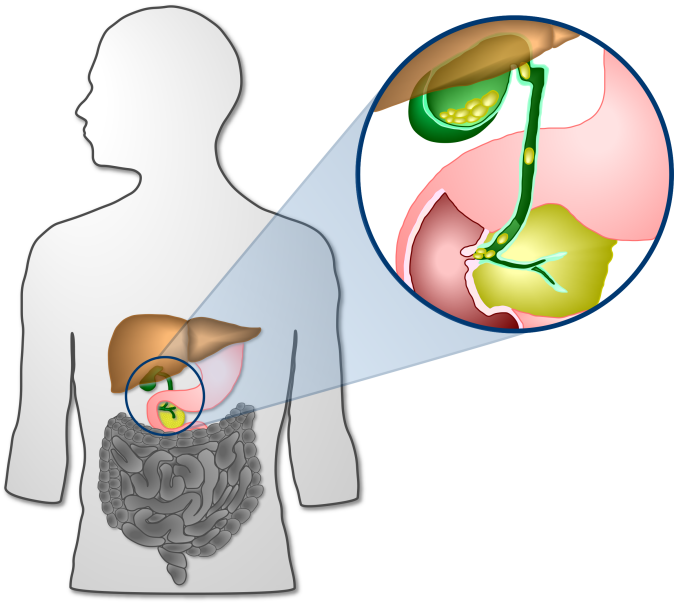

Figure 17: Diagram of the digestive system demonstrating where gallstones form in the gallbladder and can cause blockages in ducts.

Over 75% of all gallstones are cholesterol based and occur when the liver excretes more cholesterol than the bile can dissolve. Bilirubin or black pigment stones account for approximately 20% of stones as an effect of liver cirrhosis, biliary tract infections or certain blood conditions, which cause the liver to produce too much bilirubin.

To treat gallstones, there are both nonsurgical and surgical methods.[60-63] A laparoscopic cholecystectomy is the most common treatment where the gallbladder is removed with a minimally invasive surgery. The patient is either released the day of surgery or after one overnight stay with only a few days of missed work.[64] A nonsurgical method for those patients unable to have surgery is dissolution of gallstones with pharmaceutical drugs,[65] such as ursodeoxycholic acid,[66] and only work for cholesterol stones. Overall, $6.5 billion is spent annually on gallbladder disease.[59]

Cholesterol crystallization not only occurs in gallstones, but also in atherosclerosis.[67] This is what is commonly known as hardening of the arteries or plaque. In this disease, the pathology occurs over decades, starting at adolescence, through continuous evolution of arterial wall lesions.[68] At the beginning, low-density lipoproteins (LDL), which transport lipids or fats around the body, leave the bloodstream and enter the innermost coating of the artery, arterial intima, due to an inflammatory response of white blood cells.[69] As LDL levels increase in the intima, they accumulate; without adequate removal of cholesterol and fats from the macrophages by high-density lipoproteins (HDL), the build up of cholesterol and fats can lead to blockage of arteries as shown in Figure 18. These blockages cause heart attacks, strokes, etc. depending on the location.

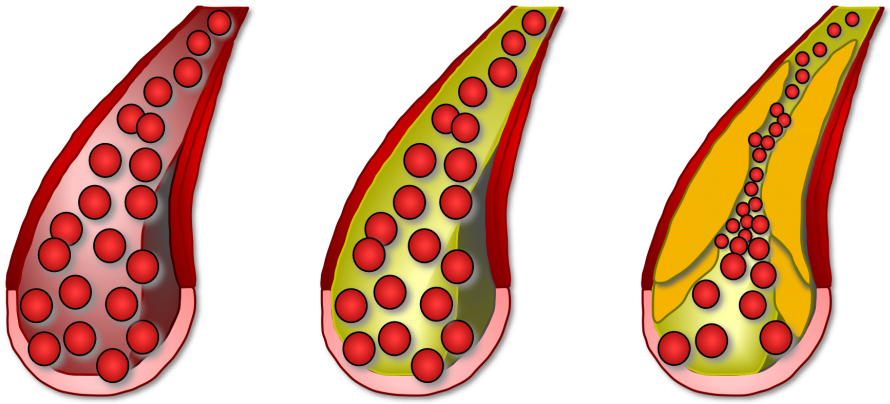

Figure 18: Progression over time of atherosclerosis from a normal artery to when the artery becomes blocked by the plaque formed.

Heart disease is the number one killer of men and women in the United States. Every year, about 700,000 Americans suffer from heart attacks and 130,000 die from strokes.[70] Most people do not realize they have the disease until it is too late. The estimated costs associated with coronary heart disease in the United States are $100 billion.[71] One major preventative medicine is a group of pharmaceuticals called statins.[72] These drugs help by decreasing the amount of cholesterol produced by the liver, which accounts for 70% of the cholesterol in the body. In 2013, $35 billion was spent on 264 million statin or cholesterol treating medication prescriptions with 25% of Americans over the age of 45 taking some type of statin.[73,74]

For both of these diseases, the knowledge is limited on the mechanism of cholesterol crystallization and how current medications, such as bile salts, affect this process. To create potential new medications to cause dissolution of cholesterol crystals in plaques and gallstones, it is imperative to understand the fundamentals.

For this project, the same strategy utilized for the hematin project was implemented by subdividing the aspects into the same four categories as shown in Figure 15: solution properties, mechanism of crystallization, inhibition and bulk assay. By

attacking this problem at all of these levels, an overall understanding of the entire system can be developed.

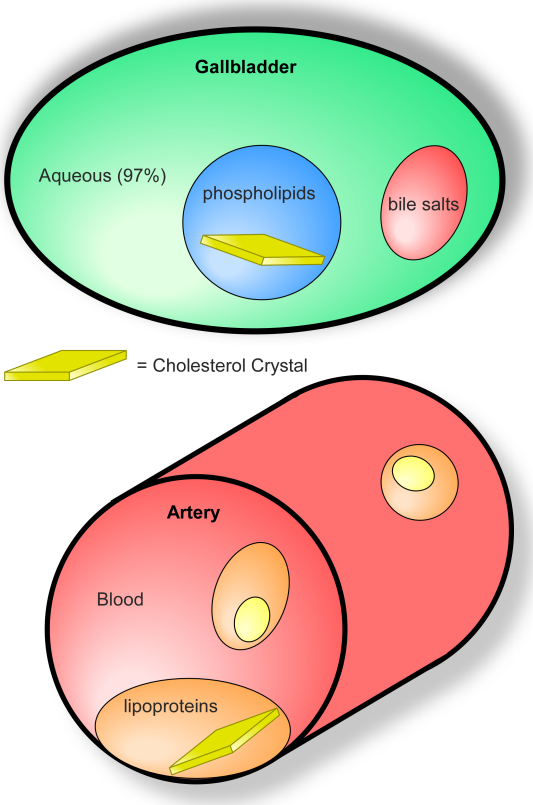

Figure 19: Diagram depicting the environments of the gallbladder and arteries where both aqueous and lipid media are present.

The environment present in both the gallbladder and arteries contains both lipid and aqueous media similar to the hematin project and the parasite DV. In the gallbladder, bile is stored which is composed of more than 90% water with lipids.[75] The lipid species are bile salts (67% of solutes by weight), phospholipids (22%) and cholesterol (4%).[57] Cholesterol accumulates in phospholipids in the gallbladder due to its low solubility in water.[76] In the arteries, blood contains blood cells suspended in blood plasma. Plasma accounts for 55% of the blood and is comprised of 92% water and 8% blood plasma proteins.[77] It also includes serum albumin, lipoproteins, antibodies, electrolytes, minerals,

and other proteins. For both systems, cholesterol crystallizes in a lipid environment as shown in Figure 19.

Initially, a variety of solvents were examined to decide which ones would be the most beneficial as a mimic for pathological crystallization. For each of these solvents, the solution properties and the effects of the addition of water were determined. This knowledge enabled a suitable solvent to be chosen as the best option for attempting to ascertain the mechanism of crystallization.

After selection of the solvent, AFM was utilized to study the surface of cholesterol crystals. Determination of the growth mechanism of cholesterol crystals and how bile salts and other medications inhibit crystallization were the main goals of this effort. Bulk crystallization studies were performed simultaneously to understand the best method for crystallization and the effects of bile salts on the morphology, aspect ratio, and nucleation.

In Chapter 6, the current understanding of atherosclerosis and gallstone formation will be reviewed. The current medications available for each disease and common surgical procedures performed will be explained.

In Chapter 7, the solution properties of cholesterol in aqueous and organic solvents and how water affects these will be examined.

In Chapter 8, bulk crystallization of cholesterol crystals will be explained along with how different factors affect this crystallization process. The efforts of uncovering the growth mechanism of cholesterol crystals will be addressed. The correlation between known crystal structures and measurements made on the surface of crystals will be discussed. The effects of bile salts will be shown.

In Chapter 9, the conclusions and summary of this project will be illuminated and how others can build upon the knowledge gained in these studies.

Chapter 2: Pathophysiology of Malaria

Malaria has been around for centuries causing loss of life dating back all the way to records in 2700 BC in China. However it was not until 1880 when Charles Louis Alphonse Laveran published a paper about his discoveries while examining a fresh unstained blood sample from a soldier in Algeria, the world began to truly understand what type of disease it was battling. He found motile pigmented bodies which he categorized as a parasitic organism.[78] However, his efforts went unnoticed at the time due to theories of a type of bacteria (bacillus) or unpleasant stench (miasma) as the culprits of malaria. Another four years had to pass before Ettore Marchiavava and Angelo Celli examined live, unstained specimens rather than stained, dead ones. It was at this time they rediscovered the etiology of malaria and named the parasite *P. malariae*. Over the next ten years, researchers correlated the periodicity of human symptoms to the life cycle of parasites and determined the existence of multiple species of parasites causing malaria.

In humans, malaria is caused by five different species of Plasmodium parasites: *P. falciparum, P. malariae, P. ovale, P. vivax, and P. knowlesi*.[79] The most common species found in humans is *P. falciparum* at approximately 75% with *P. vivax* accounting for the second most with roughly 20%. Most of the recorded deaths are African children from *P. falciparum*. *P. vivax* is more common outside of Africa, especially in South America.

2.1 Signs & Symptoms

After infection with the parasite, the signs and symptoms appear after 8-25 days. For those who travel to malaria transmission regions of the world and take preventative medication, the symptoms may take longer to develop. Initially, malaria resembles the flu and other diseases with headaches, fever, shivering, joint pain, vomiting, jaundice,

hemoglobin present in the urine, hemolytic anemia, retinal damage and convulsions.[79] A classic sign of malaria is a cycle of sudden coldness followed by shivering then subsequent fever and sweating, called paroxysm, every two or three days depending on the type of malaria.

Once infected, the body recognizes erythrocytes that contain parasites. The spleen filters the red blood cells and removes those infected. To prevent removal from the body, the parasite displays adhesion proteins on the surface of red blood cells to stick to the walls of blood vessels.[80] As a result of this, the parasite can breach the blood-brain barrier causing cerebral malaria. In cerebral malaria, the patient exhibits neurological symptoms such as abnormal posturing, nystagmus (involuntary eye movement), opisthotonus (arching of the spinal column), conjugate gaze palsy (inability of eyes to turn together in the same direction), seizures or coma.[81]

2.2 Diagnosis & Detection

Due to the fact that malaria presents similar to the flu, the most common method for diagnosis is microscopy and examination of blood films. With blood films, there are two types that are traditionally performed: thin or thick films. Examples of images from these techniques can be seen in Figure 20.[82]

With thin films, the species of parasite infection can be determined as each has distinguishing characteristics. Thin films enable preservation of the parasite's appearance during preparation. For thick films, the level of sensitivity is higher and picking up low levels of infection are easier. However, the volume is thicker making it difficult to distinguish the type of species. With both of these tests, the number of parasites in the

blood can be discerned. When monitoring treatment, this knowledge can be essential to know how effective a pharmaceutical administered is functioning.

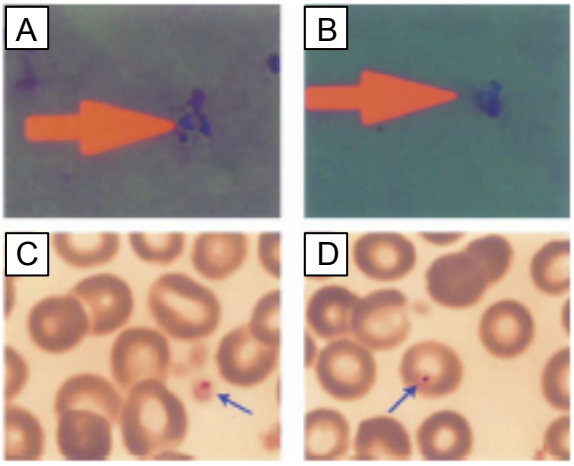

Figure 20: Microscope images of *P. falciparum* trophozoites on (A-B) thick films and (C-D) thin films.[82]

To enhance the detection of parasites in blood films, certain fluorescent dyes have been introduced which have an affinity for nucleic acid in the parasite nucleus.[83] The dye attaches to the nuclei and when excited at a specific ultraviolet wavelength, the nucleus fluoresces vividly. Depending on the type of dye utilized, it can be more or less effective as it may bind to cells other than the parasite nucleus. For example, benzothiocarboxypurine (BCP)[84] stains red blood cells and leukocytes poorly, but *P. falciparum* strongly as seen in Figure 21.[83]

In some areas of the world, microscopy is unavailable or laboratory technicians are unqualified. Therefore, other methods have been developed to aid in the diagnosis of infection, such as rapid diagnostic tests.[85,86] These tests are capable of qualitative results in 15-20 minutes and are simple to use. The only downside is the threshold of detection is 100 parasites/μL of blood compared to 5 in thick blood films.

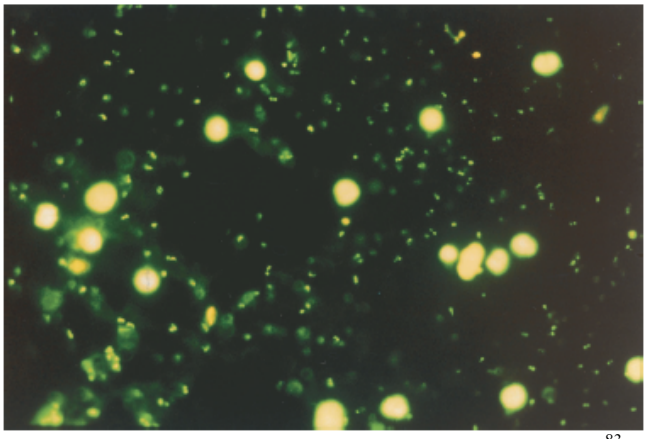

Figure 21: Fluorescence image of *P. falciparum* trophozoites stained with BCP.[83]

One popular device is the immunochromatographic test, which relies on the diffusion of a liquid across a nitrocellulose membrane. Monoclonal antibodies are attached to the membrane to capture parasite antigens from the peripheral blood. In this system, there is a mobile phase containing malaria antigen targets conjugated to a liposome containing selenium dye or gold particles. These targets form antibody-antigen complexes, which migrate across the nitrocellulose membrane. When the complexes reach the immobile monoclonal antibodies along the strip, they are captured producing a visible line. If there are no parasite antigens, the line will not appear. The strip also contains an immobile control antibody, usually a goat anti-mouse monoclonal antibody.[87] The general setup of an immunochromatographic test can be seen in Figure 22.

Currently, there are three malaria antigens targeted: histidine-rich protein 2 (HRP-2),[88] *Plasmodium* lactate dehydrogenase (pLDH),[89] and *Plasmodium* aldolase.[90] HRP-2 is a water-soluble protein produced by asexual stages and gametocytes of *P. falciparum*. Despite its abundance and usefulness, not all species of Plasmodium parasites produce this protein. Therefore, it is only suitable for detection of *P. falciparum*. pLDH is an enzyme produced in the glycolytic pathway of the malaria parasite at both the asexual and sexual stages. Four species of the parasite produce this enzyme in various isomeric

forms, making it more effective at qualitatively determining whether one is infected with malaria. If both a non-species specific monoclonal antibody and *P. falciparum* specific monoclonal antibody are attached to the membrane, the patient can verify whether they have the most common type of malaria or one of other forms. However, if a patient is infected with multiple types of malaria, the test will only indicate one as they have the same antibody targets. Aldolase is another enzyme produced by glycolytic cycle of the parasite similar to pLDH.

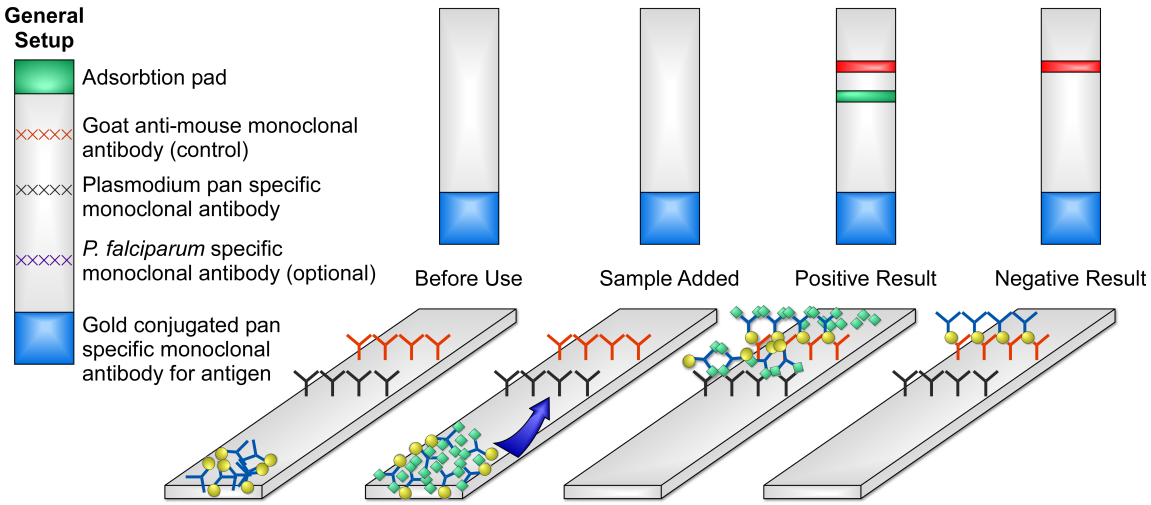

Figure 22: Schematic of immunochromatographic test for simple determination of malaria diagnosis. The results are qualitative and will not be able to indicate effectiveness of treatments.

2.3 Attempts to Eradicate Malaria & Treatments

In 1894, Sir Ronald Ross became interested in malaria parasites after Patrick Manson showed him parasites in the human bloodstream. He set out to prove the theory by Manson and Laveran that the propagation of malaria was connected to mosquitoes. After two years, Ross made his landmark discovery of malaria parasites in the stomach of an anopheline mosquito after feeding on a human infected with malaria four days previously. Over the next year, he utilized birds to demonstrate a cycle of malaria transfer. After the mosquitoes feasted on the birds, they were infected with bird malaria,

which eventually migrated to their salivary glands enabling the mosquitoes to infect more birds.

2.3.1 Removal of Mosquitoes

After this monumental discovery, Ross switched his focus toward prevention of malaria through disruption of the parasite life cycle at the mosquito stage. His thoughts were if there were no mosquitoes, there would be no transmission. Others suggested that instead of killing all mosquitoes, but rather only target the ones that transmit malaria. For most of the 20th century, the efforts to combat and control malaria focused on mosquito eradication.

Between World War I and World War II, the League of Nations and its committee dedicated to malaria was established.[78] The main goal was to investigate means to remove mosquitoes from malaria regions of the world. In 1939, Swiss scientist Paul Hermann Müller discovered the insecticidal properties of dichlorodiphenyltrichloroethane (DDT), whose structure can be seen in Figure 23. During World War II, DDT was utilized extensively to limit the havoc wrecked upon soldiers in the South Pacific by malaria and dengue fever.[91] This successful application of DDT inspired newly founded World Health Organization (WHO) to start antimalarial crusades. By 1955, this evolved into a global eradication campaign based on antimosquito efforts.[92] However, this only succeeded in developed countries. Malaria was eliminated from Taiwan, the Balkans in Europe, much of the Caribbean, parts of northern Africa, northern region of Australia and some of the South Pacific during this time. Over time, a resurgence of malaria in certain areas occurred to due to an increase in mosquito resistance to DDT, increasing parasite tolerance and a failure to sustain the program.[93] In

sub-Saharan Africa where malaria transmission is highly stable and infection severe, the spraying of DDT was ineffective due to poor infrastructure and continuous life cycle of mosquitoes. In reality, the program only succeeded in eradicating malaria from areas with high socio-economic status, an organized healthcare system, and seasonal or relatively low intensity malaria transmission. In 1969, the idea of eradication was abandoned and attention shifted to control and treatment of malaria.

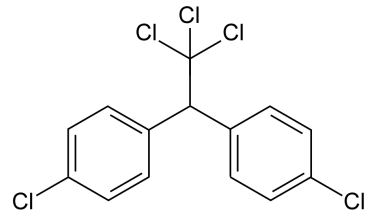

dichlorodiphenyltrichloroethane (DDT)

Figure 23: Molecular structure of insecticide used in attempts to eradicate mosquitoes and malaria.

The impact of the eradication program had other effects besides elimination of mosquitoes. As DDT was more extensively used, the environmental impact of excessive spraying was realized. DDT is readily absorbed by aquatic organisms, which propagated through the food chain to birds. Accumulation of DDT in birds, due to its lipophilic properties, resulted in a decrease in populations from inability to produce proper eggshell thickness. It is also toxic to a variety of marine animals, such as crayfish, sea shrimp and a variety of fish. For humans, DDT is an endocrine disruptor and is classified as "moderately toxic" or "moderately hazardous" by the U.S. National Toxicology Program and WHO, respectively. As a result, banning of DDT began in 1968 in Hungary followed by Norway and Sweden in 1970, West Germany and the United States in 1972, with others following suit over the next two decades. By 1991, 26 countries had total bans over the use of DDT. Eventually, in 2001 at the Stockholm Convention on Persistent

Organic Pollutants, DDT was restricted to vector control with exemptions for public health based on the WHO guidelines.

2.3.2 Antimalarial Drugs

Over the years, numerous medications have been employed to combat malaria. Each pharmaceutical compound attacks a distinct life cycle process of the parasite including: tissue schizonticides for prophylaxis, blood schizonticides, tissue schizonticides for relapse prevention (*P. vivax* and *P. ovale*), gametocytocides and sporontocides.[94] Table 1 elaborates on these categories of antimalarial activity and lists various drugs that interrupt these life cycle processes. Within these categories, various chemical targets are possible. A general approach to malaria treatment, recommended by The World Health Organization,[40] involves combination therapies. In this approach, two or more drugs with different modes of action and biochemical targets are applied simultaneously to produce a highly effective treatment.

Table 1: Categories of Antimalarial Activity

Type of Activity	Function	Drugs
Tissue schizontidicides for prophylaxis	Function against the primary tissue forms in the liver, terminating further development in the bloodstream	Pyrimethamine, Primaquine
Blood schizonticides	Act on the blood forms of the parasite, terminating clinical attacks. Most important category of antimalarials.	Chloroquine, Quinine, Mefloquine, Halofantrine, Sulfadoxine, Tetracyclines, Sulfones, Pyrimethamine, etc.
Tissue schizontidicides for relapse prevention	Attack the hypnozoites of *P. vivax* and *P. ovale* in the liver for reactivation of symptoms	Primaquine, Pyrimethamine
Gametocytocides	Destroy sexual forms of the parasite in the blood, preventing transmission cycle to mosquitoes	Primaquine Chloroquine, Quinine – *P. vivax* & *P. malariae*
Sporontocides	Prevent development of oocysts in mosquitoes	Chloroguanide, Primaquine

2.3.2.1 Quinine (QN)

One of the first natural antimalarial drugs discovered was quinine (QN) from the tree bark of the cinchona trees indigenous to South America.[95] The Quechua people

would ground the bark up and mix with sweetened water, producing tonic water, to act as a muscle relaxant. The Jesuits were the first to transport cinchona to Europe. In 1631, it was used to treat malaria in Rome where it was endemic during the 17th century. Malaria had been responsible for the death of several popes, many cardinals and countless citizens. The drug became popular in London after King Charles II consumed quinine to cure himself of malaria. Quinine was the drug of choice to treat malaria until the 1940s when others were synthesized.

Prior to 1820, the bark of the cinchona tree was dried, ground into a powder, then added to a liquid to be taken orally. Pierre Joseph Pelletier and Joseph Caventou extracted, isolated and name the compound quinine from the bark in 1820.[96] Around 1850, quinine began large-scale usage as a preventative medicine. Quinine was not successfully synthesized until 1918, but the process was elaborate, expensive and yielded low quantities with the additional problem of stereoisomers. Therefore, production is based on extraction from cinchona trees even today.

In the bark of the cinchona tree, there are other similar compounds (quinidine, cinchonine, and cinchonidine) effective against malaria. The efficacies of these four compounds were measured from 1866 to 1868 in clinical trials from 3600 patients. In this trial, they monitored the paroxysm symptoms and found a greater than 98% cure rate for all four compounds. However, after 1890, quinine was the predominant drug used based on supply concentration from the bark, which was harvested from other locations in the world besides South America.[95]

Quinine is an alkaloid molecule, which can be seen in Figure 24. Due to its extremely basic nature, it is always presented as a salt. Preparations include hydrochloride, dihydrochloride, sulfate, bisulfate, and gluconate salts.

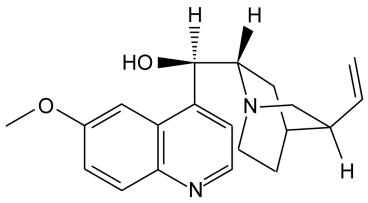

Quinine (QN)

Figure 24: Molecular structure of antimalarial quinine.

Overall, the antimalarial mechanism of action is unknown at the present time. It does possess rapid schizonticidal action against intra-erythrocytic malaria parasites and where it is hypothesized it interferes with the crystallization process of hemozoin. In *P. vivax* and *P. malariae* parasites, it also acts as a gametocytocide. After administration orally or intravenously, the body rapidly absorbs quinine reaching peak concentration after 1-3 hours.[97] It distributes throughout the entire body including cerebral spinal fluid and across the placental barrier with a half-life of 11-18 hours.

While quinine is effective against malaria, it has a low therapeutic index. The therapeutic index of drug is the comparison of the amount of the compound that causes the minimum therapeutic effect versus the amount that causes toxicity. Quinine is known to have serious side effects if dosed inappropriately. When quinine is administered at therapeutic levels, the side effects are referred to as cinchonism which include: flushed and sweaty skin, ringing of the ears, blurred vision, impaired hearing, confusion, headaches, abdominal pain, rashes, vertigo, dizziness, nausea, vomiting, and diarrhea. Very rarely, it can cause death and paralysis if injected into a nerve.

Nowadays, other medications have become the main course of treatment against malaria instead of quinine. It is now used as a second line treatment in combination with an antibiotic for uncomplicated malaria if the first line treatment does not work or is unavailable. However, in the case of severe malaria, quinine remains the main treatment method as it requires quick, safe and effective intravenous drugs.

2.3.2.2 Chloroquine (CQ)

In 1934, Johann Andersag and his coworkers at Bayer laboratories discovered a new compound, which they called Resochin, as a substitute for quinine; they synthesized and tested approximately 12,000 compounds in this process. It is chemically similar to quinine in that they both possess a quinoline base structure, which can be visualized in Figure 25. Resochin went relatively unnoticed for a decade as it was believed to be too toxic until World War II when the United States government sponsored clinical trials. At this time, the impact of the new compound would be fully revealed; it was undeniably effective as an antimalarial with the added benefits of being cheap to produce and fewer side effects than quinine. In 1946, it was officially named chloroquine (CQ).

Chloroquine functions as a blood schizonticide and against *P. vivax* and *P. malariae* as a gametocytocide analogous to quinine. The mechanism of antimalarial action is believed to inhibition of crystallization of hematin causing toxic levels of hematin to accumulate in the parasite. Another potential idea is it interferes with the biosynthesis of parasite nucleic acids. It is administered orally and diffuses into the body's adipose tissue with a high volume of distribution. The half-life is longer at 1-2 months, but the side effects are minimal with gastrointestinal problems, itches, headaches, postural hypotension, nightmares and blurred vision. The therapeutic index

for chloroquine is narrow and improper dosages can occur. When an overdose occurs, the patient can experience headache, drowsiness, visual disturbances, nausea, vomiting, cardiovascular collapse, seizures and sudden respiratory and cardiac arrest.

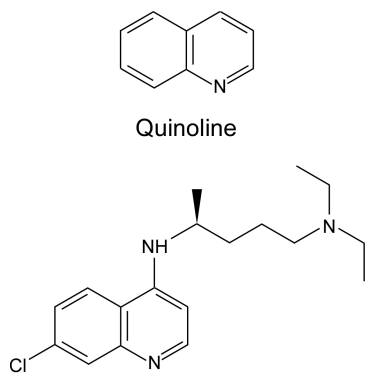

Figure 25: Structures of quinoline and antimalarial chloroquine. The group of antimalarials commonly utilized to inhibit hematin crystallization has a quinoline base structure.

In the late 1950s, the first documented case of *P. falciparum* resistance to chloroquine was reported in Colombia and at Cambodia-Thailand border. Over the next decade, the resistance of malaria spread steadily across South America and Southeast Asia.[98] In the 1970s, chloroquine-resistant malaria finally appeared in Africa and subsequently, dispersed across the continent over the next decade. *P. vivax* remained susceptible to chloroquine until 1989 when resistance was discovered in Papua New Guinea. Due to this resistance, other antimalarials were necessary for treatments as the morbidity and mortality of malaria resurged.

2.3.2.3 Artemisinin (ART)

During the time of emerging antimalarial resistance, the government of the People's Republic of China embarked on a systemic endeavor to discover if any indigenous plants used in traditional remedies possessed specific compounds to act as pharmaceuticals.[99] One plant, known as *qing hao* (or *Artemisia annua* L., sweet wormwood, annual wormwood), had been documented as a potential antimalarial as it

combats the fever and chills associated with malaria in 1596 by a herbalist, Li Shizhen.[100] Initial attempts to ascertain its capabilities as an antimalarial were unsuccessful with a hot water extract. However, a researcher, Tu Youyou, tested low temperature extraction with ethyl ether in 1971 with a profound difference in potential efficacy. Further purification of antimalarial fractions lead to the recovery of a plant constituent that never been reported in 1972. This new compound was named qinghaosu or artemisinin, ART, (Figure 26), but these results were not published until 1979. Initially, artemisinin was believed to be too unstable to be an effective antimalarial, but by 2006, artemisinin combined with other antimalarials was designated by WHO as the suggested treatment of choice for malaria.

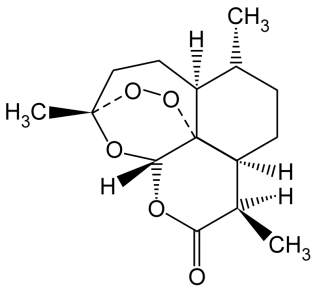

Artemisinin (ART)

Figure 26: Molecular structure of antimalarial artemisinin.

Artemisinin is a sesquiterpene endoperoxide antimalarial that inhibits the development of trophozoites functioning as a blood schizonticide. It is has also been reported to act as a gametocytocide.[101] For artemisinin, the antimalarial activity is dependent upon the endoperoxide bridge in its structure and cleavage of this bridge produces an activated form.[102,103] Intraparasitic heme or iron may react with artemisinin to cleave the endoperoxide bridge creating toxic free radicals.[104] In this form, there are numerous ways artemisinin can function as an antimalarial: inhibit crystallization of hematin, protein alkylation, or interaction with membrane containing structures.[105,106]

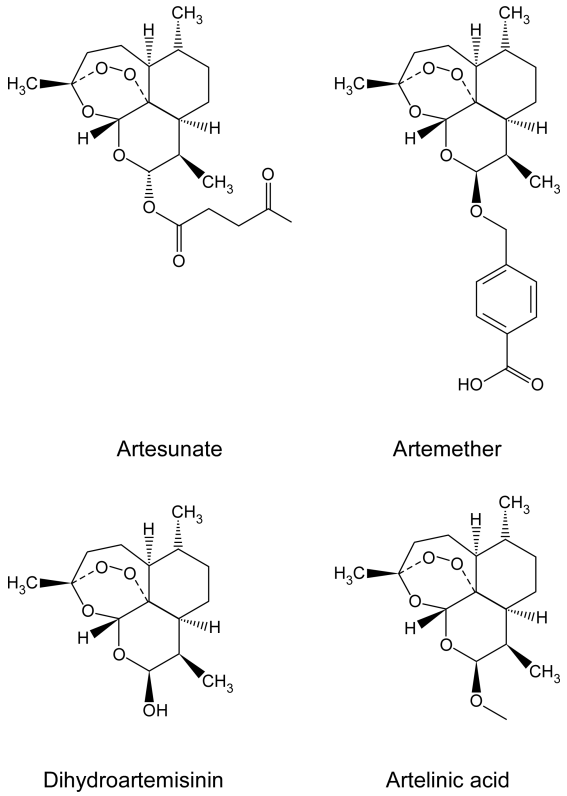

Figure 27: Chemical structures of four common derivatives of artemisinin which are prescribed to treat malaria.

The physical properties of artemisinin limit its efficacy as an antimalarial. It has poor bioavailability; therefore, several semisynthetic derivatives have been manufactured including artesunate, artemether, dihydroartemisinin, and artelinic acid to improve solubility in either aqueous or lipid media (Figure 27). The half-life of artemisinin is on the order of an hour, requiring daily doses over several days.[107] Normally, artemisinin is not used as a lone treatment due to recrudescence. It is paired with another antimalarial possessing a longer half-life. While artemisinin is extremely effective, it is much more expensive than chloroquine and limits its availability to those infected as most live in poverty.[108]

In 2008, strains of artemisinin resistant malaria emerged in western Cambodia.[109,110] Resistance to artemisinin-based therapies is spreading to other areas in Southeast Asia and Africa.[111,112] Unregulated use of artemisinin based therapies, poor

quality artemisinin based therapies with sub-therapeutic quantities, and widespread availability and use of artemisinin lead to the development of resistant parasites.[113]

2.3.2.4 Other Antimalarial Drugs in Use

During this same time, other antimalarials were discovered or synthesized as replacements due to resistance of parasites.[114] Antibiotics were utilized in attempts to help limit the occurrence of resistance in combination therapies with other antimalarials. Table 2 is a summary of common pharmaceutical compounds in use for treatments against malaria. For all of the drugs in the table, parasites demonstrate resistance in some form.

Table 2: Common Antimalarials and Their Applicability

Drug	Structure	Life Cycle Target	Hypothesized Mechanisms	Usefulness
Amodiaquine [AQ][115]	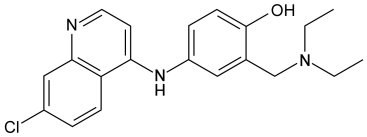	Blood schizonticide	Inhibit hematin crystallization	Second cheapest drug to produce; Only used in Africa
Mefloquine [MQ]	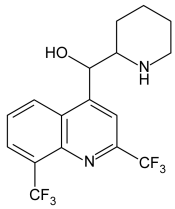	Blood schizonticide	Complexation between mefloquine and hematin for crystallization inhibition	Long half-life (2-4 weeks); Taken prior to traveling to malaria endemic regions
Sulfadoxine [SX]	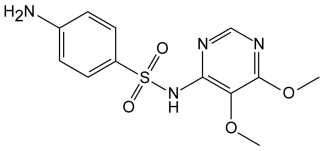	Blood schizonticide	Interferes with folate synthesis disrupts DNA replication, cell division and reproduction	Half-life 7-9 days; Combined with Pyrimethamine usually
Doxycycline (Tetracyclines) [DC]	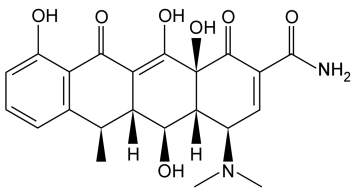	Tissue schizonticide – prevention; Blood schizonticide	Targets apicoplasts in parasites	Cheap and effective drug used in combination with another antimalarial with hematin crystallization inhibition; slow onset

Table 2 continued

Drug	Structure	Life Cycle Target	Hypothesized Mechanisms	Usefulness
Pyronaridine [PY]	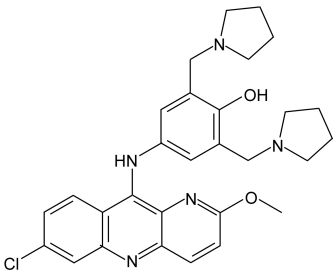	Blood schizonticide	Inhibits hematin crystallization	Long shelf life; long post-treatment prevention
Pyrimethamine	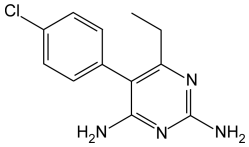	Tissue schizonticide – prevention & relapse; Blood schizonticide	Inhibits folic acid metabolism	Combined with Sulfadoxine usually
Proguanil (Chloroguanide)	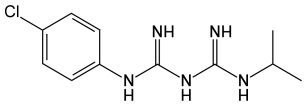	Blood schizonticide; Sporontocide	Inhibits folic acid metabolism	Taken daily; Prevents reproduction of parasites
Atovaquone	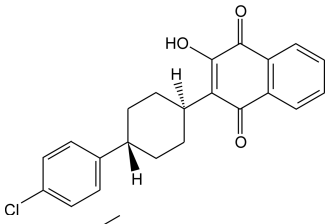	Tissue schizonticide – prevention & relapse	Collapses mitochondrial membranes	Used to treat malaria in developed countries
Halofantrine	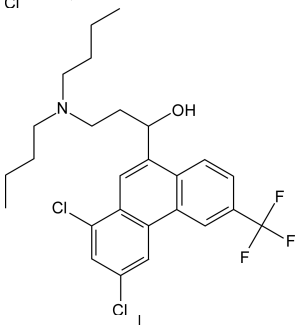	Blood schizonticide	Complexation to inhibit hematin crystallization	Unreliable adsorption; Used minimally overall, mostly severe/resistant malaria
Primaquine	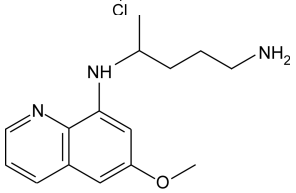	Tissue schizonticide – prevention & relapse; Gametocytocide; Sporontocide	Block oxidative metabolism	Only drug affecting certain life cycles of parasite
Piperaquine	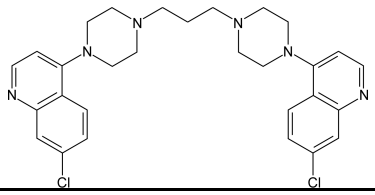	Blood schizonticide	Inhibit hematin crystallization	Slow absorption; Long half-life

Table 2 continued

Drug	Structure	Life Cycle Target	Hypothesized Mechanisms	Usefulness
Tafenoquine	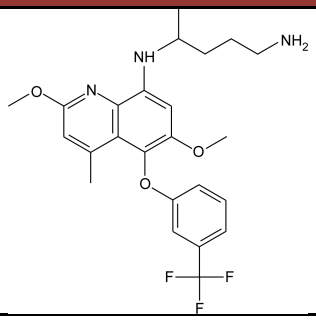	Tissue schizonticide – relapse; Gametocytocide	Collapses mitochondrial membranes	Long half-life (2-3 weeks); Effective against *P. vivax*; improved therapeutic index

2.4 Parasite Resistance

As the Plasmodium parasites became resistant to various antimalarials, it became imperative to know why the parasite was able to survive for the implementation of new drugs. Would the parasite have immunity against new pharmaceuticals introduced? Biologists studied how the parasite mutated and why extremely effective antimalarials no longer functioned properly to answer this question.

For chloroquine, the drug accumulates in the parasite's digestive vacuole where is supposedly interferes with the heme detoxification process. In resistant strains of *P. falciparum*, the concentration of chloroquine inside the digestive vacuole is dramatically lower.[98] When comparing a chloroquine-resistant strain versus a chloroquine-sensitive strain of malaria, the *pfcrt* gene was identified as a candidate for resistance. The PfCRT protein localizes to the digestive vacuole membrane and contains ten putative transmembane domains; effectively, this gene determines whether or not an antimalarial enters the digestive vacuole. Point mutations in the PfCRT gene enable the parasite to survive antimalarials that require entrance into the digestive vacuole including CQ, amodiaquine (AQ), mefloquine (MQ), etc. The parasite mutates differently for each new

drug launched into use. Different affected genes include: *pfcrt*, *pfmdr1*, *pftctp*, and *pfmrp1*.

Resistance occurs for antimalarials that do not accumulate in the digestive vacuole as well. Both sulfadoxine (SX) and pyrimethamine inhibit part of the folic acid synthesis cycle, specifically dihydropteroate synthetase (DHPS) and dihydrofolate reductase (DHFR). For sulfadoxine resistance, the DHPS gene mutates while for pyrimethamine, the DHFR gene is altered.

The number of years required for the parasites to mutate and show resistance to a drug varies; however, the amount of time is declining. Table 3 compares a variety of antimalarials with their dates of introduction and the first reported resistance.[116] From this table, it can be gleaned that not only is there a need for new antimalarials but also a way to understand how antimalarials function to create a platform for pharmaceutical design. Since antimalarials are phased out quickly due to resistance, new ones must be available to replace them.

Table 3: Antimalarial Resistance

Drug	Year Introduced	First Reported Resistance	Difference (years)
Quinine	1632	1910	278
Chloroquine	1945	1957	12
Proguanil	1948	1949	1
Sulfadoxine-Pyrimethamine	1967	1967	0
Mefloquine	1977	1982	5
Atovaquone	1996	1996	0

2.5 Crystal Structure of Hemozoin

The size and morphology of hemozoin crystals extracted from several Plasmodium species has been identified by electron microscopy as shown in Figure 28.[117,118] The hemozoin crystals formed inside of the parasite's digestive vacuole are

approximately 100 × 100 × (300-500) nm^3 in size. The synthetic crystal β-hematin is identical to hemozoin.[8] X-ray diffraction (XRD) has shown that the crystals of both hemozoin and β-hematin are triclinic, with space group $P\bar{1}$. In both natural and synthetic crystals, hematin is present as "head-to-tail" dimers, bound by a coordination bond between the carboxyl residues and the Fe^{3+} ion.[119]

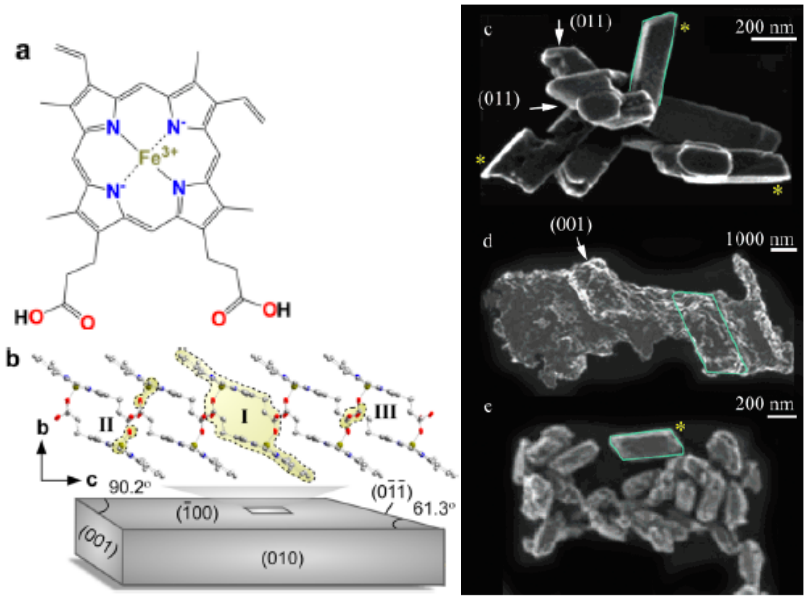

Figure 28: Illustration of the crystal structure of hemozoin. (A) Chemical structure of hematin. (B) Diagram of β-hematin crystals, packing structure and bonds necessary. (C-E) SEM images of crystals extracted from different parasites. (C) *P. falciparum* (D) *S. mansoni* (E) *H. columbae*.

Depending on the solution, hematin will form other types of dimers and oligomers, distinct from head-to-tail dimers, including: π–π dimers, in which two hematin monomers are in parallel positions, the two Fe atoms face outward, and the monomers are linked by overlapping π electron density; μ-oxo dimers, in which two parallel hematin monomers are bound by an O atom linking their facing Fe atoms; and larger oligomers, in which μ-oxo dimers catenate by π–π linkages. These dimers and oligomers can potentially interfere with the process of crystallization. Illustrations of these dimers are shown in Figure 29.

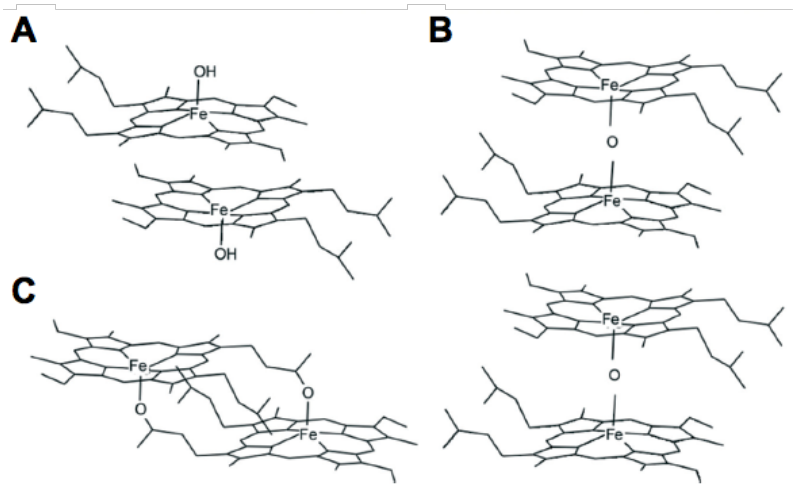

Figure 29: Structures of hematin dimers. (A) π–π dimers, (B) stacked μ-oxo dimers, and (C) head-to-tail dimers found in synthetic and naturally existing hematin crystals.

2.6 Previous Growth Methods

Attempts to replicate hematin crystallization *in vitro* have traditionally focused on the use of aqueous solvents.[120-122] For all procedures in aqueous solutions, the low solubility must be overcome otherwise crystallization will not proceed. To improve solubility, several methods have been employed (Table 4) including: addition of acetate, dimethyl sulfoxide (DMSO), sodium hydroxide (NaOH), introduction of lipid droplets and alcohol interfaces.

When comparing the crystals grown from each environment, there are clear difficulties associated with many growth media. If hematin crystallization occurs in 0.1 M aqueous acetate solution (pH 4.8), the resulting crystals do not possess the morphology indicative of hemozoin crystals *in vivo*.[121] The only success at achieving crystals in aqueous solutions is through the use of high ionic strength growth media that are not physiologically relevant. This suggests that a strictly aqueous environment may not be sufficient for hematin crystallization. Other groups that attempted to form beta-hematin crystals in an aqueous environment with lipid droplets succeed at producing crystals with the correct morphology.[123] Additionally, groups have used DMSO as an organic phase in

hematin crystallization; however, DMSO incorporates into the crystal structure.[124] These results suggest that an organic phase facilitates hematin crystallization. Recently, transmission electron micrographs[45,125] and X-ray tomography images[126] of parasites have shown hemozoin crystals seemingly immersed in lipid nanospheres and attached to DV membranes coated with lipid.[45,126]

Table 4: β-Hematin Crystal Morphology Based on Growth Conditions

Growth Environment	β-hematin Crystals	Inconsistencies
4.5 M acetate, pH 5.0	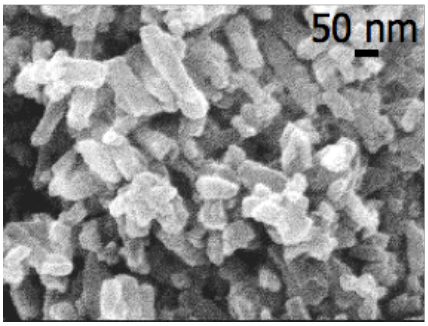	High ionic strength solution – not physiologically relevant
DMSO & water	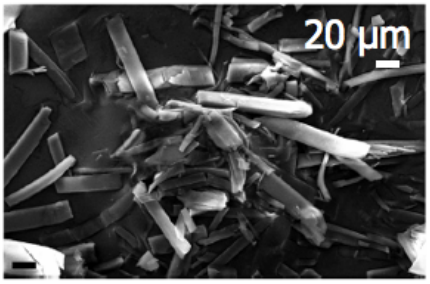	DMSO incorporates into crystal structure
0.1 M acetate, pH 4.8	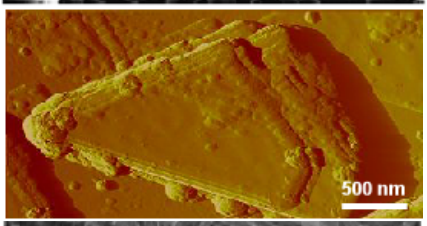	Morphology does not match crystals found in Plasmodium parasites
monopalmitoyl glycerol droplets & water, pH 4.8	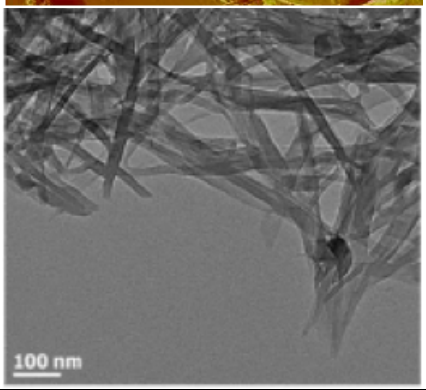	Correct morphology of crystals, but lipids are expensive and most are not liquid are room temperature for further studies

Table 4 continued

Growth Environment	β-hematin Crystals	Inconsistencies
octanol & water, pH 4.8[127]	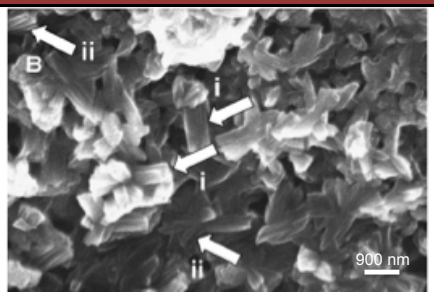	Correct morphology, alcohol substitute for lipid blend
anhydrous octanol		No crystals produced in this solvent

From these previous studies, a starting point can be exposed. Physiologically relevant aqueous solutions and purely organic solutions are unable to produce the correct morphology crystals or crystals in general. Therefore, the solution properties of physiologically relevant environments need to be scrutinized to understand how crystal growth may be influenced and proceed.

Chapter 3: Solution Properties Governing Hematin Crystallization

The crystallization process is heavily dependent upon the growth environment and the properties of the solute. For this project, the solution properties of hematin and antimalarial drugs are used to shed light on the location of crystal growth of β-hematin in the two bulk phases of the DV: aqueous and lipid.

3.1 Lipid Environment as Growth Medium

The lipid blend identified within the parasite digestive vacuole is a mixture of five neutral lipids: monopalmitoyl glycerol, monostearoyl glycerol, dipalmitoyl glycerol, dioleoyl glycerol, and dilinoleoyl glycerol. These lipids are reportedly present in the digestive vacuole in a molar ratio of 2:4:1:1:1, respectively.[45] The chemical structure of the lipids is shown in Figure 30. Only two of the five lipids, dioleoyl glycerol, and dilinoleoyl glycerol, are liquid at 25°C.[128] To test the phase of the lipid blend, a mixture of the five lipids in proportions according to their reported physiological molar ratio was prepared. At room temperature the mixture is solid; the melting point of the lipid blend is reported at approximately 37°C.[129] Thus, it is feasible that this mixture is indeed present as a liquid subphase within the parasite DV. The lipid blend is not a practical solvent for *in vitro* tests of hematin crystallization inhibitors owing to the high cost of the constituents, the large quantity of lipids required for high-throughput characterization, and the inability to perform experiments at room temperature.

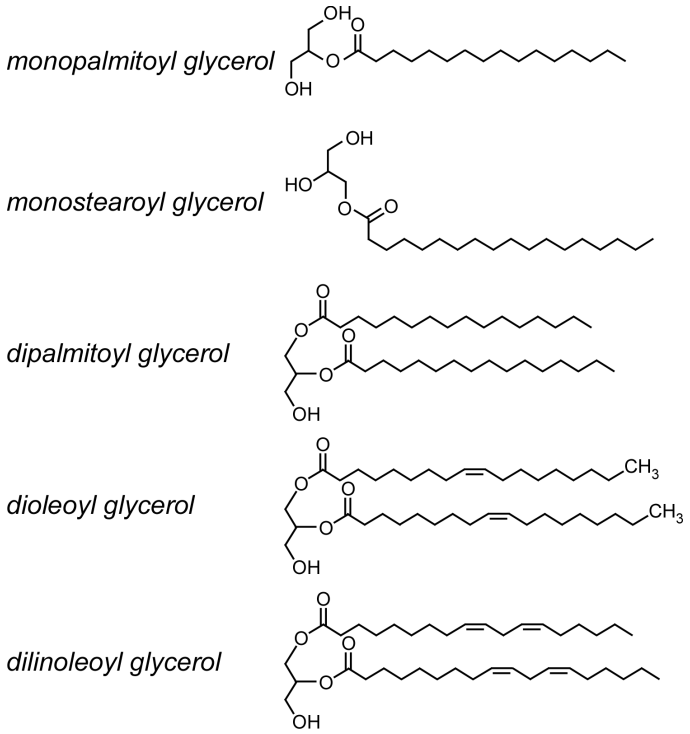

Figure 30: Chemical structures of five neutral lipids identified in the digestive vacuoles of malaria parasites.[45]

Given the challenges associated with using a lipid blend, our group searched for an alternative organic solvent with properties similar to the lipid blend, but one that is inexpensive, available in large volume, and liquid at room temperature. To this end, n-octanol was selected as a surrogate organic solvent. Octanol possesses a long aliphatic carbon chain and a polar alcohol group that mimics the amphiphilicity of the lipids. Octanol is routinely used to model lipids during determinations of the lipophilicity of drugs. Another property of the surrogate solvent that may be significant for hematin crystallization is the presence of water. The organic phase in the parasite digestive vacuole is in direct contact with an aqueous phase that maintains a pH between 4.8 and 5.5.[130,131] To estimate the amount of dissolved water within the organic subphase, the lipid blend was prepared and placed it in intimate contact with water for one hour to generate a water-saturated organic phase. The latter was extracted and the solubility of

water in the lipid blend was determined using thermogravimetric analysis (TGA). The mass fraction of evaporated solvent was recorded as a function of temperature increasing from 25 to 120°C. Three different runs with ramp rates, 0.1, 0.3, and 1.0 °C min^{-1}, yielded identical results. As shown in Figure 31A, an increase in temperature from 25 to 85°C results in a loss of mass from the lipid blend, but no further loss was observed between 85 and 120°C. An identical study performed with an anhydrous lipid blend revealed no mass loss at temperatures lower than 120°C. These temperatures are significantly lower than the boiling points of the lipids; therefore, it can be concluded that the evaporated compound is water.

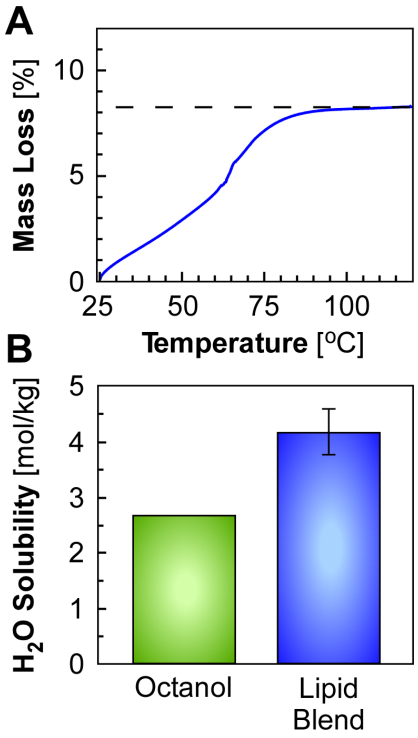

Figure 31: (A) Thermogravimetric analysis of the biomimetic blend of five lipids at a ramp rate of 0.3°C/min shows the mass loss of water as a function of temperature. (B) Comparison of the water solubility in n-octanol (reported by Segatin et al.)[132] and the biomimetic lipid blend.

The average amount of dissolved water in the lipid mixture is 8.5 ± 0.5% mass, corresponding to a solubility of 4.2 ± 0.3 mol kg^{-1}. In comparison, the water solubility in

n-octanol is slightly lower (2.7 mol kg^{-1}), as shown in Figure 31B.[132] Previous results have indicated that anhydrous n-octanol does not support hematin crystallization.[16]

The factors that underlie the need for water in the crystallization solvent are likely related to the shared structure of both physiological and synthetic hematin crystals. In these crystals, hematin assembles into dimers bound by reciprocal COO^{-}-Fe(III) coordination bonds, and connected through chains of -COOH-HOOC- hydrogen bonds.[133] The formation of hydrogen bonds requires the presence of water and hydrogen ions. Hence, as a biomimetic solvent here we use n-octanol as a surrogate for the lipid blend, saturate it with citric buffer, and refer to it as CBSO.

3.2 Hematin Solubility in Aqueous & Organic Environments

For crystallization to occur, the solvent must be supersaturated with the solute. To understand how hematin crystallizes in CBSO in comparison to an aqueous environment, the solubility of hematin in CBSO was measured. To determine the solubility of hematin in saturated octanol, UV-Vis spectrophotometry and the Beer-Lambert Law,

$$A = \varepsilon bC, \qquad [1]$$

where A is the absorbance, ε is the extinction coefficient, b is the path length of the cuvette, and C is the concentration of the solute, were utilized.

As hematin dissolves in either anhydrous or water saturated octanol, a solid insoluble residue remains. Hence, hematin concentration in this solvent cannot be evaluated from the mass of dissolved material. To transfer known amounts of soluble hematin to octanol, hematin was dissolved at a known concentration in NaOH. This solution was incubated for two weeks in contact with octanol, as illustrated in Figure 32 and Figure 33a. Preliminary tests revealed that vigorous stirring led to the formation of

emulsions of water in octanol and octanol in water, stabilized by layers of hematin on the droplet interfaces; therefore, the aqueous-octanol mixture was only gently stirred at the beginning of incubation. Within several minutes after this stirring, the mixture splits into two layers with the octanol phase on the top. During the incubation, both water and hematin transfer to the octanol phase. The amount of hematin in octanol was determined from the difference of the concentrations in NaOH before and after the incubation with octanol, as discussed below.

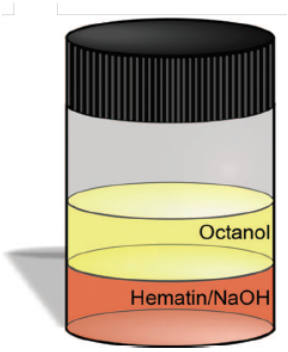

Figure 32: Illustration of experimental procedure to determine the extinction coefficient of hematin in water-saturated octanol.

The commercial hematin powder fully dissolves in 0.1 M NaOH. Thus, we used its mass to determine the concentration of hematin in this solution. After the exchange with octanol, the residual hematin concentration was measured spectrophotometrically. To determine the extinction coefficient of hematin in 0.1 M NaOH, solutions with varying hematin concentration were prepared. The absorbance spectra of the solutions in the 200–800 nm wavelengths range was recorded; an example is displayed in the inset of Figure 33c. The dependence of the absorbed intensity at 607 nm on the hematin concentration is linear, Figure 33b, and its slope yields the extinction coefficient of hematin in 0.1 M NaOH at this wavelength $\varepsilon = 3.86 \pm 0.06$ cm^{-1} mM^{-1}.

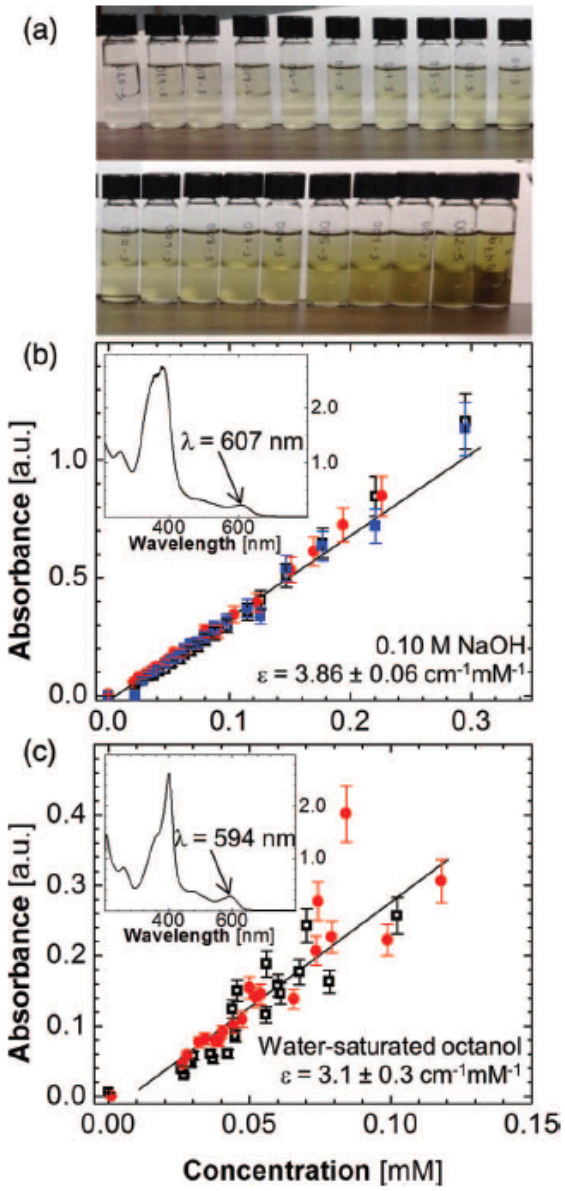

Figure 33: Determination of the extinction coefficient of hematin in water-saturated octanol. (a) 20 vials with two layers as illustrated in Figure 31. (b) Extinction coefficient of hematin in 0.1 M NaOH at 607 nm. (c) Extinction coefficient of hematin in water-saturated octanol at 594 nm.

Finally, the extinction coefficient of hematin in water-saturated octanol was determined. Two mL of 0.1 M NaOH solution with varying concentration of hematin was placed in 5 ml glass vials. To each vial, 2 mL anhydrous octanol was added and equilibrated it for a week at 25^{o}C. The spectra of the octanol and NaOH layers were recorded in each vial after filtration through 0.22 μm filters. The hematin spectra in

octanol, illustrated in the inset of Figure 33c, exhibit a local absorbance maximum at 594 nm. The dependence of the absorbed intensity at this wavelength on the hematin concentration is linear, Figure 33c, and its slope yields the extinction coefficient of hematin in water-saturated octanol, $\varepsilon = 3.1 \pm 0.3\ cm^{-1}\ mM^{-1}$.

Citric buffer (pH 4.80) was prepared by dissolving citric acid at 50 mM in DI water and titrating with 0.10 M NaOH under continuous stirring to the desired pH. The buffer was stored with a maximum shelf life of 1 month. Before each experiment, the buffer pH was verified. To prepare citric buffer-saturated octanol (CBSO), n-octanol (ca. 15 mL) was deposited over citric buffer stock solution (5 mL) held in a pre-cleaned 40 mL glass vial. The resulting two-phase solution was sealed and allowed to equilibrate without stirring at 23°C for 30 min. During this time, the organic layer becomes saturated with water, forming the CBSO solution. The top CBSO layer was carefully removed with a pipette far from the interface to avoid resuspension of the two phases.

To determine the solubility of hematin in CBSO, 2–5 mM hematin powder was added to 5 mL CBSO held in 20-mL glass vials that were subsequently sealed with Parafilm. Sets of three vials were stored at four temperatures: 5 °C, 25 °C, 37 °C, and 45 °C. A 300-μL aliquot was removed weekly from each of the 12 solutions, diluted with CBSO, filtered through a 0.22-μm polyethersulfone (PES) filter, and the concentration of dissolved hematin was determined spectrophotometrically. This procedure was repeated until the concentrations in each vial reached a plateau, defined by three consecutive readings of similar value. Microscopic observations revealed that the initial amorphous hematin powder appeared to fully dissolve and β-hematin crystals with typical rodlike habit had formed. The final steady-state concentrations were averaged over the three

samples at each temperature. The resulting mean was used as the solubility c_e of hematin in CBSO with respect to β-hematin crystals. The data for the four tested temperatures are plotted in Figure 34a, where they are compared with a determination using AFM. Solubility in AFM studies was determined as the concentration of hematin at the point of zero step velocity (i.e., the x intercept in Figure 35). In Figure 34, the solubility of hematin in CBSO at 25 °C is compared to that in aqueous citric buffer at the same temperature and pH 4.8.

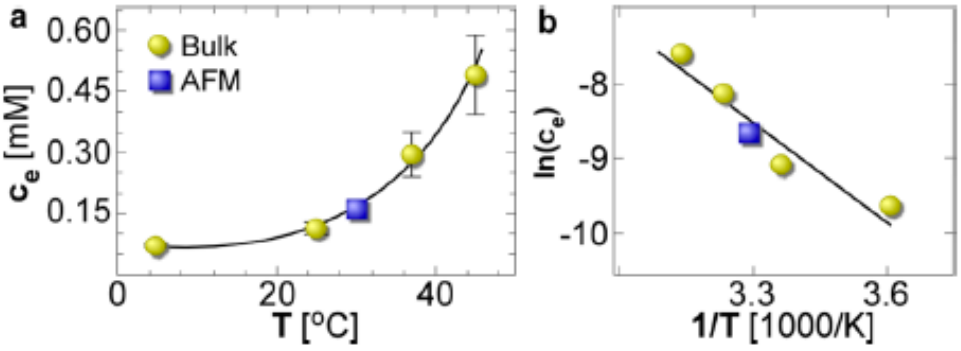

Figure 34: Characterization of the crystal−solution equilibrium from bulk crystallization experiments (yellow circles) and by in situ atomic force microscopy (blue squares). (a) The temperature dependence of hematin solubility in CBSO. (b) The solubility data in van 't Hoff coordinates.

Spectroscopic analyses revealed that this solubility is ~10^5 higher than in aqueous buffer at pH 4.8 (Figure 35), which is not surprising given that hematin is a hydrophobic molecule. Because crystal growth rates roughly scale with the solubility, this disparity in the magnitude of hematin solubility indicates that crystallization from an organic phase is a significantly faster method of heme detoxification than from an aqueous phase.[13]

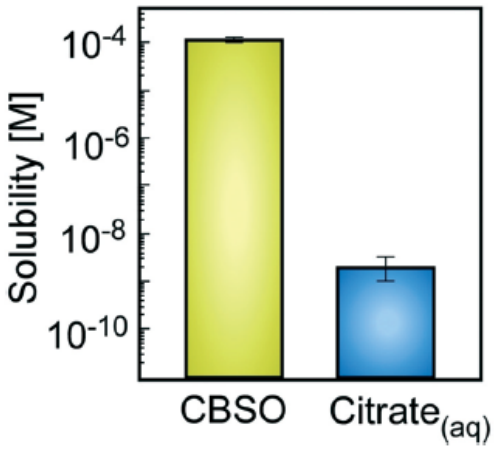

Figure 35: Comparison of the solubility of hematin in citric buffer saturated octanol (CBSO) and aqueous citric buffer, pH 4.8 at 25°C.

A dependence of hematin solubility c_e in CBSO on temperature is presented in Figure 34a. The data in Figure 34 reveal excellent agreement between the solubility measured by two separate techniques: bulk crystallization and in situ AFM. To evaluate the standard enthalpy ΔH^o_{cryst} of hematin crystallization in CBSO, it is noted that, in the crystallization equilibrium,

$$\text{hematin (solution)} \leftrightarrows \text{hematin (crystal)}, \qquad [2]$$

the product is a solid phase and has activity of one. The activity of the soluble hematin was assumed to be equal to its concentration. This assumption is justified by the low values of the solubilities in Figure 34 that correspond to long intermolecular separations, at which the intermolecular interactions are weak and the activity coefficients are near unity. With this, the equilibrium constant for crystallization is

$$K_{\text{cryst}} = c_e^{-1}. \qquad [3]$$

The temperature T dependence of solubility $c_e(T)$ is given by the classical van't Hoff equation

$$\frac{\partial \ln c_e}{\partial (1/T)} = \frac{\Delta H^o_{cryst}}{R}, \qquad [4]$$

where R is the universal gas constant. The slope of the c_e data plotted in van 't Hoff coordinates ln c_e as a function of $(1/T)$ in Figure 34b yields ΔH^o_{cryst}= −37 ± 8 kJ mol^{-1}.

The solubility data can also be used to determine the Gibbs free energy of crystallization ΔG^o_{cryst} and the crystallization entropy ΔS^o_{cryst}. ΔG^o_{cryst} is related to the crystallization equilibrium constant K_{cryst} as

$$\Delta G^o_{cryst} = -RT\ lnK_{cryst} = RT\ lnc_e. \qquad [5]$$

Equation 5 yields ΔG^o_{cryst} = −22 ± 3 kJ mol^{-1} at 25 °C. The difference between ΔH^o_{cryst} and ΔG^o_{cryst} provides an estimate for ΔS^o_{cryst}

$$\Delta S^o_{cryst} = {(\Delta H^o_{cryst} - \Delta G^o_{cryst})}/{T}. \qquad [6]$$

ΔS^o_{cryst} = −49 ± 7 J mol^{-1} K^{-1} was obtained.

The crystallization entropy reflects the loss of translational and rotational degrees of freedom when a molecule from the solution incorporates into a crystalline lattice, partially balanced by the gain of vibrational degrees of freedom of the newly established crystal contacts. The molecular processes underlying ΔS^o_{cryst} are similar to those during the entropy loss of a molecule binding to another molecule. Estimates of the latter process for molecules with sizes similar to that of hematin yield ΔS^o_{cryst} in the range of −100 to −280 J mol^{-1} K^{-1}. Thus, the magnitude of ΔS^o_{cryst} for hematin is lower than the estimates for similarly sized molecules, which suggests a process leading to entropy increase during hematin incorporation into the growth sites on crystal surfaces. This process could possibly be the release of *n*-octanol molecules, which may be ordered at the crystal–solvent interface and surrounding hematin molecules in the solution.

3.3 Mechanism of Crystallization

Hematin crystals that form in physiological (hemozoin) and synthetic (β-hematin) processes are faceted with smooth faces oriented along crystallographic planes with low Miller indices and high density of molecules. To elucidate the growth mechanism of hematin crystals, our group employed time-resolved in situ AFM to image large crystals. They discovered hematin crystals follow a classical mode of crystal growth, in which new layers are generated by 2D nucleation and spread to cover the entire facet as seen in Figure 36.

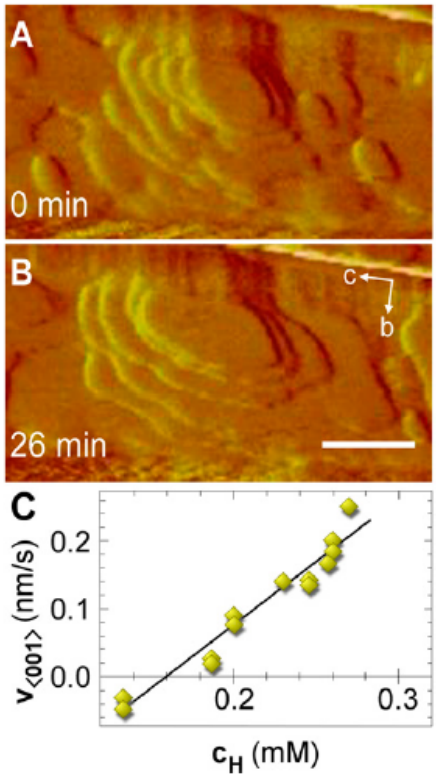

Figure 36: Layer growth on β-hematin [100] surfaces. (A and B) Time-resolved in situ AFM images of layer growth in solution at c_H = 0.28 mM. (Scale bar, 250 nm.) (C) Step velocity in the [001] direction as a function of hematin concentration c_H.

3.4 Thermodynamic Properties of Crystallization

Analyses of successive snapshots from AFM movies in our group reveal that new layers may either grow (I–III in Figure 37 A–D), dissolve (IV in Figure 37 A–D), or

retain a steady size during continuous imaging (V in Figure 37 C and D) depending on their radius R. They observed a reduction in the critical radius R_{crit} for island growth or dissolution with increasing hematin concentration (Figure 37E), which is consistent with classical nucleation theory (CNT) applied to 2D crystal islands on a substrate. According to CNT, islands form as a result of fluctuations of the concentration of molecules on the surface.

The dependence $R_{crit}(c_H)$ is governed by the Gibbs–Thomson relation, according to which

$$R_{crit} = \frac{\Omega\gamma}{k_B T ln(^{c_H}/_{c_e})}, \quad [7]$$

where $\Omega = 0.708$ nm^3 is the volume of one molecule in the crystal; γ is the surface free energy of the layer edge; k_B is the Boltzmann constant; T is temperature; c_H is hematin concentration; and c_e is hematin solubility in CBSO. The γ is estimated using the Turnbull empirical rule,

$$\gamma = \frac{0.3\left|\Delta H^o_{crys}\right|}{\Omega^{2/3}}, \quad [8]$$

where $\Omega = 0.708$ nm^3 is the volume of one molecule in the crystal and $\Delta H^o_{cryst} = -37 \pm 8$ kJ mol^{-1} as calculated from bulk solubility temperature dependence. The correspondence between the experimentally determined R_{crit} and the a priori CNT prediction in Figure 37E indicates that the generation of new layers on growing β-hematin surfaces is governed by the thermodynamics of hematin crystallization.

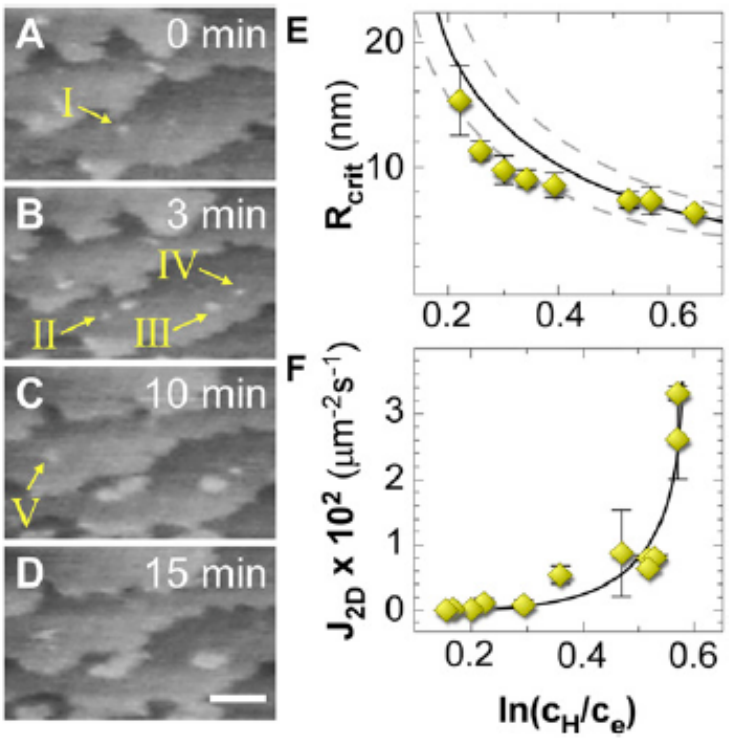

Figure 37: Generation of crystal layers. (A–D) Time-resolved in situ AFM images showing growing and dissolving islands on a (100) face at c_H = 0.25 mM. (Scale bar, 125 nm.) (E) Dependence of the critical radius of 2D nuclei R_{crit} on $\ln(c_H/c_e)$. (F) Rate of 2D nucleation of new layers.

3.5 Inhibition by Chloroquine

To date, definitive evidence for antimalarial mode(s) of action remains elusive. Our group was able to identify the mechanism of β-hematin crystal growth inhibition by chloroquine. *In situ* AFM measurements revealed that the addition of chloroquine to hematin growth solutions leads to slower step growth, fewer 2D nuclei, and more rugged step edges (Figure 38 A-E). The impact of chloroquine at concentrations c_{CQ} = 0–2 μM on layer generation and step propagation is summarized in Figure 38 F–H. There is an exponential decay in the rate of 2D nucleation of new layers per unit area per time, $J_{2D,}$ with increasing c_{CQ} that is accompanied by a monotonic decrease in v (Figure 38 G and H). They observed a complete suppression of layer nucleation and step growth at c_{CQ} = 2 μM.

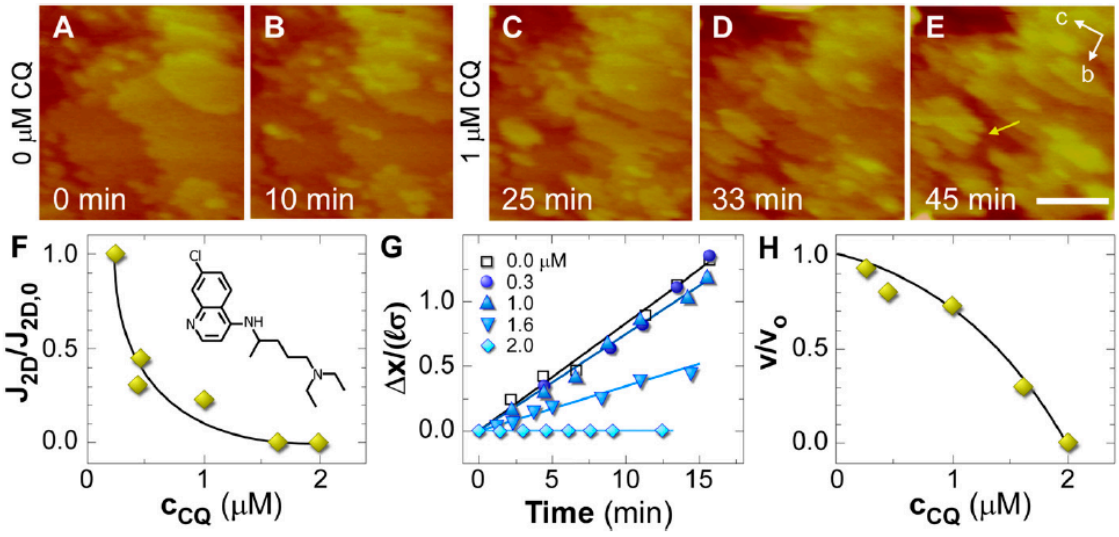

Figure 38: CQ inhibition of β-hematin growth. (A–E) Time-resolved in situ AFM images of a (100) face growing in solution at c_H = 0.28 mM. (Scale bar, 250 nm.) (A-B) Absence of CQ. (C-E) 1 mM CQ. Effect of CQ on (F) rate of 2D nucleation, (G) step displacement, and (H) step velocity.

3.6 Drug Solubility

An argument that is frequently presented in the literature in favor of hematin crystallization in an aqueous medium is the presumed low solubility of quinoline-class antimalarials in organic solvent, which would seemingly reduce their efficacy as inhibitors of crystal growth in the lipid phase. If the solubility of drug in the organic solvent exceeds 1 μM, a low threshold of efficacy of chloroquine in hematin crystallization inhibition,[134] the partitioning of drug from an aqueous phase to the organic phase would not limit its efficacy.

The solubility of eight drugs listed in Figure 39 was determined. As discussed earlier, the general approach to malaria treatment, recommended by The World Health Organization,[40] involves combination therapies. In this approach, two or more drugs with different modes of action and biochemical targets are applied simultaneously to produce a highly effective treatment.[48] For example, an antibiotic such as doxycycline (DC), which causes abnormal cell division, and an antimalarial such as quinine (QN), which inhibits

crystallization of hematin, are administered together to eradicate the parasite from the body. For these reasons, six common antimalarials – amodiaquine (AQ), mefloquine (MQ), pyronaridine (PY), artemisinin (ART), chloroquine (CQ), and quinine (QN) – and two antibiotics, sulfadoxine (SX) and doxycycline (DC) were selected. The solubility of each drug was measured in CBSO and citric buffer to assess the difference between organic and aqueous solvents, respectively.

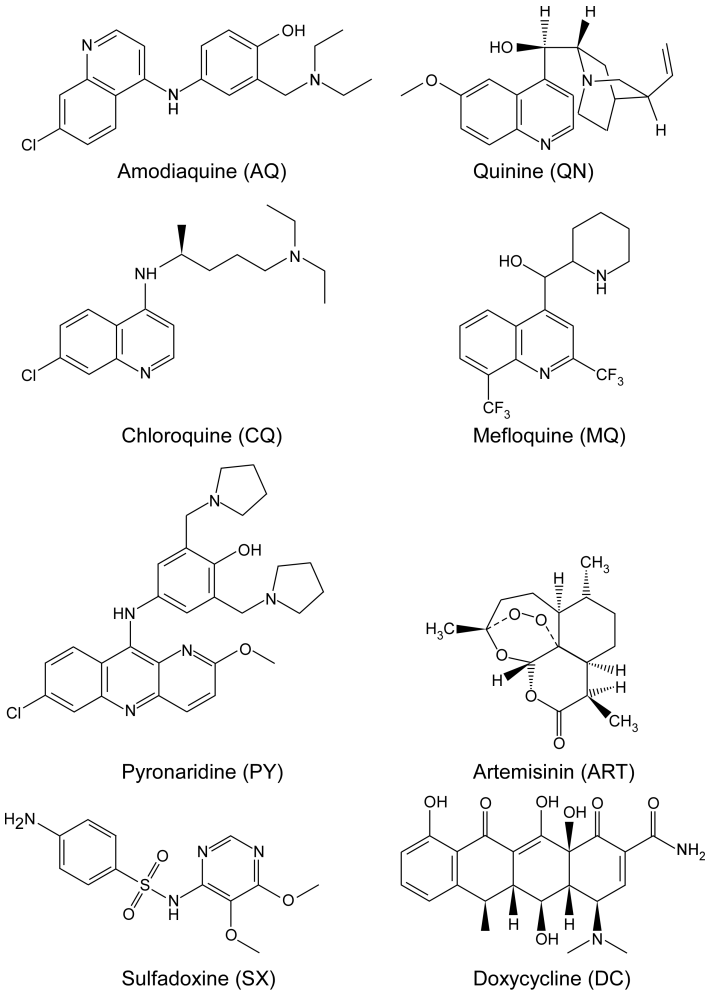

Figure 39: Molecular structures of six antimalarials (AQ, QN, CQ, MQ, PY, ART) and two antibiotics (SX and DC) that are commonly used in malaria combination therapies.

3.6.1 Extinction Coefficients

The concentrations of antimalarials, and antibiotics were determined using UV-

Visible spectrophotometry and the Beer-Lambert Law (Equation 1). The extinction coefficients of the five antimalarials, amodiaquine, quinine, chloroquine, mefloquine, and pyronaridine, and the two antibiotics, doxycycline and sulfadoxine, were determined in citric buffer and either citric buffer saturated octanol (CBSO) or water-saturated octanol (WSO). Tests revealed that the ε values in WSO are similar, within several percent deviation, to those in CBSO; hence, the ε values measured in WSO were used to determine the drug concentrations in CBSO. To determine ε in the respective solvent, a known amount of a drug was fully dissolved in a known volume of solvent. These stock solutions were diluted to eight concentrations and filtered through 0.22 μm polyethersulfone (PES) filters. Absorbance spectra in the wavelength range 200 – 800 nm were recorded for each concentration for each drug. A wavelength of peak absorbance was identified and ε at that wavelength was determined using the Beer-Lambert law as illustrated in Figures 40 – 42; the ε values are shown in Table 5. Each determination was based on two or three independent concentration series.

The extinction coefficient of sulfadoxine in citric buffer was determined analogously; however, sulfadoxine powder dissolves very slowly in CBSO. To prepare sulfadoxine solutions in CBSO with known concentration, 2 mL of sulfadoxine was kept in citric buffer in contact with 2 mL of CBSO for one week. The sulfadoxine concentration in CBSO was calculated from the decrease of the sulfadoxine concentration in the citric buffer layer and the respective ε was determined as with the other drugs.

Artemisinin does not absorb light in the UV-visible range. The concentration of an artemisinin stock solution was determined by keeping a known amount of the drug in contact with a volume of CBSO that was slowly increased over 45 days, until the entire

artemisinin powder dissolved.

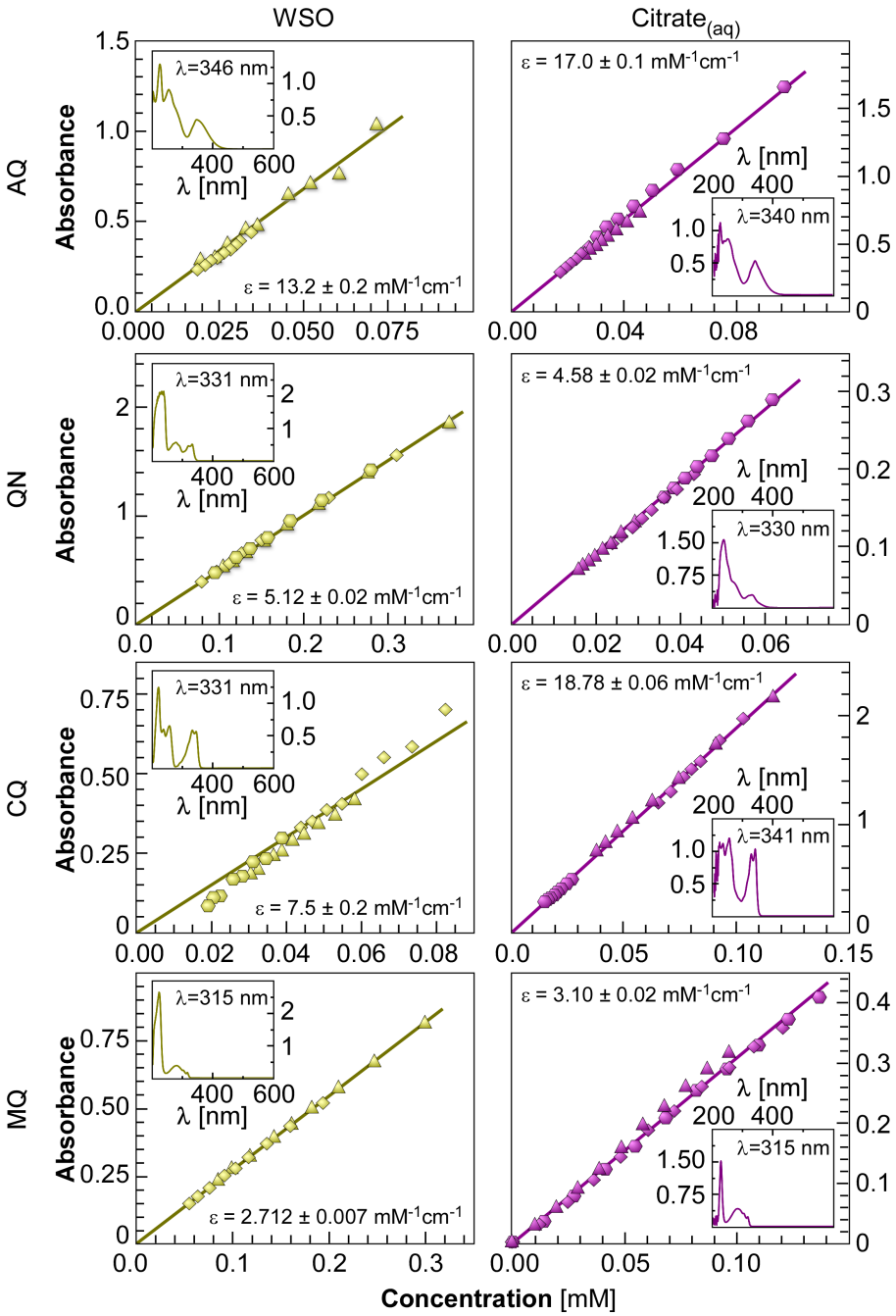

Figure 40: Determination of the extinction coefficients of antimalarials AQ, QN, CQ, and MQ in water-saturated octanol (left column) and aqueous citric buffer at pH 4.8 (right column).

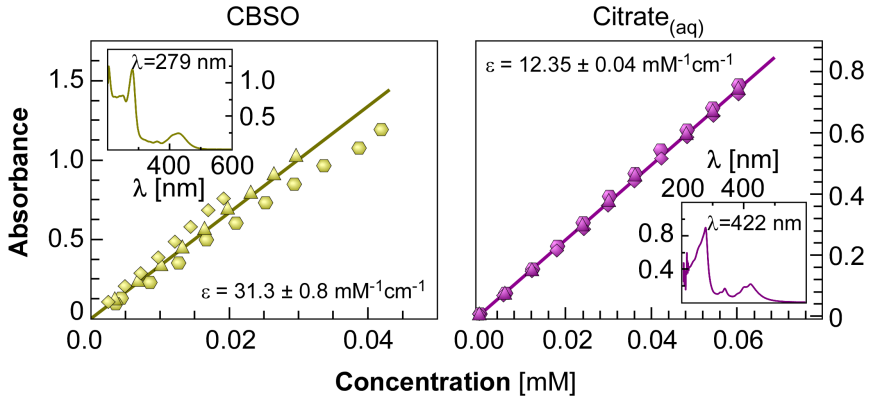

Figure 41: Determination of the extinction coefficients of PY in CBSO (left column) and aqueous citric buffer at pH 4.8 (right column).

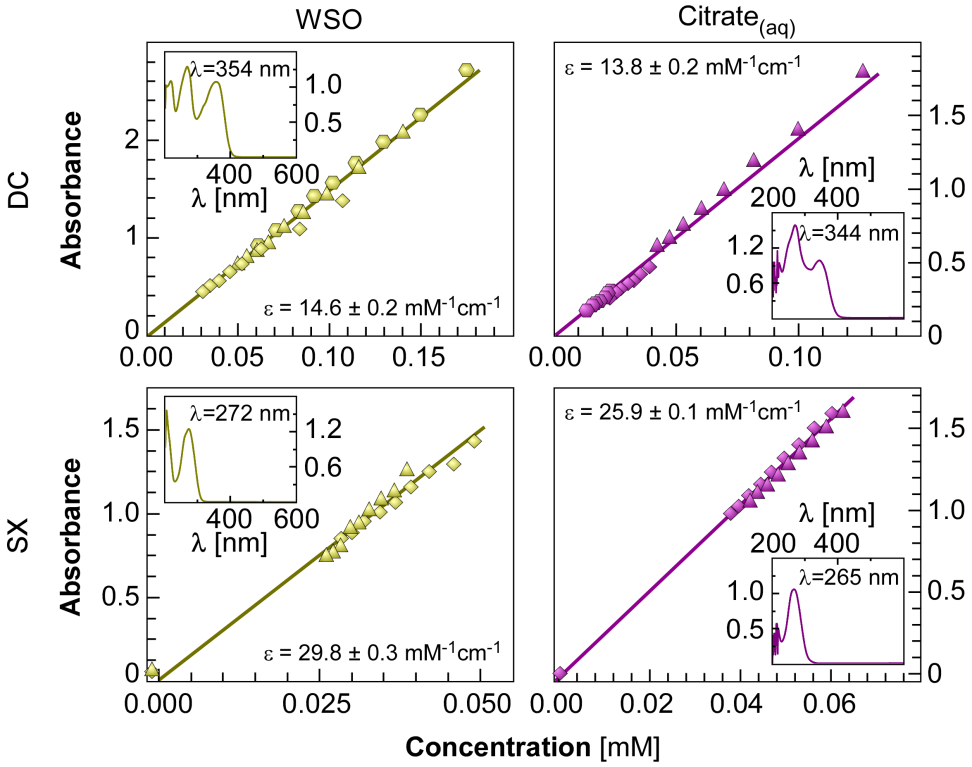

Figure 42: Determination of the extinction coefficients of the antibiotics DC and SX in WSO (left column, yellow symbols) and aqueous citric buffer at pH 4.8 (right column, purple symbols).

Table 5: Extinction coefficients of antimalarials in CBSO and citric buffer at pH 4.80

Drug	ε [$mM^{-1}cm^{-1}$] at λ (nm)			
	CBSO or WSO		**$Citrate_{(aq)}$**	
Hematin [H]	3.1 ± 0.3	(594 nm)		
Amodiaquine [AQ]	13.2 ± 0.2	(346 nm)	17.0 ± 0.1	(340 nm)
Chloroquine [CQ]	7.5 ± 0.2	(331 nm)	18.78 ± 0.06	(341 nm)
Quinine [QN]	5.12 ± 0.02	(331 nm)	4.58 ± 0.02	(330 nm)
Mefloquine [MQ]	2.712 ± 0.007	(315 nm)	3.10 ± 0.02	(315 nm)
Pyronaridine [PY]	31.3 ± 0.8	(279 nm)	12.35 ± 0.04	(422 nm)
Doxycycline [DC]	14.6 ± 0.2	(354 nm)	13.8 ± 0.2	(344 nm)
Sulfadoxine [SX]	29.8 ± 0.3	(272 nm)	25.9 ± 0.1	(265 nm)

3.6.2 Solubility Determination

The concentration of antimalarials in CBSO and citric buffer was determined by UV-Visible spectrophotometry using the Beer-Lambert law (Equation 1) and the extinction coefficients from Table 5. To determine the solubility of antimalarial drugs in each solvent, solid drug powder was placed in contact with 5 mL of solvent at room temperature in a clean 6 mL vial. This procedure was repeated until the powder no longer dissolved, and the vial was then sealed with a plastic cap. A total of three vials were prepared for each drug-solvent combination for each temperature that was analyzed. The solutions were incubated at four temperatures: 5 (or 9), 25, 37, and 45°C. Every week, a small aliquot was removed from each vial and filtered (0.22 μm PES membrane) to determine the concentration using the same spectrophotometric procedure described above. The change in concentration was tracked as a function of time and the solubility was determined as the plateau across three time points. In the case of pyronaridine, its relatively high solubility in citric buffer enabled only one determination at 25°C due to a limited supply of reagent. Conversely, the low solubility of artemisinin required an alternative method involving the slow addition of solvent to a known mass of dry powder

over the course of one month, until the entire artemisinin powder dissolved. Given the long timeframe of the latter measurement, this procedure was only performed at a temperature of 25°C.

Drug solubility was determined spectrophotometrically by monitoring the evolution of soluble drug concentration over a 50-day period. A representative data set for chloroquine in CBSO (Figure 43A) shows that the soluble drug concentration reaches a plateau with prolonged time.

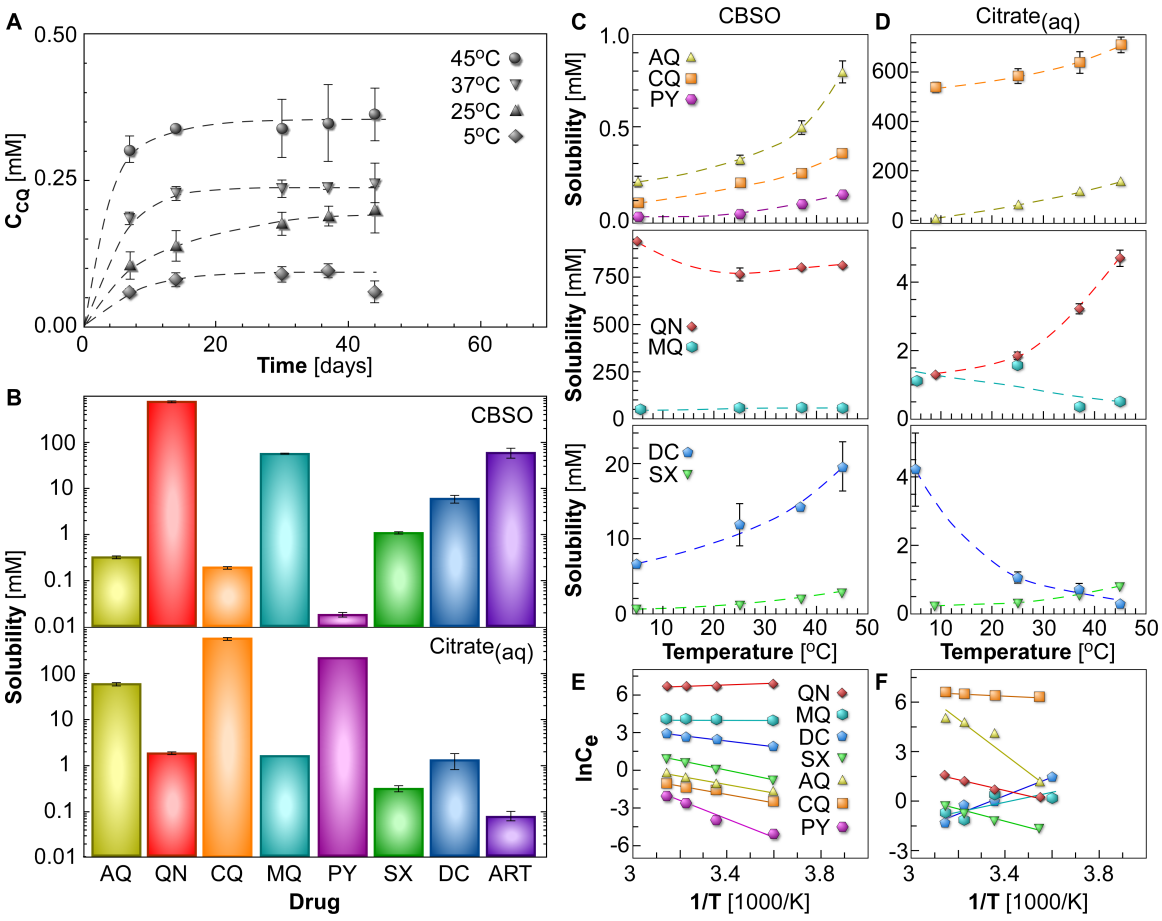

Figure 43: Drug solubility in CBSO and citric buffer.

The thermodynamic equilibrium and the average concentration value at the plateau was interpreted as solubility. The solubility for each drug at 25°C is listed in Figure 43B for CBSO (top plot) and citrate buffer (bottom plot). The majority of drugs

were found to have a solubility that exceeds 100 μM in both solvents, with the exception of pyronaridine in CBSO and artemisinin in citric buffer. When comparing the solubility of antimalarials, it was observed that quinine, mefloquine and artemisinin have higher solubility in CBSO (that exceed 10 mM). The antibiotics sulfadoxine and doxycycline exhibit comparable solubility in both solvents, with slightly higher values in CBSO. Note that even the drugs that exhibit lower solubility in CBSO than in citric buffer are soluble at concentrations sufficient to inhibit hematin crystallization.

The effect of temperature on drug solubility was quantified within the range 5 – 45°C, which encompasses the conditions selected for bulk crystallization assays *in vitro* (25°C) and the physiological environment of hemozoin formation *in vivo* (37°C). Notably, drug solubility within this temperature range does not fall below 1 μM, the approximate threshold concentration for effective inhibition of hematin crystal growth. The determinations in CBSO (Figure 43C) reveal that all tested drugs generally exhibit higher solubility at higher temperature. The solubility of amodiaquine exhibits a 1.5-fold increase. The solubility of mefloquine and quinine is nearly independent of temperature. For the other drugs, the solubility increases only marginally between 25 and 37°C. The effect of temperature on drug solubility in citric buffer (Figure 43D) reveals disparate effects. The solubility increases with temperature for the majority of drugs tested; however, the solubility of doxycycline, and to a lesser extent mefloquine, decreases with increased temperature. The solubility of pyronaridine at 25°C is 223.3 ± 0.6 mM, which lies between that of amodiaquine and chloroquine; however, limited pyronaridine availability prohibited an exhaustive analysis over the full temperature range.

Van ’t Hoff plots of the temperature dependence of solubility (Figure 43E and 4F)

yield the enthalpy ΔH and entropy ΔS of drug crystallization from the slope and intercept, respectively, of the linear relation between ln C_e and T^{-1}:

$$lnC_e = \frac{\Delta H}{RT} - \frac{\Delta S}{R}. \quad [9]$$

Equation 9 is based on the crystallization equilibrium constant $K_{eq} = C_e^{-1}$. The values of ΔH and ΔS for each drug extracted from data in Figure 43E and F are listed in the Table 6.

Table 6: Thermodynamics of crystallization of antimalarials and antibiotics

Drug	CBSO		Citrate$_{(aq)}$	
	ΔH [kJ mol^{-1}]	**ΔS [J mol^{-1}K^{-1}]**	**ΔH [kJ mol^{-1}]**	**ΔS [J mol^{-1}K^{-1}]**
Amodiaquine [AQ]	-24 ± 4	70 ± 10	-80 ± 20	290 ± 60
Chloroquine [CQ]	-25 ± 2	71 ± 7	-5.4 ± 0.8	71 ± 3
Quinine [QN]	3 ± 2	47 ± 6	-27 ± 4	100 ± 10
Mefloquine [MQ]	-2 ± 1	38 ± 4	21 ± 16	-70 ± 50
Pyronaridine [PY]	-56 ± 8	160 ± 30		
Doxycycline [DC]	-19 ± 2	83 ± 5	47 ± 6	-160 ± 20
Sulfadoxine [SX]	-30.9 ± 0.7	105 ± 2	-26 ± 3	80 ± 10

Collectively, the studies suggest that CBSO is a suitable biomimetic solvent for hematin crystallization. These pivotal pieces of information about the bulk properties of hematin and antimalarials in solution aid in the creation of a platform for screening and design of new compounds. However, a fast and easy method for calculating inhibition of crystallization is required.

Chapter 4: Design of a Biomimetic Assay

Assays play an integral role in the discovery of new pharmaceutical drugs for diseases.[55] With high-throughput assays, companies test libraries of drugs containing thousands of compounds to determine their applicability. Current methods for discovery of new antimalarials are parasite-based assays, which do not indicate the functionality of the compounds whether they act by corrupting the reproductive cycle of the parasite, inhibiting crystallization or some other means.

4.1 Previous Aqueous Assays

Multiple types of aqueous assays currently exist to determine the half maximal inhibitory concentration (IC_{50}) values, most of which are unseeded. The values between each of the assays coincide with each other. The most effective one was designed by Ncokazi et al.; it does not require centrifugation and reaches completion in less than two hours. However, seeded assays do not provide IC_{50} values that coincide with the unseeded assays, but these assays can provide knowledge for the design of a new biomimetic assay.

In an assay designed by Egan and coworkers, they formed β-hematin crystals through a reaction of hemin to hematin by adjusting the pH from 13 to 4.5 using 1 M hydrochloric acid and 12.9 acetate solution.[135] The reaction was allowed to proceed until various time intervals where the solution was analyzed with UV-visible spectroscopy by adding pyridine to form a complex between hematin and pyridine. Pyridine only complexes with non-crystalline hematin, thereby removing any residual amorphous material present.[136] Due to this complexation, the depletion of hematin in solution over time can be measured to determine a rate of crystallization, which is equal to the rate of

depletion. This procedure can be visualized in Figure 44. Others have utilized this assay and adapted it to a high-throughput configuration in 96-well plates.

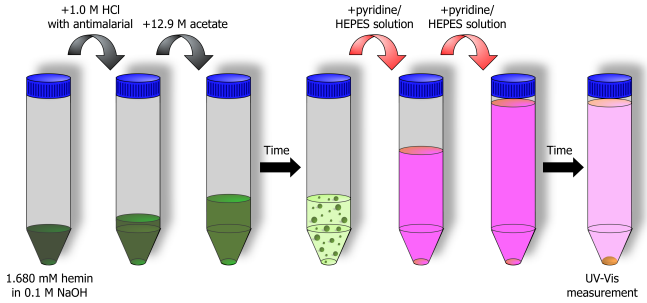

Figure 44: Schematic drawing of unseeded assay designed by Timothy Egan's group. The assay monitors the depletion of hematin in solution over time.

Another assay approach was created by Chong and coworkers, where a supersaturated hematin solution with seed crystals in 0.1 M ammonium acetate provided the crystallization environment for β-hematin crystals.[137] The analysis of growth was complicated with two separate spectrophotometry measurements: one after the addition of 3% SDS/0.225 M $NaHCO_3$ to dissolve any amorphous material and the second after the introduction of 10 M NaOH to dissolve the crystals. The rate of crystallization was calculated by determining the concentration of crystalline material from the differences in spectroscopic measurements over time. In this assay, the induction time for crystallization was decreased through the use of seed crystals lowering the thermodynamic energy barrier.

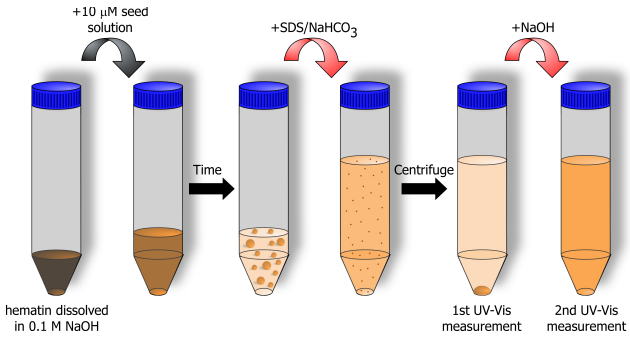

Figure 45: Illustration of seeded assay designed by David Sullivan's group.

4.2 New Biomimetic Crystallization Assay

A filtered solution of 0.60 mM hematin in CBSO was prepared using the method described below. Hematin seed crystals were added to this solution at a molar ratio of 1:4 seeds to hematin. Portions of the seeded growth solution (ca. 0.2 mL) were extracted by pipette while continuously stirring and transferred to polypropylene centrifuge tubes containing 0.2 mL of an antimalarial drug solution to yield a final hematin concentration of 0.3 mM. Each centrifuge tube was shaken to ensure proper mixing and incubated in the dark at 22.6 ± 0.2°C. To monitor the time evolution of the concentration of uncrystallized hematin, three tubes were removed and analyzed every hour over a five-hour period (for experimental statistics). First, pyridine (21.1 μL, 5% v/v) was added to re-solubilize the hematin precipitated as amorphous solid (pyridine does not induce crystal dissolution within the time scale of the determination). To separate the crystals, each tube was centrifuged at 4000 rpm and 20°C for 10 minutes. The concentration of hematin in the supernatant was determined spectrophotometrically by measuring the absorbance at λ = 525 nm. The entire procedure is illustrated in Figure 46. For each trial, the rate of crystallization r (mM h^{-1}) is determined from the slope of hematin concentration as a function of time. The percent inhibition of crystallization is calculated using the relation

$$Percent\ Inhibition = \left(1 - \frac{r_{inhibitor}}{r_{control}}\right) \times 100\% \,, \qquad [10]$$

where r_i is measured in the absence (i = control) and presence (i = inhibitor) of drug.

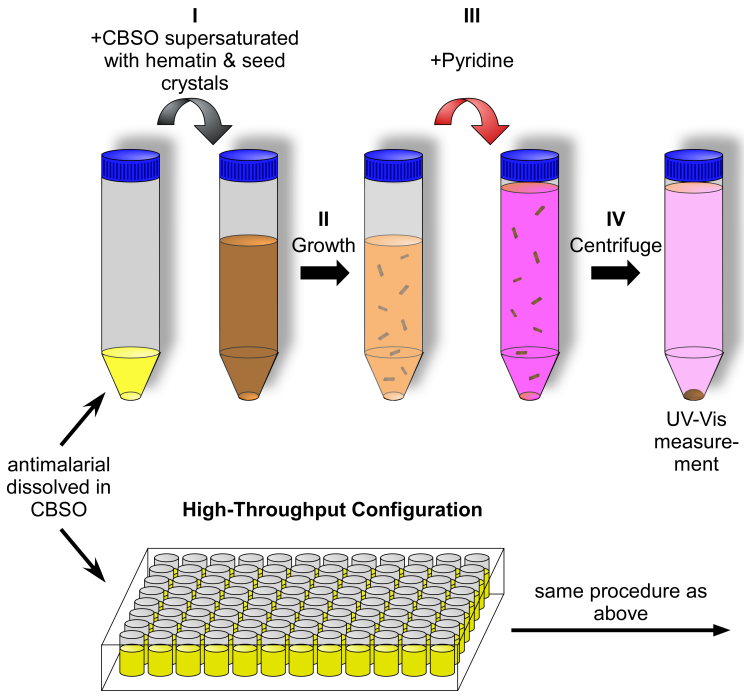

Figure 46: Schematic of the biomimetic assay to quantify the efficacy of potential antimalarial drugs as inhibitors of hematin crystallization. Benchmark studies in centrifuge tubes were adapted to a high-throughput configuration using multi-well plates.

The above procedure was adapted to a high-throughput configuration (Figure 46) with only minor modification. The volume of growth solution was reduced to accommodate measurements in microwell plates. The concentration of filtered hematin solution in CBSO was increased to 0.60 mM while maintaining the same ratio of seed crystals to hematin. For this study, a V-bottom Corning polypropylene 96 well plate was used. A small volume of hematin/seed solution (ca. 100 μL) was transferred by pipette into wells containing an equal volume of CBSO with the desired drug concentration. The plates were immediately shaken to ensure proper mixing and the procedure described above was used to determine the rate of crystallization and percent inhibition. To remove solids from each sample prior to UV-Vis spectroscopy measurements, the plate was centrifuged at 3,000 rpm and 20°C for 10 minutes, then 100 μL of the supernatant in each well were transferred to a flat bottom Corning polypropylene 96 well plate. The absorbance at λ =

525 nm was measured for all samples using a Tecan Infinite200 Pro microplate reader (an entire 96-well plate requires 1.5 minutes of scanning time).

4.3 Seed Crystal Preparation

All glassware was thoroughly cleaned with 0.1 M NaOH to remove residual hematin. The glass containers were then washed with soap and rinsed with DI water and acetone.

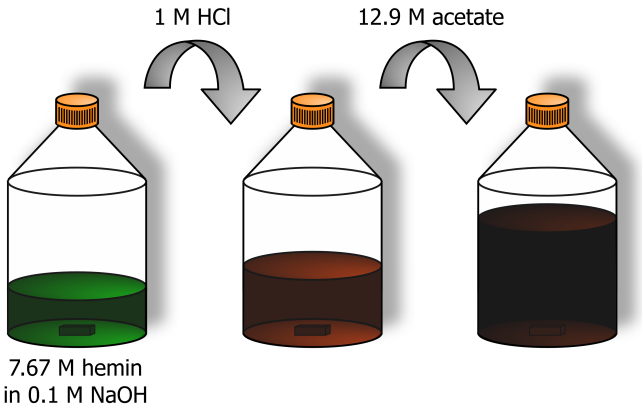

Figure 47: Process of manufacturing β-hematin seed crystals for biomimetic assay.

To prepare β-hematin seed crystals, a 7.7 mM hemin solution was first prepared by dissolving hemin in 0.1 M NaOH in a sealed glass container that was heated at 60°C in a water bath under continuous stirring at 150 rpm.[138] Within 10 min, the solution was neutralized using 1.0 M HCl; it was found that exposing hemin to NaOH for more than 20 minutes resulted in an amorphous product. A 12.9 M acetate buffer at pH 4.5 was prepared by mixing sodium acetate trihydrate and glacial acetic acid, which was then stored at 60°C for an hour and subsequently incubated at 70°C for 22 hours. This buffer was added to the hematin solution at 1:1 ratio. The mixture was placed in a freezer at -18°C for 15 minutes, and the formed residue was filtered through a 0.20 μm Nylon filter and rinsed sequentially with 100 mL DI water, 100 mL of a 0.225 M $NaHCO_3$ solution containing 0.105 M SDS, and 100 mL DI water. The filter cake was placed in a glass

Petri dish over a layer of Drierite and dried for 48 hours in an incubator at 37°C. It was then removed and crushed into a fine powder using a mortar and pestle. This powder was stored for a maximum of three weeks in a sealed vial in the dark. This procedure can be visualized in Figure 47.

4.4 Seed Crystal Characterization

Powder X-ray diffraction (XRD) patterns of seed crystals were collected on a Siemens D5000 X-ray diffractometer with CuKα radiation (40 kV, 40 mA, λ = 1.54 Å). Crystal size and morphology were analyzed by scanning electron microscopy (SEM) using a FEI XL-30FEG microscope. Seed samples for microscopy imaging were mounted on metal specimen stands using adhesive carbon tape (Ted Pella Inc.) and coated with ca. 25 nm carbon using an AJA UHV six-source sputtering device.

4.5 Preparation of Hematin and Antimalarial Solutions

Hematin solutions for crystal growth experiments were prepared by placing 20 mL CBSO and an amount of hematin powder sufficient for a 6 mM solution in a 20 mL glass vial. The unsealed vial was kept at 100°C in the absence of direct light. Solution samples were periodically extracted from the solution by pipette. Each aliquot was filtered through a 0.2 μm polyvinylidene fluoride (PVDF) membrane, and the hematin concentration was measured spectrophotometrically using a Beckman Coulter DU 800 Spectrophotometer with Tungsten and D2 lamps.

Solutions of antimalarials or antibiotics were prepared by placing solid drug powder in contact with 20 mL of CBSO in a clean glass vial sealed with a plastic cap. The solutions were incubated in the dark at 22.6 ± 0.2°C, and then were filtered with a 0.2 μm PVDF membrane. The exact drug concentration was determined

spectrophotometrically using extinction coefficients determined from data in Figures 40 – 42. When necessary, the concentration was adjusted by dilution with CBSO.

4.6 Screening Drug Efficacy as Hematin Crystallization Inhibitors

The most significant feature of the proposed assay is the use of CBSO as a solvent. To monitor the extent of hematin crystallization in CBSO, crystalline hematin was quantified as the difference between initial hematin in the solution and the amount present during crystallization, as in previous studies.[135,137] A problem encountered in this approach is the presence of amorphous hematin, which sequesters a fraction of hematin in a third phase and lowers the measurement of the concentration of uncrystallized hematin. To address this issue, Egan and coworkers[136] proposed the addition of pyridine prior to concentration determination. Pyridine forms a relatively strong complex with hematin and dissolves potential amorphous residue.[136] In the presence of excess pyridine, all non-crystalline hematin is complexed with pyridine. The amount of hematin-pyridine complex is used as a measure of uncrystallized hematin in solution when determining the rate of hematin crystal growth. The UV-Vis spectra in Figure 48A reveal a significant shift in the hematin absorbance peaks due to the addition of pyridine. These shifts indicate complexation between hematin and pyridine. The isosbestic point at 513 nm (constant absorbance at varying pyridine concentration) suggests the formation of a 1:1 hematin:pyridine complex. At pyridine concentration above 5.4% v/v, the spectra do not change in response to additional pyridine, indicating complete hematin complexation. Hence, pyridine concentration at 5 % v/v was chosen as optimal for the assay.

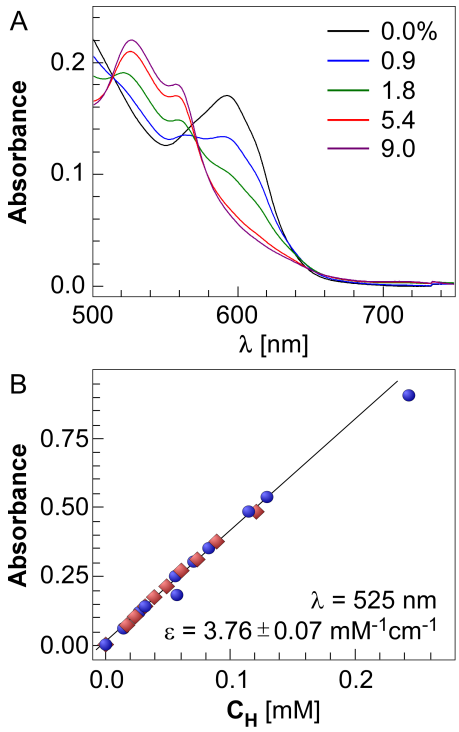

Figure 48: (A) UV-Vis absorbance spectra of hematin in CBSO at pyridine concentrations from 0 to 9% v/v. (B) Determination of the extinction coefficient ε of the hematin-pyridine complex at 5% v/v pyridine in CBSO solution at a wavelength λ = 525 nm.

To quantify the amount of hematin held in a pyridine complex in the presence of 5% v/v, the extinction coefficient of the hematin:pyridine complex was determined. The data on the absorbance at the top of the peak at 525 nm in Figure 48B yield ε = 3.76 ± 0.07 $mM^{-1}cm^{-1}$. In the high-throughput version of the assay implemented in 96 well plates, this value of ε was used to determine the optical path length in the wells. Solutions of eight distinct hematin concentrations containing 5% v/v pyridine were loaded into eight wells of the 96-well plate. The absorbance of each well was measured using a Tecan Infinite200 Pro microplate reader. The polypropylene plate bottom contributes a constant A_0 to the total absorbance leading to a non-zero intercept in the Beer-Lambert law,

$$A = A_0 + \varepsilon bc. \qquad [11]$$

A linear fit of this relation to the data in Figure 49 yields the optical path b = 0.193 cm

and $A_0 = 0.130 \pm 0.004$.

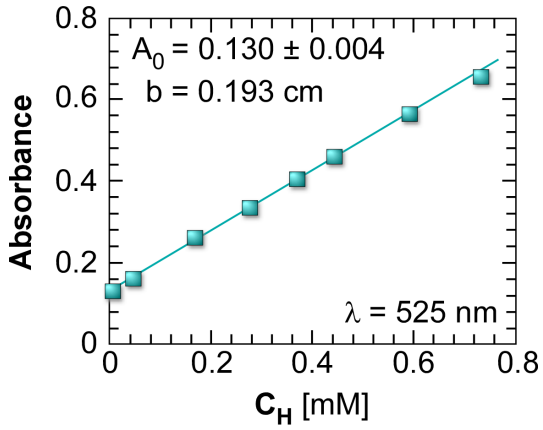

Figure 49: Characterization of the optical absorbance at wavelength λ = 525 nm of hematin in the presence 5% v/v pyridine in CBSO held in a polypropylene 96-well plate.

Seed crystals (Figure 50A) were employed to bypass nucleation and reduce the time of crystallization for more efficient screening of inhibitors, similar to Chong and coworkers.[137] Since β-hematin crystal surfaces oxidize in contact with air, seeds should not be stored for long periods of time. Each batch of seeds was analyzed by powder X-ray diffraction (XRD) to test their crystallinity. It was found that published protocols for seed synthesis can yield either crystalline or amorphous product (Figure 50B). The lack of crystallinity may lead to irreproducible crystallization kinetics. For example, a hematin crystallization assay was performed using three different approaches: (i) absence of seeds, (ii) use of amorphous seeds, and (iii) use of crystalline seeds. The data in Figure 50C demonstrate that there is a marked difference in the induction period and crystallization rates between the three approaches. In the absence of seeds, there is a short induction period (ca. 1 day) followed by a rate of growth much slower compared to the crystalline seeded growth assays. The addition of either amorphous or crystalline seeds eliminates the induction period and leads to more rapid depletion of solute. The use of amorphous seeds can falsely give the appearance of crystallization where the apparent

rate of growth (i.e., slope of curves in Figure 50C) lies between the values of non-seeded and crystalline seed assays. In these studies, it could not be determined whether the reduction in free hematin concentration was associated with heterogeneous nucleation and growth of new crystals or condensation of amorphous solid (i.e., the mass of products was insufficient for XRD analysis). This observation underscores the importance of verifying the crystallinity of seed batches.

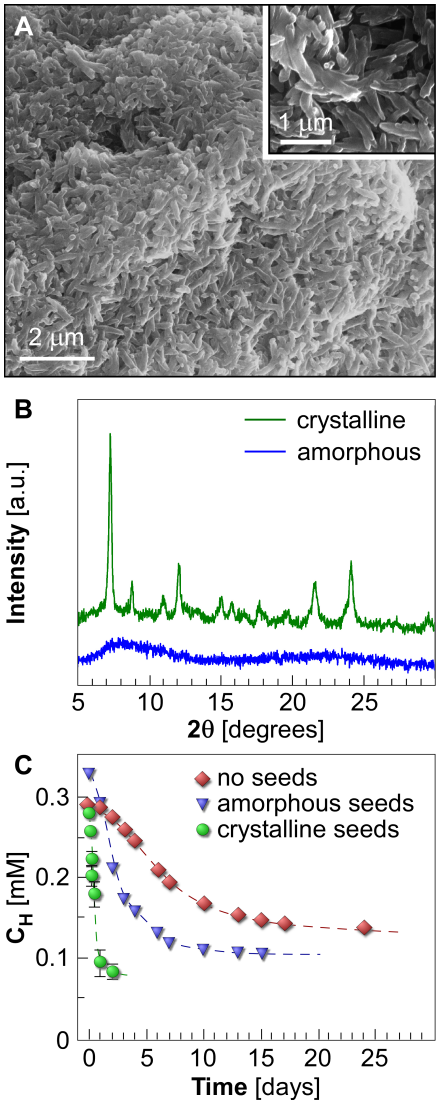

Figure 50: (A) Scanning electron micrograph of hematin crystal seeds. (B) Powder XRD patterns of amorphous hematin and crystalline β-hematin. (C) Evolution of the concentration of soluble hematin in the absence of seeds and in the presence of amorphous and crystalline seeds.

An important aspect of the proposed procedure is that hematin crystallization in the presence or absence of inhibitors can be assessed in a relatively short period of time (≤ 5 hours), which is practical for drug screening assays. Within the first five hours of crystallization the growth rate is approximately linear. Variations from one seed batch to another lead to disparities in the measured rate of crystallization. To account for this experimental uncertainty, the effect of antimalarials on hematin crystallization is reported using the percent inhibition, defined in Equation 10 as the ratio of growth rate in the presence of inhibitor relative to that of the control in the absence of drug. Using this relative change in growth rate minimizes variability between different seed batches. An example of hematin growth in the presence of the antibiotic doxycycline is provided in Figure 51. Figure 52 shows the change in spectra correlating to the data in Figure 51. The rate of crystal growth, measured as the slope of the linear correlation (solid lines), decreases monotonically with increasing drug concentration. From these plots, drug potency and its efficacy are extracted for inhibiting the growth of hematin crystals.

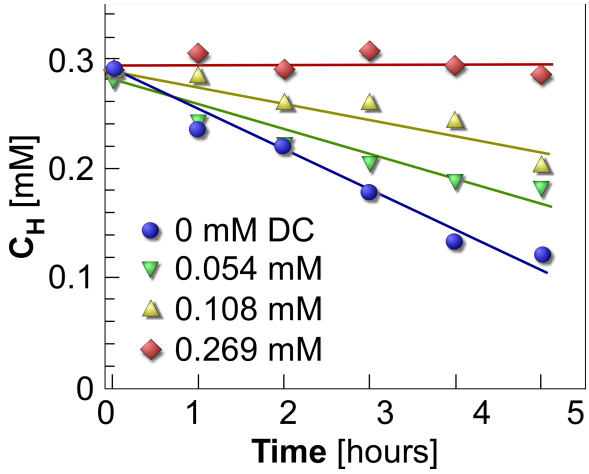

Figure 51: The evolution of free hematin concentration C_H over five hours in the presence of varying concentration of doxycycline (DC).

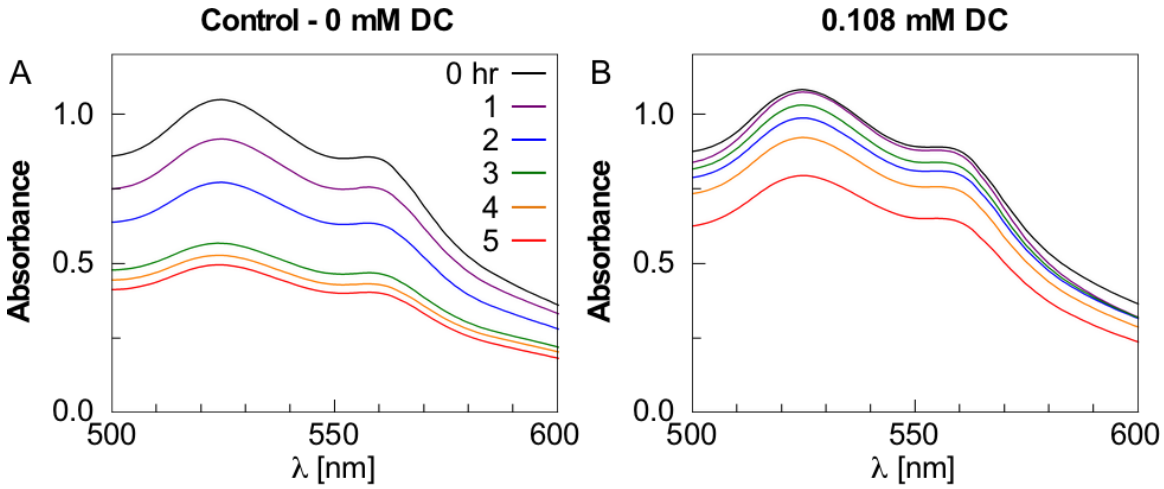

Figure 52: UV-Vis spectra from a bulk crystallization assay indicating a decrease in the concentration of free hematin for measurements in (A) the absence of inhibitor (control) and (B) in the presence of 0.108 mM doxycycline (DC). These spectra correlate to the data presented in Figure 51.

In Figure 53A, the percent inhibition of hematin crystallization is reported as a function of inhibitor concentration for four quinoline-class antimalarials: amodiaquine, quinine, chloroquine, and mefloquine. As shown in Figure 39, each drug is comprised of different functional moieties, but they share a common quinoline base. With the exception of mefloquine, all of the tested antimalarials are capable of inhibiting growth by more than 80%. The findings reveal that 0.1 mM concentration of amodiaquine is sufficient to nearly suppress hematin crystallization. Few studies in literature report growth inhibitors capable of reaching such high efficacy in bulk crystallization assays without leading to the promotion of polymorphs or the precipitation of amorphous product. Reported values of percent inhibition for a wide range of crystalline materials tend to be around 60%,[139] which is the approximate value observed for hematin growth in the presence of mefloquine. The other two antimalarials tested here (chloroquine and quinine) inhibit growth in the range 60 – 90%, which is similar to highly effective inhibitors reported in prior studies of inorganic crystals.[140-143] The general trends in Figure 53A are consistent with a Langmuir-like behavior wherein the coverage of

inhibitor on hematin crystal surfaces reaches a maximum (corresponding to the plateau in percent inhibition) beyond which any further addition of inhibitor has no appreciable effect on crystal growth.

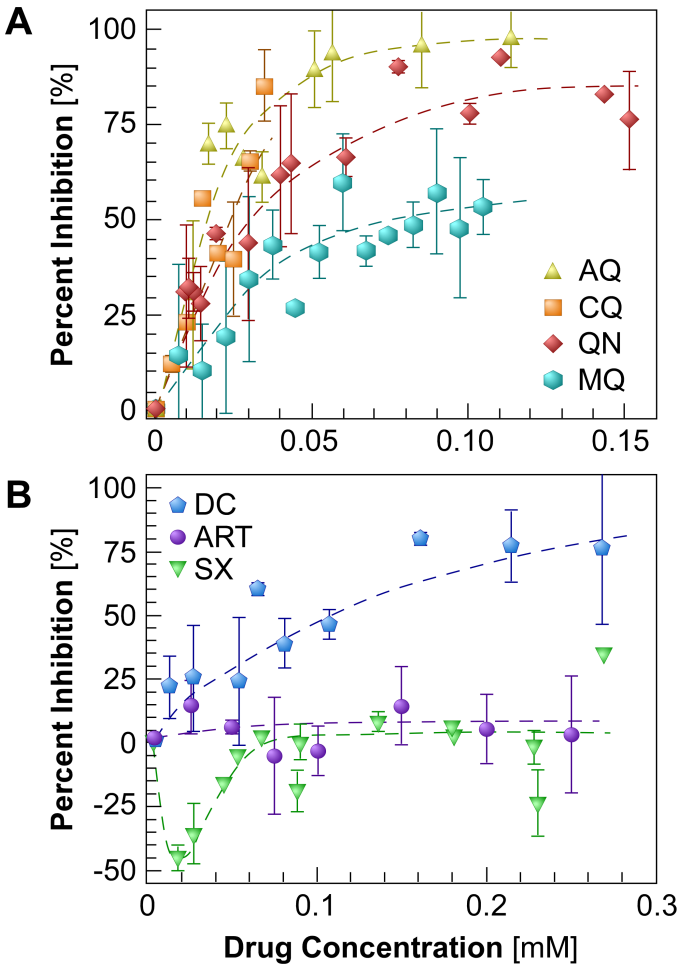

Figure 53: Percent inhibition of hematin crystallization. (A) The effect of four antimalarials: amodiaquine (AQ), chloroquine (CQ), quinine (QN), and mefloquine (MQ). (B) The effect of artemisinin (ART) and two antibiotics: sulfadoxine (SX) and doxycycline (DC).

The effect of one additional antimalarial, artemisinin, along with two antibiotics, doxycycline and sulfadoxine, was determined. The solubility of pyronaridine in CBSO (Figure 43) was not sufficient to generate a full inhibition curve. As shown in Figure 53B, quantification of hematin crystallization in the presence of artemisinin reveals no apparent change in growth rate with drug concentration, which is not surprising

considering prior studies suggest that an activated form of artemisinin (with the endoperoxide bridge cleaved) is the effective suppressor of malaria parasites.[100,144] Conversely, doxycycline was found to be a weak inhibitor of hematin crystallization that is capable of achieving comparable percent inhibition as the antimalarials in Figure 53A, but at much higher drug concentration. Unexpectedly, measurements of sulfadoxine revealed promotion of hematin crystal growth (observed as negative percent inhibition) at low drug concentration (< 0.06 mM), and no appreciable influence on crystal growth at higher concentrations. Presently, there are three proposed mechanisms for modifier promotion of crystal growth: (i) solute-promoter interactions increase the local supersaturation at crystal interfaces due to an enhanced attraction of solute molecules to the surface,[145] (ii) reduction of the energy barrier(s) for solute attachment by disruption of the solvation layers at the crystal surface as a result of promoter-crystal interactions,[146-148] and (iii) adsorbed promoters decrease the energy of advancing layers at step edges on the crystal surface.[149] Drawing upon examples from literature for other types of crystalline systems, it is reported for calcite ($CaCO_3$) crystallization that certain molecules act as a growth promoter at low concentration and switch to a growth inhibitor at higher concentration.[146,150] Prior studies seem to indicate that the promotion-to-inhibition transition occurs when the adsorbate coverage on crystal surfaces is sufficient to induce step pinning. In other examples, such as calcium oxalate monohydrate crystallization, molecules have been observed to act strictly as a promoters, irrespective of their concentration.[140] In this study of hematin crystallization, the exact mode of action governing sulfadoxine promotion of growth is not well understood.

Table 7: Comparison of antimalarial and antibiotic IC_{50} values.

		IC_{50} values	
Compound	**Assay**	**CQ-susceptible parasites (strain)[a]**	**CQ-sensitive parasites (strain)[a]**
Amodiaquine [AQ]	16 μM	7.8 nM (3D7)[151] 8.5 nM (HB3)[151] 3.0 nM (NF54)[152] 10.1 nM (NF54)[153]	9.3 nM (wild)[154]
Chloroquine [CQ]	25 μM	14.0 nM (3D7)[151] 18.5 nM (HB3)[151] 13.0 nM (NF54)[155] 10.0 nM (NF54)[152] 12.9 nM (NF54)[153] 25 nM (3D7)[156] 41 nM (HB3)[156]	29.0 nM (KH-266)[157] 76 nM (wild)[154]
Quinine [QN]	32 μM	34.2 nM (3D7)[151] 36.8 nM (HB3)[151] 22.0 nM (NF54)[158] 132.0 nM (NF54)[153] 134 nM (3D7)[156] 109 nM (HB3)[156]	178 nM (L3)[159] 90.1 nM (KH-266)[157] 150 nM (wild)[154]
Mefloquine [MQ]	71 μM	43.9 nM (NF54)[153] 51 nM (3D7)[156] 36 nM (HB3)[156]	11.4 nM (L3)[159] 67.7 nM (KH-266)[157]
Pyronaridine [PY][160]	--------	1.9 nM (NF54)[153] 24 nM (3D7)[156] 16 nM (HB3)[156]	
Doxycycline [DC]	110 μM	10.8 μM (3D7)[156] 12.1 μM (HB3)[156]	11.3 μM (wild)[154]
Sulfadoxine [SX]	No inhibition	---------	23.7 μM (wild)[161]

[a] NF54 = African origin *Plasmodium falciparum* strain; 3D7 = parasite line cloned from NF54; HB3 = *Plasmodium falciparum* strain from Honduras; L3 = strain of *Plasmodium falciparum* from Ivory Coast; wild = strain from Gabon; KH-266 = Southeast Asia origin *Plasmodium falciparum* strain

When comparing the relative effect of antimalarial drugs at 50% inhibition of hematin growth, the following order of inhibitor potency (from lowest to highest drug concentration) was observed: amodiaquine > chloroquine > quinine > mefloquine >> doxycycline >> sulfadoxine. Interestingly, this trend is almost identical to the IC_{50} values of each drug reported in literature for parasite models using a variety of *Plasmodium* strains (see Table 7). The IC_{50} value refers to the inhibitory concentration (IC) of drug

where the response (i.e., parasite population) is reduced by half. Prior studies reveal the following order of drug potency (from lowest to highest IC_{50}): amodiaquine > chloroquine > mefloquine > quinine >> doxycycline >> sulfadoxine. Comparison of our assay with parasite models shows excellent agreement, with the exception of one outlier: the relative potency of mefloquine and quinine in our assay does not match the parasite model. Caution should be taken when directly comparing the results of *in vitro* and *in vivo* studies. Nevertheless, the similarity in IC_{50} trends suggests that the bulk crystallization assay is an effective tool for identifying lead drug candidates and comparing relative efficacy.

4.7 High-throughput Assay

The commercial relevance of drug-screening assays relies on their ability to identify lead candidates in a rapid timeframe. As a proof of concept, the biomimetic assay developed above was adapted to high-throughput screening of numerous prospective drugs in parallel. Instead of centrifuge tubes, 96-well plates were employed. In this high-throughput configuration, the solution volume in individual runs was reduced from 400 μL (centrifuge tubes) to 200 μL (plate wells). The modified platform was tested using the conditions described above.

In the multi-well plates, hematin crystallizes at a much slower rate than in the centrifuge tubes. Slower rates of crystal growth impede the quantification of the percent inhibition of hematin crystallization as the differences between hematin growth in the absence and in the presence of inhibitor are commensurate with the error of UV-Vis measurements; and this similarity increases the likelihood of identifying false positives during inhibitor screening. To address this problem, the starting hematin concentration

C_H was adjusted to increase the supersaturation, which alters the rate of crystallization. As shown in Figure 54A, the growth rate increases monotonically as a function of C_H. The data in Figure 54 illustrate the good reproducibility of the assay in multi-well plates, i.e., growth rates obtained using two separate crystal seed batches, each in duplicate, agree. For all measurements reported herein, a hematin concentration of 0.60 mM was used that induces growth at a rate observed for the 0.3 mM concentration in the centrifuge tubes.

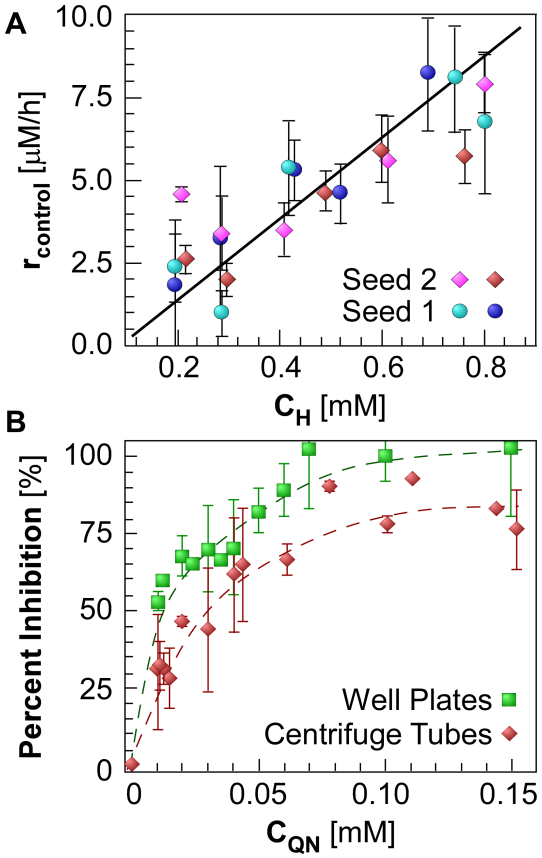

Figure 54: (A) Effect of starting hematin concentration C_H on the rate of growth using a 96-well-plate configuration. (B) Percent inhibition of hematin crystallization as a function of quinine concentration, C_{QN}, in biomimetic assays employing centrifuge tubes and a 96-well plate.

In Figure 54B, the percent inhibition of hematin measured in the multi-well plate and centrifuge tubes was compared, selecting quinine as a representative growth inhibitor. The general trend of the two curves is similar, which confirms that the high-

throughput configuration can be used to screen inhibitors of hematin crystallization. For reasons that are not entirely clear, the percent inhibition measured in the multi-well plate is slightly higher. Potential reasons for this observation may be attributed to the fact that multi-well plates have smaller volume (which may slow down buoyancy-driven convection), the plates are made of different polymeric material (which may potentially alter crystal and/or inhibitor adsorption on container walls), and the multi-well plate requires higher supersaturation. Despite these small differences, this proof-of-concept study indicates that the biomimetic assay proposed here has the potential to be applied as a screening platform for hematin crystallization in order to identify and characterize new generations of antimalarial drugs.

Chapter 5: Conclusions of Hematin Project

In summary, hematin solubility and crystallization was examined in media that mimic aqueous and lipid regions of the parasite DV. The formation of hemozoin *in vivo* is not well understood—notably the regions within the vacuole where hematin nucleates and crystallizes. These studies reveal that hematin solubility in an aqueous solution at pH 4.8 is nearly four orders of magnitude lower than that in an organic solvent (water-saturated octanol) that mimics the environment in the lipid nanospheres within the DV.

The effects of antimalarial and antibiotic drugs on bulk hematin crystallization were assessed in a biomimetic growth medium. Systematic analysis of drug-solvent thermodynamics confirmed that all drugs are sufficiently soluble in CBSO, resulting in concentrations that are high enough to inhibit hematin crystals. Although these studies do not conclusively identify the exact regions within the parasite digestive vacuole where hematin crystals are formed, the collective mesoscopic and microscopic investigations reported here strongly suggest that the organic lipid environment mediates hemozoin formation.

Bulk crystallization in CBSO employing hematin crystal seeds was shown as an effective method of quantifying inhibitor efficacy. Moreover, comparison of seeded growth assays for various drugs revealed their relative potency. Here, several advantages of the biomimetic bulk crystallization assay over current parasite models was reported. For instance, seeded growth in CBSO requires relatively short time (ca. $\leq$ 5 hours) to assess the efficacy of growth inhibitors. Crystallization-based assays also provide more information regarding the mechanism of drug action. Notably, crystalline product from drug screening assays can be analyzed by more rigorous techniques, such as electron or

scanning probe microscopy, to examine the effects of inhibitors on crystal size, habit, and surface topography from the macroscopic to near molecular length scale. Identifying effective crystal growth inhibitors can also help develop structure-performance relationships wherein the properties of the drug (i.e., molecule structure and functionality) could potentially serve as heuristic guidelines to design molecular analogues for additional testing, thereby reducing the number of compounds that need to be screened prior to identifying a lead candidate(s).

A high-throughput configuration was described that is potentially viable for conducting bulk crystallization in parallel, thus offering an efficient method of screening antimalarial drug compounds. One aspect of this approach that is lacking is the ability to discern the bioavailability of these compounds. To this end, *in vivo* tests are essential, and could be combined with bulk crystallization assays wherein the latter would serve as a pre-screening stage to collect useful information on drug-crystal interactions for the design of new compound libraries, and improve the overall efficiency of drug screening.

.

Chapter 6: Gallstones & Atherosclerosis

The presence of gallstones dates back centuries with multiple gallstones found in a mummified Egyptian priestess.[162] However, the disease was first described by a Florentine pathologist, Antonio Benivenius, in 1507 posthumously.[163] Not only were gallstones found in mummified Egyptians, atherosclerotic lesions were found in pharaoh mummies from more than 3500 years ago.[164] Hippocrates described the sudden cardiac death of humans during his lifetime as a physician. At approximately 300 B.C., Erasistratus documented the symptoms of peripheral arterial disease by the intermittent cramping in the leg, or claudication. From the 1550s to 1800s, several famous physicians, including Gabriele Falloppio and Caleb Hillier Parry, observed pathological findings in arteries in various regions of the body and suggested the presence of calcified atherosclerotic lesions. In 1835, Jean Lobstein coined the term arteriosclerosis.

Both of these diseases have been present for centuries afflicting hundreds of thousands of individuals.[165] During this time, knowledge has been accumulated regarding various treatment methods, likelihood of incidence, risk factors, and the pathology.

6.1 Gallstones

Gallstone disease, or cholelithiasis, is one of the most common and most expensive to treat of digestive disorders that require admission to hospital. In Europe and the United States, gallstones are found in 15-20% of the adult population, but 40-60% of these people are asymptomatic.[166] Each year in the United States, more than one million people are newly diagnosed with gallstones. The direct costs of diagnosis and treatment are more than $5 billion annually.

6.1.1 Types of Gallstones

In humans, three types of gallstones can occur: cholesterol stones, black pigment stones and brown pigment stones.[56] Approximately 75% of gallstones are cholesterol based with black pigment stones accounting for 20% and brown pigment stones are found in 5% or less.[167] A variety of human gallstones can be seen in Figure 55.[168]

Figure 55: Variety of human cholesterol gallbladder stones with different shapes, sizes and compositions of cholesterol.[168]

Cholesterol and black pigment stones develop only in the gallbladder in a bacterially sterile environment.[56] In contrast, brown pigment stones form due to a chronic anaerobic bacterial infection of bile, which usually occurs in the extrahepatic bile ducts and intrahepatic bile ducts. Rarely do brown pigment stones occur in the gallbladder and only after an inflammation of the gallbladder, or cholecystitis. The presence of brown pigment stones is principally in underdeveloped countries.

6.1.1.1 Black or Brown Pigment Stones

The pathogenesis of black pigment stones results from shifts in the lipid and lipopigment compositions of bile stored in the gallbladder. Black and brown pigment stones consist of calcium salts of bilirubin, shown in Figure 56.[169] Bilirubin is a yellow

breakdown product of normal heme catabolism. This is the compound responsible for the yellow color of bruises.

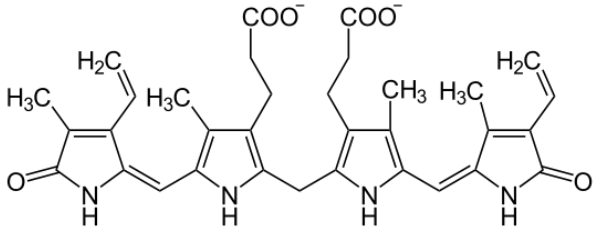

Figure 56: Molecular structure of bilirubin in black and brown pigment stones.

Bilirubin constructs polymers with large amounts of mucin glycoproteins in black pigment stones.[170] Black pigment stones are common in individuals who have underlying conditions causing their body to produce excess bilirubin, such as cirrhosis (liver does not function properly) or chronic hemolytic conditions (thalassemias or sickle cell anemia).

Meanwhile, brown pigment stones are composed of calcium salts of unconjugated bilirubin with varying amounts of protein and cholesterol. In the primary bile ducts, stones that originate there are usually associated with a bacterial infection resulting in brown pigment stones. The bacteria in the biliary system release β-glucuronidases.[56] These hydrolyze glucuronic acid from conjugated bilirubin resulting in unconjugated bilirubin. The unconjugated bilirubin precipitates in the form of calcium salts.

6.1.1.2 Cholesterol Stones

Cholesterol stones are composed of more than 80% cholesterol as seen in Figure 57. They often contain alternating layers of cholesterol crystals and mucin glycoproteins. Some calcium salts and bile pigments can also be included in the stone. The addition of the proteins improves the strength of cholesterol stones are pure cholesterol crystals are soft.[56]

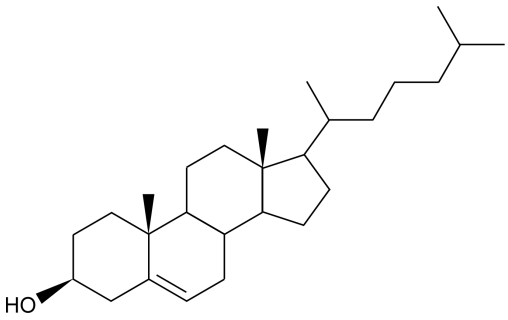

Figure 57: Chemical structure of cholesterol.

For cholesterol crystals to form, the cholesterol concentration in bile exceeds the solubility in solution.[171] It then precipitates out as crystals, producing stones. Cholesterol is only slightly soluble in aqueous media (~10^{-8} M).[76] However, bile also contains mixed micelles of bile salts and phospholipids, mostly phosphatidylcholine.[4,171,172] The concentrations of the bile salts and phospholipids control the degree of cholesterol saturation as illustrated in Figure 58.[168]

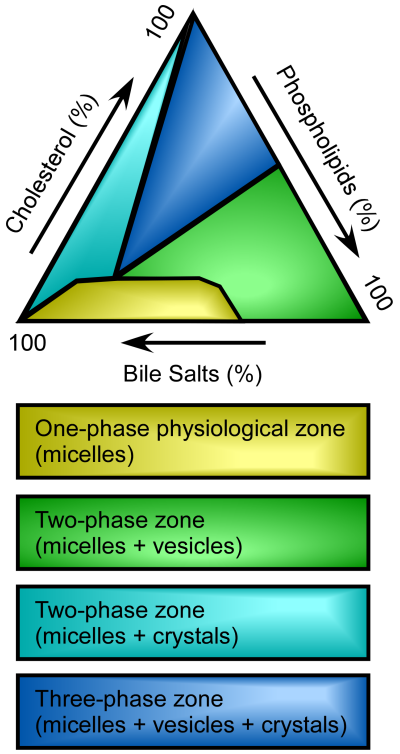

Figure 58: Ternary phase diagram of cholesterol, phospholipids and bile salts illustrating how cholesterol solubility is dependent upon the concentration of phospholipids and bile salts.[168]

Cholesterol is solubilized into vesicles in supersaturated bile by phospholipids.[173] From these vesicles, monohydrate crystals can precipitate becoming entrapped in gallbladder mucin gel with bilirubinate.[174] These will agglomerate into a gallstone as shown in Figure 59.[175] Cholesterol is most soluble when the lipid concentration contains more than 50% bile salts with smaller concentrations of phospholipids. Overall, the greater degree of cholesterol supersaturation, the higher the risk for gallstones which correlates to solubility as the driving force of crystallization. The solubility of cholesterol in human gallbladder bile ranges from 5-50 mM.[176]

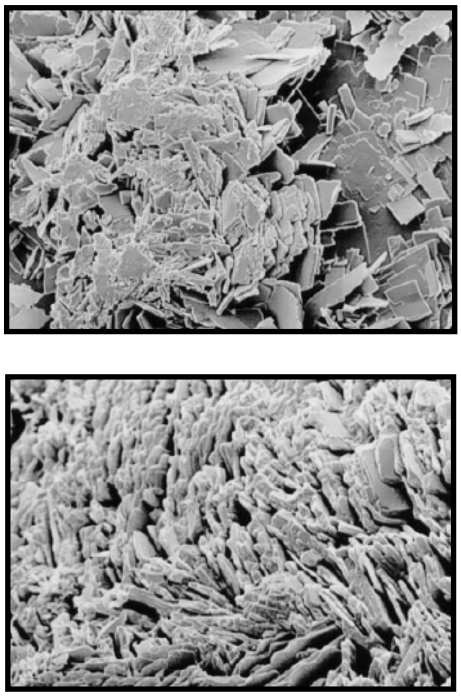

Figure 59: SEM images of cholesterol monohydrate crystals aggregated in gallstones.[175]

6.1.2 Signs & Symptoms

Approximately half of people with gallstones are asymptomatic. However, if the flow of bile is slowed or blocked, a number of problems can occur. When a gallstone causes blockage of the cystic duct, there are severe episodes of pain (biliary colic).[177]

During this, the gallbladder contracts vigorously against the blockage resulting in spasmodic severe pain. The pain occurs in the upper right portion of the abdomen, center of the abdomen just below your breastbone, back pain between the shoulder blades and/or pain in the right shoulder. These episodes usually last only an hour or two and occur infrequently. Other symptoms include jaundice (yellowing of the skin and the white part of the eyes), dark urine, light-colored bowel movements, fever and chills.

One effect of gallstones is an inflamed gallbladder, or cholecystitis. There are other causes of inflammation such as excessive alcohol use, infections or tumors, but the most common culprit is gallstones. The body reacts by swelling and pain of the gallbladder walls. This inflammation can last for several hours or up to a few days with possible fever.[178] At this time, the gallbladder is susceptible to infection by intestinal bacteria, which occurs about 20% of the time. Occasionally, the gallbladder will rupture, resulting in a surgical emergency.

If the gallbladder experiences gallstones or inflammation often, it can become rigid and scarred causing a dysfunctional gallbladder or chronic gallbladder disease. For this, the symptoms are more vague but constant. The person experiences abdominal fullness, indigestion, increased gas and chronic diaherra.

6.1.3 Diagnosis & Detection

To diagnose whether gallstones are present, doctors will most commonly recommend an abdominal ultrasound or computerized tomography (CT) scan.[179] With images from these instruments, the doctor can analyze them for the presence of gallstones. These tests are safe, non-invasive, widely available and are low cost

procedures. Blood tests can also reveal abnormalities associated with gallstones, such as infection, jaundice, pancreatitis or other complications.

Other methods will use special dyes to highlight the regions of the bile ducts and ascertain whether a gallstone is causing a blockage; tests include hepatobiliary iminodiacetic acid (HIDA) scan,[180] magnetic resonance imaging (MRI) or endoscopic retrograde cholangiopancreatography (ERCP).[181] During an ERCP, the gallstone can be removed if found.

In this procedure, an endoscope with a small camera mounted on the end is inserted down the esophagus. Air is pumped into the stomach and duodenum making it easier to see. The bile and pancreatic ducts are located where they empty into the duodenum. A catheter is inserted through the endoscope and into the ducts where a special dye is injected, making the ducts more visible for the x-ray imaging. The doctor can break up or remove stones present or a variety of other procedures depending on the affliction.

6.1.4 Treatment Methods

Prior to the late 1800s, treatment for gallstones was cholecystostomy. In this treatment, doctors would perform surgery where they would open the body and gallbladder to remove the stones and drain the fluid. At the time, they feared removing the gallbladder entirely from the body would kill the patient. However, this procedure only provided temporary relief as fistulas formed and continued pain ensued.[182]

German physician Carl Johann August Langenbuch became frustrated with his patients suffering after these gallbladder procedures and aimed to find a cure. In 1882, Langenbuch performed an open cholecystectomy, surgical removal of the gallbladder, on

a man who had ached with gallstones for 16 years.[183] Overnight, he cured the man's painful condition providing a solution which would not only not kill patients, but provide a painless future. Open cholecystectomies became the gold standard for gallstone treatment for almost a full century.

During this time, other methods of treatment were developed for those patients who could not undergo surgery. In 1937, a report of complete dissolution of gallstones by bile acids was published.[62] In the 1970s, bile acid chenodeoxycholic acid emerged as an oral drug for removing gallstones.[65] In the 1980s, another bile salt ursodeoxycholic acid was introduced as another prescribed drug to cause dissolution of gallstones.[66] Both bile acids are shown in Figure 60. In this method, chenodeoxycholic acid increases the solubility of cholesterol in bile, causing dissolution. For ursodeoxycholic acid, it reduces the synthesis of cholesterol in the liver and its secretion into the bile. For this method to be applicable for a patient, the gallstones must be composed of cholesterol (pigment stones would be unaffected) and the size of the stones must be less than 1.5 cm. Only 20% of all patients who undergo cholecystectomies meet these requirements.[184] In bile acid therapy, the efficacy is dependent upon the size and content of the stones as well as patient compliance. Bile acids must be taken daily for up to two years. This particular method has not become popular in the United States, due to its limited efficacy, inconvenience and improvement of other methods.

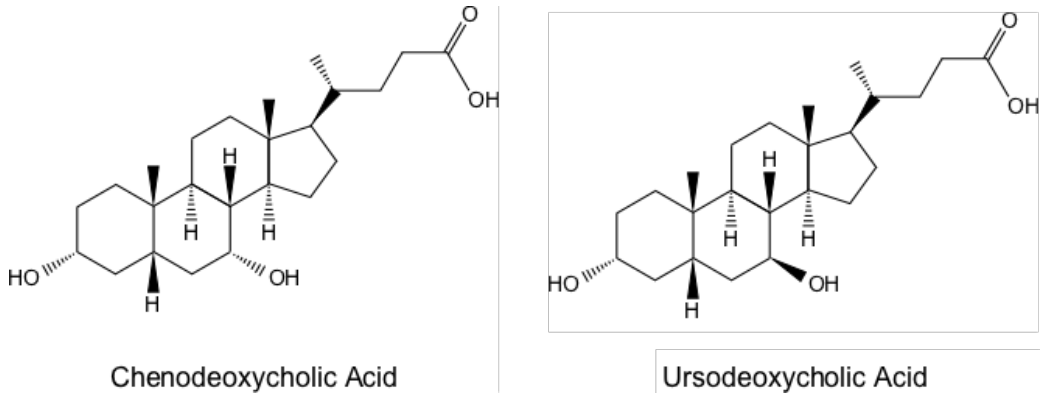

Figure 60: Structures of two bile acids used in oral dissolution therapy for gallstones.

There are other dissolution therapies in clinical investigations. One method in particular uses a percutaneous catheter placed through the liver introducing solvents into the gallbladder to dissolve cholesterol gallstones.[185] A nasobiliary catheter can be utilized as well.[186] Methyl *tert*-butyl ether is main solvent tested with repeated instillations and drainage to dissolve the stones in 24 hours. A side effect is mild acute inflammation in the gallbladder mucosa and it must be monitored to prevent seepage into the duodenum, where it causes severe mucosal irritation. An alternative less toxic solvent being tested is *n*-propyl acetate. However, this method has a similar problem with recurrence of stones after treatment.[187]

In 1986 in Munich, the first use of extracorporeal shockwave lithotripsy plus oral bile acids was performed.[63] In this therapy, acoustic shockwaves, generated by spark-gap, electromagnetic or piezoelectric technology, are sent through the body to break stones into small pieces. The additional bile acid dissolution therapy should help dissolve or pass the stones into the small intestine. The main downside to both the bile acids therapy or shockwave lithotripsy is the recurrence of stones in 30-50% of the cases five years afterward.[188,189]

The major revolution for gallstone treatment came in 1985 and 1987 when laproscopic cholecystectomies were performed by Erich Mühe and Philippe Mouret, respectively.[190] In this procedure, a small incision is made where a laparoscope, thin lighted tube with a camera, is inserted and several other small incisions are made where surgical instruments are inserted. After the two and a half hour procedure, patients were ready to leave the hospital later that day.[191] With the laparoscopic cholecystectomy, the rectus abdominus muscle is not cut during an incision like in an open cholecystectomy decreasing the recovery time by a month. In Figure 61, the algorithm for treatment based on the patient results in most individuals receiving a laparoscopic cholecystectomy.[168] Every year, about 700,000 individuals have cholecystectomies.

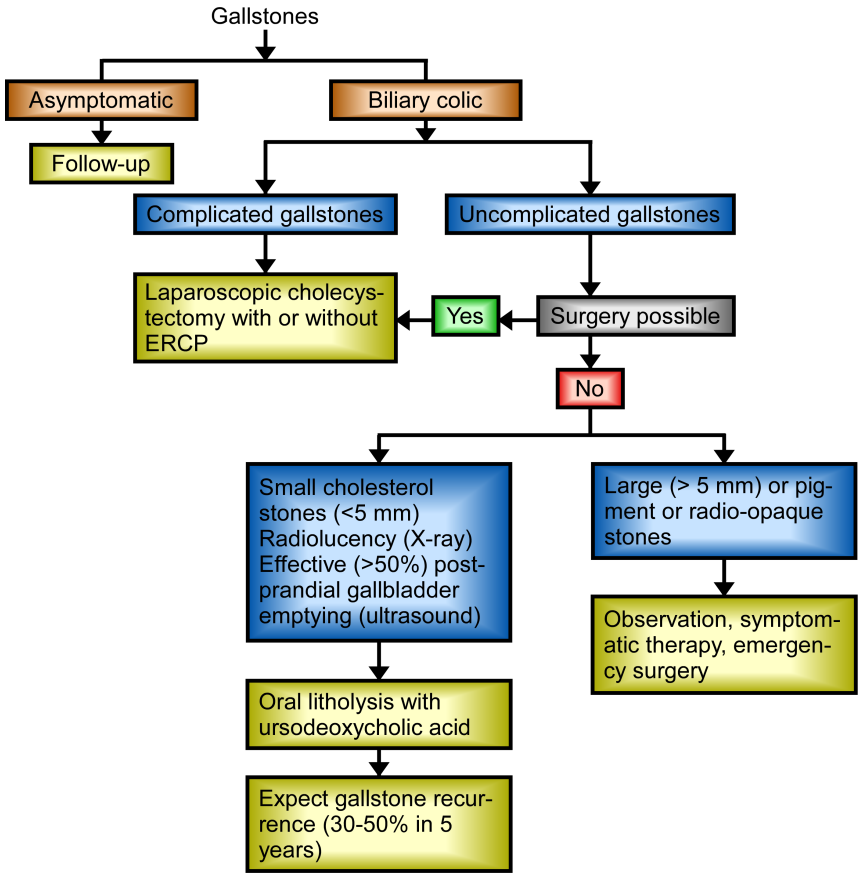

Figure 61: Algorithm for treatment of gallstones based on symptoms and conditions of patient.[168]

6.1.5 Risk of Gallstones

Certain features can increase a person's risk factor: age, female gender, oral contraceptive use, rapid weight loss, pregnancy (having given birth), obesity, type 2 diabetes, dyslipidaemia (hypertriglyceridacemia and low HDL serum cholesterol), hyperinsulinaemia, and sedentary life-style.[192-197] Specific ethnic groups are also more prone to gallstones including specific Indian tribes from around the world. In the United States, gallstones have a low presence in African Americans and higher prevalence in Mexican Americans.

6.2 Atherosclerosis

In the United States, cardiovascular, lung and blood diseases attribute for a large morbidity, mortality and economic burden on individuals and families. In 2010, these diseases accounted for over 1 million deaths, approximately 41 percent of all deaths in the United States.[198] The economic costs of illness, injuries and death from these diseases in 2009 were $424 billion, accounting for 23 percent of medical costs. Of all diseases, cardiovascular is the leading cause of death, representing 32 percent of all deaths. Atherosclerosis is one of the most common forms. Most of our knowledge of this disease comes for the last century.

6.2.1 Formation of Plaque

In atherosclerosis, or arteriosclerotic vascular disease, an artery wall thickens as a result of build-up of fatty materials or plaque. To begin, atherosclerosis develops from low-density lipoproteins (LDL), as shown is Figure 62.[199] LDL is a globular shaped molecule with a hollow core used to transport cholesterol throughout the body. The cholesterol is used to generate brain tissues, vitamin D, etc. Cholesterol can only move in

the bloodstream by transportation by LDL due to its low solubility in water, which constitutes 70% of blood.

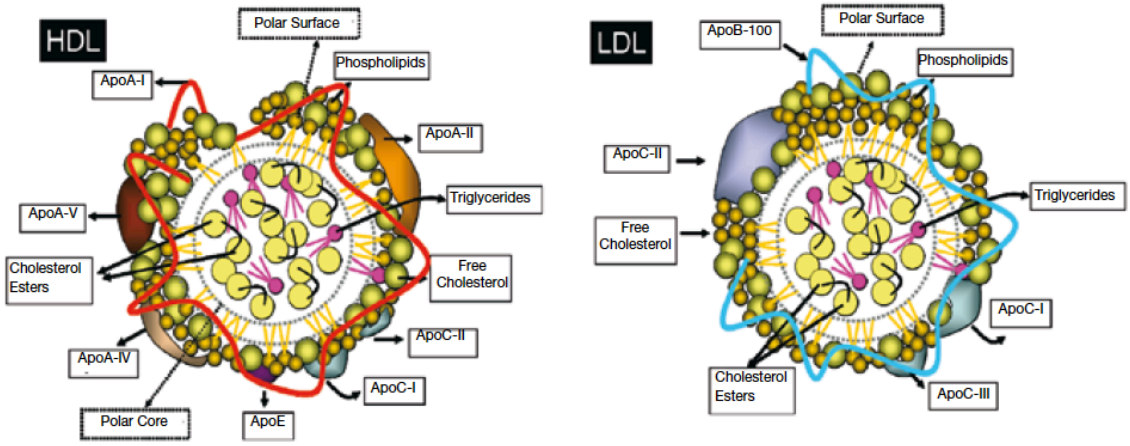

Figure 62: Schematic of high-density lipoprotein (HDL) and low-density lipoprotein (LDL). Apo refers to apolipoprotein.[199]

LDL molecules become oxidized by free radicals, mostly oxygen free radicals. When oxidized LDL contacts an artery wall, it damages the endothelial cells triggering a series of reactions to repair the damage. The immune system sends white blood cells, specifically macrophages and T-lymphocytes, to absorb the oxidized LDL, forming specialized foam cells.[200] High-density lipoproteins (HDL), seen in Figure 62, are recruited by the foam cells to remove the fats (cholesterol).[199] However, if the white blood cells are unable to process oxidized LDL or HDL levels are insufficient, rupture ensues. This rupture deposits cholesterol into the artery wall, triggering more white blood cells. Thus, the cycle repeats.[201]

Eventually, inflammation of the artery occurs. The muscle cells enlarge and create a hard cover over the affected area due to the cholesterol plaque. The hard cover produced reduces blood flow and increases blood pressure as this narrows the artery in question.[202]

In the atheromatous plaque formed in the arteries, there are three components. The first component is the soft, flaky, yellowish material at the center of large plaques, composed of macrophages called the atheroma. Underlying areas of cholesterol crystals comprise the second component. The last section is the calcification at the outer base of more developed lesions.

The progression of atherosclerosis is slow and cumulative over decades and complications arise suddenly. Commonly, a soft plaque will suddenly rupture creating a thrombus, a blood clot in a vessel which remains there.[203,204] The blood flow will rapidly slow or completely cease due to the thrombus, resulting in the death of the tissues fed by the artery in question in five minutes. This is known as an infarction. Infarctions specific to coronary arteries are referred to as heart attacks, and strokes are infarctions in arteries in the brain.

6.2.2 Symptoms

The atherosclerosis process usually begins in adolescence and is found in most arteries. However, it is mostly asymptomatic and left undetected by most diagnostic methods during life.[205] The first sign of atherosclerosis for about 65% of men and 47% of women is heart attack or sudden cardiac death. Depending on the location of the blockage, other symptoms could persist.[206] Other symptoms could be stroke, chest pain, leg pain, leg cramps, erectile dysfunction, shortness of breath, arrhythmias (irregular heartbeats), sudden numbness, weakness and dizziness. Overall, most signs and symptoms will not appear until the arteries are severely narrowed or blocked.

6.2.3 Diagnosis

The most commonly performed non-invasive testing method for blood flow limitations is cardiac stress testing.[207] In this method, the heart's ability to respond to an external stress, induced by exercise or drug stimulation, is measured. Usually a treadmill, stationary bicycle or hand crank will be used to testing.

Angiography is another common method where the lumen of blood vessels is visually examined by injecting a radio-opaque contrast agent into the blood vessel.[208] The vessels are imaged using X-ray based techniques. This is particularly useful for blood vessels near the heart and brain. Examples of arteries before and after treatment can be seen in Figure 63.[209]

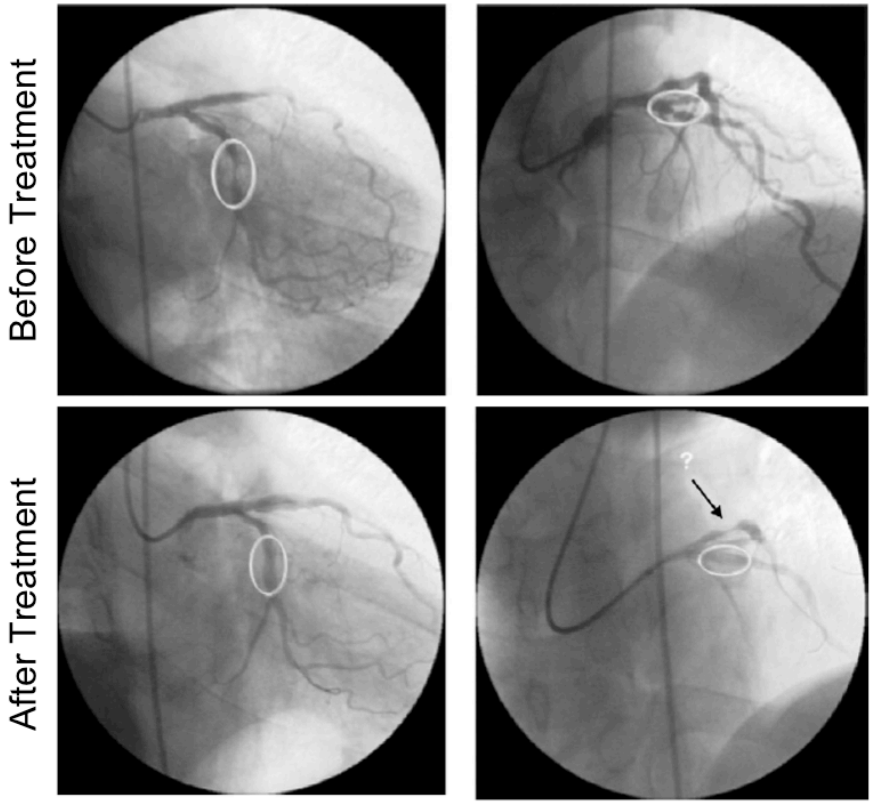

Figure 63: Angiographs of arteries before treatment (above images) and after treatment (lower images) illustrating narrowing of arteries and blood flow.[209]

Nuclear stress tests are implemented to visualize the blood flow after injection of a radiotracer. This test will identify regional areas of reduced blood flow. If a patient has ECG abnormalities or severe motor disability, this test can cause stress and cardiac damage.

For most artery flow disruptions, the lumen (inside space of tubular structure, such as artery) is narrowed by less than 50% at these locations. In cardiac stress testing, the detection limit is for 75% or greater lumen narrowing. Nuclear stress methods may be able to detect as little as 50%.

6.2.4 Risk Factors

While the exact cause of atherosclerosis is unknown, there are certain traits, conditions or habits that can increase an individual's likelihood of acquiring it.[210] A number of these can be controlled or monitored to prevent or delay atherosclerosis while others are entirely unavoidable.

The formation of plaques is dependent upon LDL and HDL. The levels of both LDL and HDL in the bloodstream can be indicators of the chance of atherosclerosis. High LDL and low HDL levels increase the risk of plaque development as these are integral in the formation cycle. Other factors which increase a person's risk of atherosclerosis are high blood pressure, smoking, insulin resistance, diabetes, obesity or overweight, lack of activity, age and family history of early heart disease.[211] With high blood pressure, more force is exerted on the arteries in your body leading to more serious problems. If a person smokes, the blood vessels in the body can be damaged or tightened. It also raises cholesterol levels and blood pressure. As the body ages, the signs and

symptoms of atherosclerosis begin to appear. For men, risk increases after age 45 while for women, it is after age 55.

6.2.5 Treatments

When attempting to provide treatment for atherosclerosis, doctors endeavor to lower risk factors or if the condition is more severe, they will elect for a surgical option. There are a variety of risk factors that can be controlled with pharmaceuticals; others can be simply a lifestyle change such as not smoking or performing regular exercise.

6.2.5.1 Statins

One common method is the prescription of a type of drug called a statin. Statins function by competitively inhibiting HMG-CoA reductase (3-hydroxy-3-methyl-glutaryl-coenzyme A reductase).[72] In the mevalonate pathway producing cholesterol, HMG-CoA reductase is the rate-controlling enzyme.[212] Statins are similar in structure to HMG-CoA on a molecular level enabling them to bind to the enzyme's active site competing with HMG-CoA. Effectively, the rate at which mevalonate is produced in decreased creating a cascade effect through the pathway lowering the amount of cholesterol manufactured as seen in Figure 64.[212]

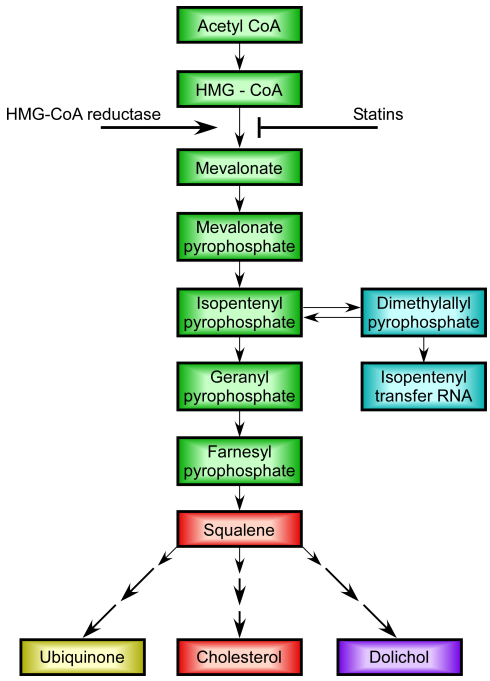

Figure 64: Mevalonate pathway where cholesterol is produced. Statins interfere with this process by interacting with HMG-CoA reductase binding preventing further assembly of cholesterol.[212]

Statins have only been marketed in the last thirty years as initial research to discover a cholesterol-lowering drug began in 1971 by Akiro Endo working for Sankyo. His team extracted mevastatin from the fungus *Penicillium citrinum*. The drug was never marketed as it caused serious side effects of tumors, muscle deterioration and even death. In 1978, Merck isolated lovastatin from the fungus *Aspergillus terreus*, but it was not marketed for 9 years until 1987 as Mevacor. Nowadays, there are numerous statins available on the market as shown in Table 8, with varying degrees of potency.

Table 8: Statin Drugs Available as Pharmaceuticals

Statin	Structure	Brand Name	Derivation	Year Approved
Atorvastatin	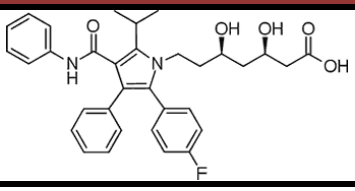	Lipitor, Ator	Synthetic	1996

Table 8 continued

Statin	Structure	Brand Name	Derivation	Year Approved
Cerivastatin	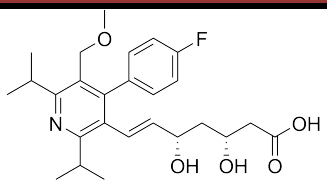	Lipobay, Baycol (removed from market in 2001 due to severe side effects)	Synthetic	1997
Fluvastatin	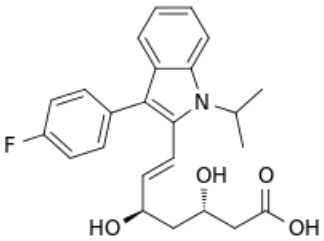	Lescol	Synthetic	1994
Lovastatin	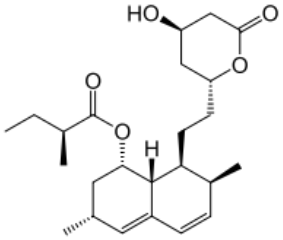	Mevacor, Altocor, Altoprev	Natural	1987
Mevastatin	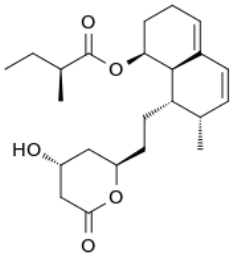	Compactin	Natural	Never marketed
Pitavastatin	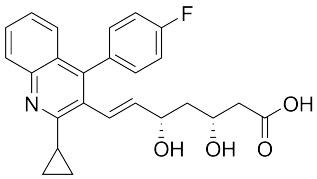	Livalo, Pitava	Synthetic	2003-Japan, 2009 - US
Pravastatin	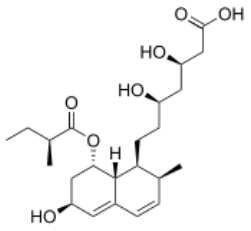	Pravachol, Selektine, Lipostat	Natural	1991

Table 8 continued

Statin	Structure	Brand Name	Derivation	Year Approved
Rosuvastatin	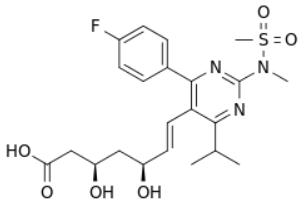	Crestor	Synthetic	2003
Simvastatin	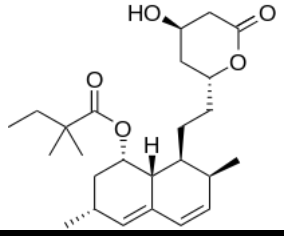	Zocor, Lipex	Synthetically produced, but is found in natural process	1989

6.2.5.2 Prescribed Pharmaceuticals to Lower Risk Factors

To prevent blood clots, doctors may prescribe aspirin as an anti-platelet medication. It attempts to avert further harmful blockages. To lower an individual's blood pressure, a variety of drugs can be utilized. Beta-blockers lower the heart rate and blood pressure, reducing the risk of heart attacks and heart rhythm problems. Other medications which lower the blood pressure include calcium channel blockers, diuretics, and angiotensin-converting enzyme (ACE) inhibitors.

6.2.5.3 Surgical Options

When the atherosclerosis begins to show signs of severe symptoms or blockages threatening survival, doctors will opt for more aggressive treatments. One common method is angioplasty where an empty, deflated balloon (balloon catheter) is passed over a wire into specific locations. The balloon is inflated to a desired size, expanding vessels to improve blood flow and compresses the plaque deposits.[213] Occasionally, a mesh tube

(stent) will be placed in the artery to ensure it remains open. A diagram of this procedure visualizes the process in Figure 65.

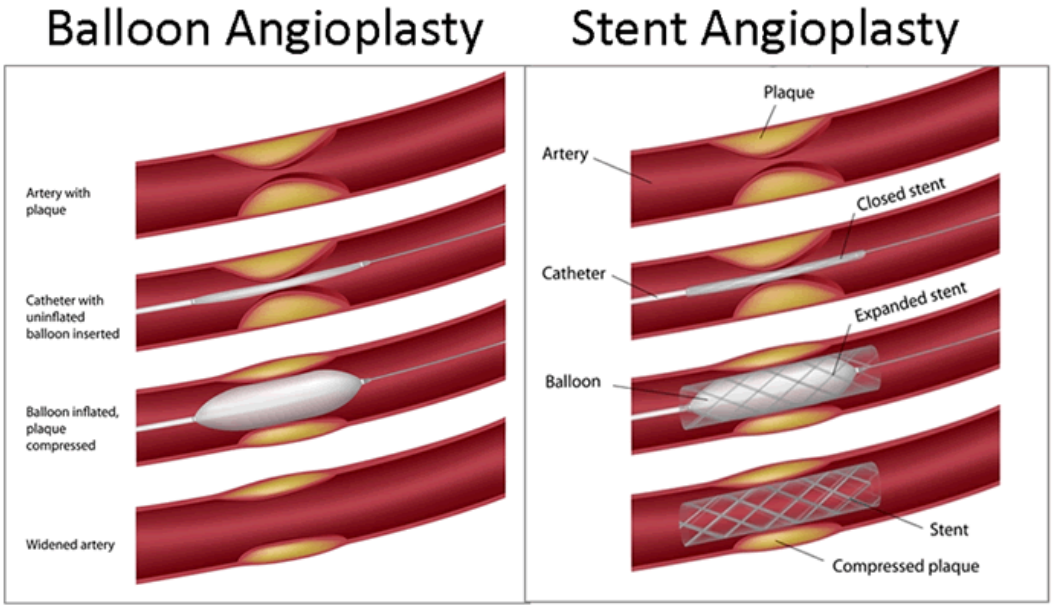

Figure 65: Procedures for balloon angioplasty and stent angioplasty. The main difference is whether or not a structural device (stent) is left behind to help maintain flow through the artery.

In other cases, the fatty deposits need to be surgically removed from the artery in a process called endarterectomy. In this procedure, an incision is made on the body to locate the artery with deposit. The vessel is clamped around the deposit to open it and remove the fatty deposit entirely. The artery is closed and patched after deposit removal. This commonly occurs for the carotid artery.

Instead of removal of a deposit, a doctor may elect to perform a bypass surgery. In this method, a vessel from another part of the body or a tube made of synthetic fabric is used to allow blood to flow around the blocked or narrowed artery.

6.3 Cholesterol Structure

Cholesterol is capable of forming multiple polymorphs depending on the growth conditions. The two most common ones are cholesterol monohydrate and anhydrous

cholesterol. Cholesterol monohydrate crystals have a bilayer structure with space group P1. In their triclinic structure, the polar 3-hydroxyl ends form hydrogen bonds with each other and water molecules. The unit cell crystallographic dimensions are as follows: a = 12.39 Å, b = 12.41 Å, c = 34.36 Å, $\alpha = 91.9^{o}$, $\beta = 98.1^{o}$, and $\gamma = 100.8^{o}$.[214] These crystals exhibit a platelike morphology, which can be seen in Figure 66.[215] The largest plate face is the c face, or (001) face, which is a result of faster growth within the bilayer plane than growth between bilayers. This is an effect of stronger intermolecular interactions in the bilayer plane.

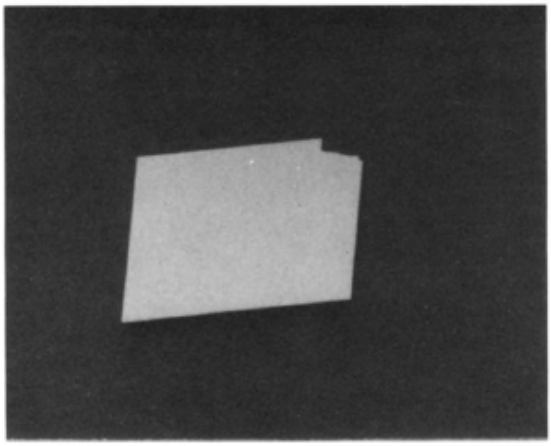

Figure 66: Photo of cholesterol monohydrate crystal depicting the platelike morphology.[215]

Anhydrous cholesterol crystals are triclinic with a space group of P1 similar to cholesterol monohydrate. The unit cell dimensions are a = 14.17 Å, b = 34.21 Å, c = 10.48 Å, $\alpha = 94.6^{o}$, $\beta = 90.7^{o}$, and $\gamma = 96.3^{o}$.[216] The observed morphology is clearly distinct from cholesterol monohydrate as needlelike crystals are produced as seen in Figure 67.[215]

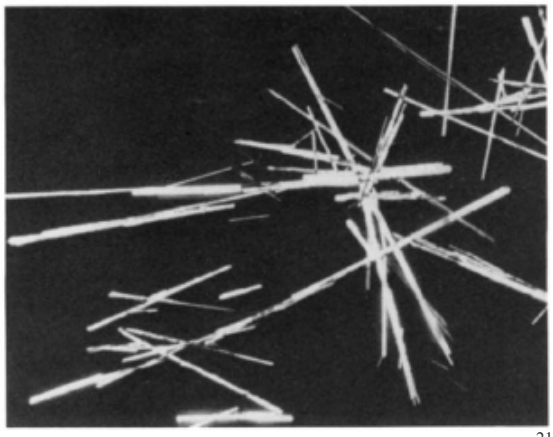

Figure 67: Anhydrous cholesterol crystals illustrating needlelike morphology.[215]

Polymorphs of anhydrous cholesterol can be produced depending on the conditions. One method is the loss of water from the crystal structure of cholesterol monohydrate. To rehydrate the crystal back to the original cholesterol monohydrate, at least 24 hours were required and the rate of hydration was dependent on the polymorph of anhydrous cholesterol.[215] Figure 68 illustrates the differences in rate of hydration.

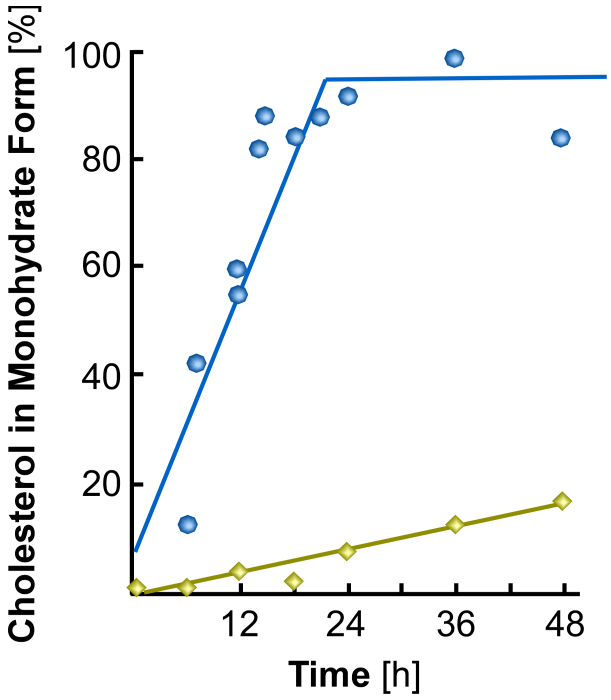

Figure 68: Rate of hydration of cholesterol in bulk water. Blue circles represent anhydrous cholesterol and water equilibrated at 20°C and yellow diamonds are anhydrous cholesterol and water at 45°C.[215]

Depending on the system, cholesterol solubilizes in varying quantities. Sonicated systems of synthetic homogenous chain lecithins have been shown to solubilize up to 3 moles of cholesterol for every 1 mole of phospholipid.[217] Liposomes produced from certain organic solvents contain about 2 moles of cholesterol in 1 mole of phospholipid in a metastable state.[218] The solubility limit of cholesterol in phospholipids is attributed to the molecule's intrinsic hydrophobicity and the interactions between the sterol hydroxyl group with the polar moiety of the lipid.[219,220]

6.4 Methods of Crystallization

To crystallize anhydrous cholesterol, pure cholesterol is dissolved in hot acetic acid.[215] The solution is then cooled slowly to change the solubility and crystallization to occur. To isolate the crystals, the solution was filtered on filter paper and placed in an 80^{o}C heated desiccator under vacuum to remove any lingering acetic acid. The crystals were stored in the dark in a desiccator over phosphorus pentoxide at 4^{o}C.

To grow cholesterol monohydrate crystals, a method of slow evaporation over 10 days from solutions of 95% ethanol and 5% distilled water has been utilized. During the slow evaporation process, platelike crystals began to form. The crystals are originally transparent or clear, but after a few hours of exposure to air a transformation to opaque crystals transpires due to dehydration of the crystalline structure. It is desired to extract hydrated crystals for experiments before dehydration occurs or implement another method of storage. To prevent autoxidative degradation[221,222], crystals can be stored in water in the dark at 4^{o}C for up to three months.

Using thermogravimetric analysis, the amount of water in a known mass of crystals can be determined by increasing the temperature while monitoring the mass of

the sample. For anhydrous cholesterol crystals, there is no change in mass; however, cholesterol monohydrate crystals experience a loss of mass, which can be attributed to water in the crystalline structure.

Other groups have attempted to uncover relationships between the solvent utilized for crystallization and its effect on the polymorph and morphology of cholesterol crystals produced. In one study, the morphology of cholesterol crystals grown in methanol, ethanol, acetone, and acetonitrile with 5% water and as extra dry pure solvents was examined. For these experiments, supersaturated solutions were produced by heating the solutions and then after a reduction of temperature at a rate of 4^{o}C per hour, cholesterol crystals formed. Needlelike crystals form in solutions of methanol and acetonitrile and in pure acetone. If anhydrous ethanol is used, cholesterol hemiethanolate crystallizes as the solvent is occluded in the structure. The angles of these crystals (71^{o} and 110^{o}) differ from cholesterol monohydrate (79^{o} and 100.8^{o}) as shown in Figure 69. Cholesterol monohydrate crystals form in 95% ethanol with 5% water and 95% acetone with 5% water.

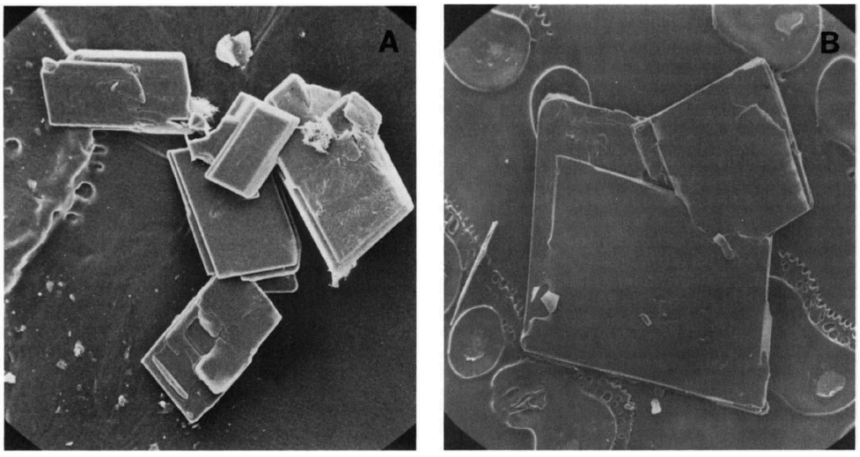

Figure 69: Cholesterol crystals. (A) Grown from pure ethanol and (B) 95% ethanol with 5% water.[223]

Lia Addadi and coworkers wanted to demonstrate cholesterol crystallization from two-dimensional domains in lipid bilayers.[224] Cholesterol is known to be an essential lipid in vertebrates as it is involved in membrane structure and function; yet to transport this molecule to various parts of the body, it requires assistance.[6] In this method, lipid bilayers with varying compositions and two-dimensional cholesterol domains function as nucleation sites for three-dimensional cholesterol crystals. However, these crystals only nucleate if there are domains of cholesterol in the lipid bilayers. For this system, it requires a three-phase setup as shown in Figure 70. The lipid bilayers were supported on coverslips which float on an aqueous phase. The aqueous phase contains methyl-β-cyclodextrin, which acts as a carrier of cholesterol. Beneath the aqueous solution, a saturated cholesterol solution in chloroform exists as a source where the cyclodextrin extracts cholesterol and transports it to the bilayers on the coverslip. Attempts to remove the crystals produced from the lipid bilayers failed suggesting the embedment of crystals in the bilayers. Most of the crystals produced by this method were cholesterol monohydrate parallelogram-shaped plates, yet some appeared as curved cylindrical particles and transformed into plates over a longer time. If the cholesterol in the bilayer did not segregate into domains but remained homogeneous throughout the lipid bilayer, no crystals were formed.

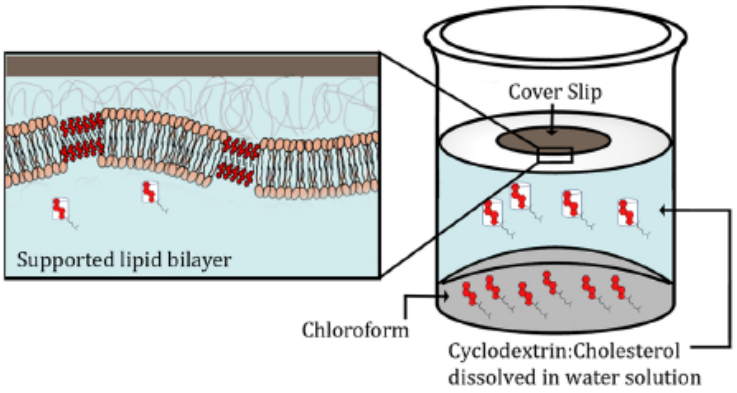

Figure 70: Three-phase setup for growth of cholesterol crystals with transport from an organic source across an aqueous medium to lipid bilayers.[224]

In contrast, others believe the direct formation of platelike cholesterol monohydrate crystals is incorrect. In a study by Martin Carey and coworkers, they utilized a model bile system composed of taurocholate, egg yolk lecithin and cholesterol in a molar ratio of 97.5:0.8:1.7. The model bile was dissolved or diluted to a specific concentration to create micelles and vesicles. Between 2–4 hours after dilution, thin filamentous structures were observed by optical, fluorescence and scanning electron microscopy. Within 12 to 24 hours, the filaments had aggregated into "wheat sheaf" bundles. Over the course of days, the progression from filaments to other structures occurs. During 2–7 days, thicker needlelike and helical structures appear along with platelike crystals. In videos of optical microscopy, the filaments coiled into spirals and helices which eventually formed tubelike structures. These tubes fractured at the ends to produce platelike crystals. Occasionally, the filaments would grow into flat ribbons, which will subsequently break directly into plates. Also, platelike crystals were produced without any transitions. This transformation of crystals is illustrated in Figure 71.[225] Using X-ray diffraction, the cholesterol crystal polymorph produced at various stages can be verified. The filaments exhibit peaks from anhydrous cholesterol crystals at 8-12 hours

in addition to cholesterol monohydrate peaks; however, only cholesterol monohydrate was detected after 24 hours.

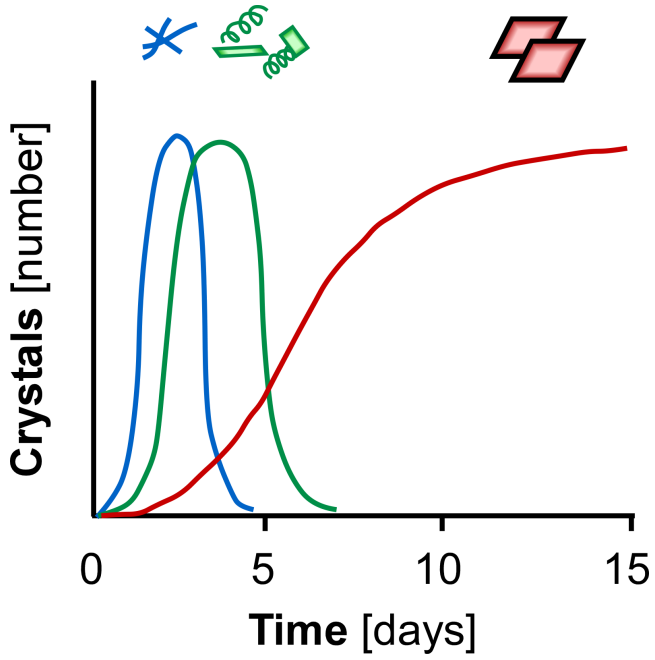

Figure 71: Illustration of transformation of crystals from filaments to ribbons, spirals or helices to plates.[225]

Although the growth medium described above is not physiological, other compositions of model biles were tested along with human gallbladder biles to evaluate their physiological relevance. The other systems experienced similar transformations from filaments to plate crystals. However, it should be noted this phenomenon has never been observed for atherosclerosis plaques or biomimetic models.

Prior studies in the literature have predominantly focused on the lipids present in the gallbladder and how they affect the crystallization of cholesterol. To date, there lacks fundamental systematic analyses of cholesterol crystallization. Dissolution has been observed using *in situ* AFM, but growth has not, leaving the mechanism of crystallization unknown. Therefore, this project attempts to address these unanswered questions.

Chapter 7: Solution Properties of Cholesterol in Various Solvents

Before elucidating the growth mechanism of cholesterol crystals, a physiologically-relevant solvent (growth medium) must be identified. The solvent should possess similar characteristics of both environments of gallstones and atherosclerosis. With this in mind, the search for a biomimetic environment(s) was the first major objective of this project.

7.1 Solubility of Cholesterol

The solubility of cholesterol determines how crystallization occurs in the body. Variations in cholesterol solubility emerge as the concentrations of lipids are altered based on biological responses of the body. These are observed in ternary diagrams of bile salts, phospholipids and cholesterol as well as the compositions of phospholipids in membranes. For all of these techniques, micelles, vesicles or lipid bilayers serve as potential heterogeneous interfaces for cholesterol crystals to grow and/or adhere. However, these systems are difficult to mimic for AFM measurements. As such, alcohols with varying chain length (as lipid surrogates) were selected and the percentage of water dissolved in the alcohol was adjusted to tune cholesterol solubility. Alcohols contain both a hydrophilic and hydrophobic moieties similar to lipids and are capable of solvent structuring.

7.1.1 Preparation of Alcohol Solvents

Initially, methanol, ethanol, butanol, hexanol and octanol were chosen as suitable solvents for investigation. Alcohols larger than octanol (8-chain length alcohol) are more susceptible to phase change with temperature variation. For example, decanol (10-chain length alcohol) can easily change from liquid to solid depending on slight fluctuations in

temperature. Therefore, no alcohols with a chain length larger than octanol were investigated. The water solubility in each solvent was tested to evaluate the percentages of water to test for cholesterol solubility.

Fresh deionized water was added to 20 mL glass vials with alcohols creating 10 mL solutions with varying percentages of water by volume. The solutions were allowed to equilibrate over the course of two days with occasional stirring to ensure mixture of water into the alcohol. If droplets were present after this time, the solution was considered immiscible at that volume percentage of water. Methanol and ethanol were miscible at all volume percentages of water. Butanol is miscible up to 15% by volume (i.e, a 20% solution was two-phase). For hexanol, water becomes immiscible at approximately 7.5% by volume of water. The solubility of water in octanol was found earlier to be 2.7 mol kg^{-1} (3.85% v/v).

The pH of blood is 7.35–7.45 while the pH of gallbladder bile is between 5.6 and 8.0. As an attempt to vary the aqueous solution present in the alcohol, phosphate buffer (pH 5.6) was added in varying percentages by volume to ethanol. At 30% v/v in ethanol, the phosphate precipitates out of solution. Therefore, solubility determination for this set with phosphate buffer was discontinued.

7.1.2 Extinction Coefficients of Cholesterol

To measure the solubility in these environments, two different methods were employed. In the first method, the Beer-Lambert Law (Equation 1) and UV-Vis spectrophotometry were employed; however, the extinction coefficients for each solvent with varying percentages of water needed to be determined first.

A known mass of cholesterol was dissolved in a fixed volume of solvent in a glass vial. The solution was allowed to sit for at least one day in the dark at 25^{o}C to ensure full dissolution. The solution in the vial was examined in an inverted microscope to ensure no solid residue was lingering. The entire solution was filtered with a 0.2 μm polytetrafluoroethylene (PTFE) filter. The filtered solution was diluted with filtered solvent (0.2 μm PTFE filter) to make ten different concentrations. The absorbance spectrum of each solution was measured from 200-800 nm in a quartz cuvette designed for this wavelength range. Peaks were chosen for each spectrum for every solvent. The absorbance at this peak was plotted as a function of concentration. This method was performed in triplicate for each solvent. The extinction coefficient for each solvent was calculated from this data. All of the extinction coefficients for cholesterol can be seen in Figures 72-74 and Table 9. For all regression analysis, the intercept was forced to go through the origin and any absorbance values above 1.1 were not included as the Beer-Lambert Law tends to fail above this region as an effect of turbidity.

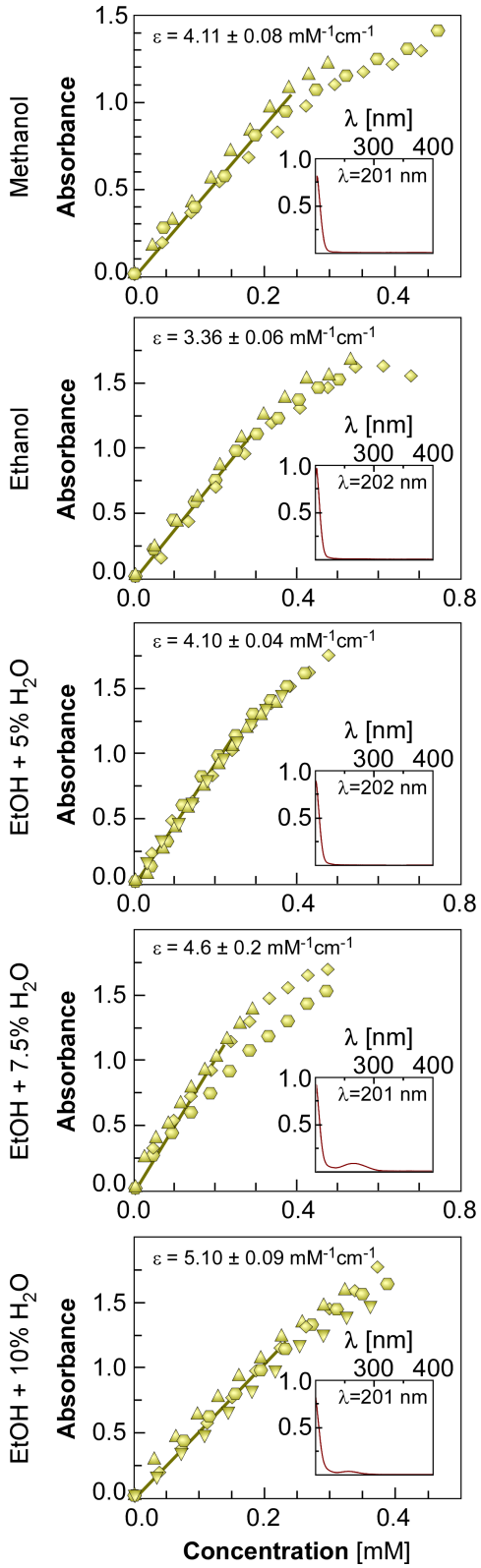

Figure 72: Extinction coefficients of cholesterol in methanol and ethanol based solvents. Insets are spectra of cholesterol in the designated solvent.

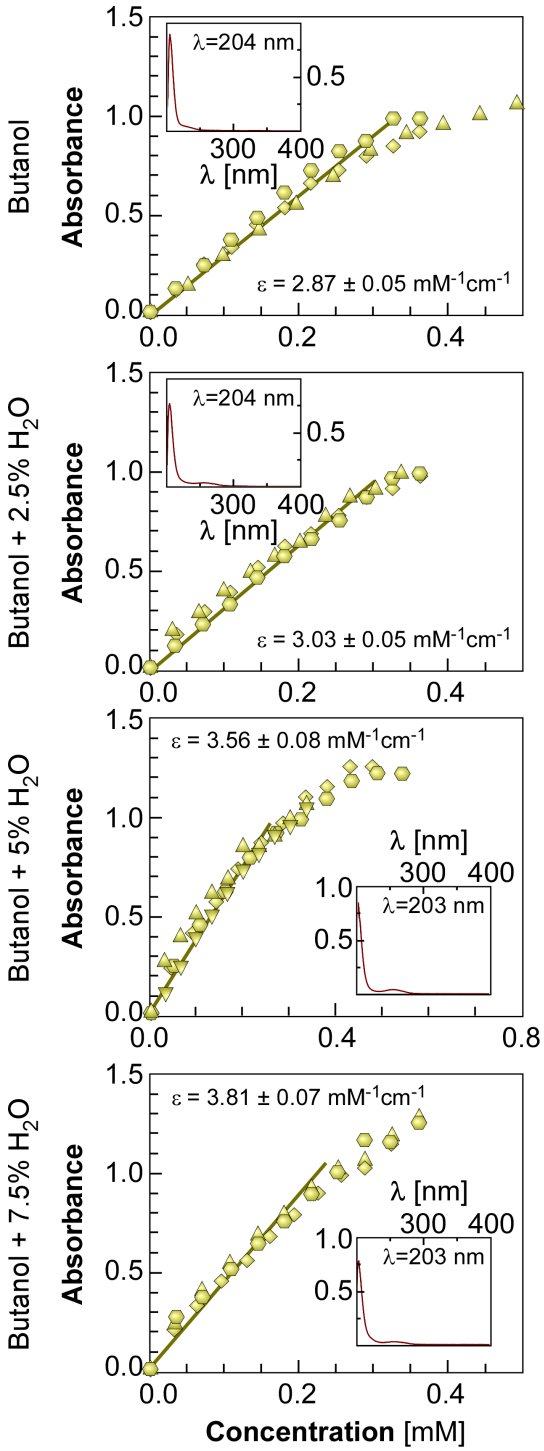

Figure 73: Extinction coefficients of cholesterol in butanol based solvents. Insets are spectra of cholesterol in the designated solvent.

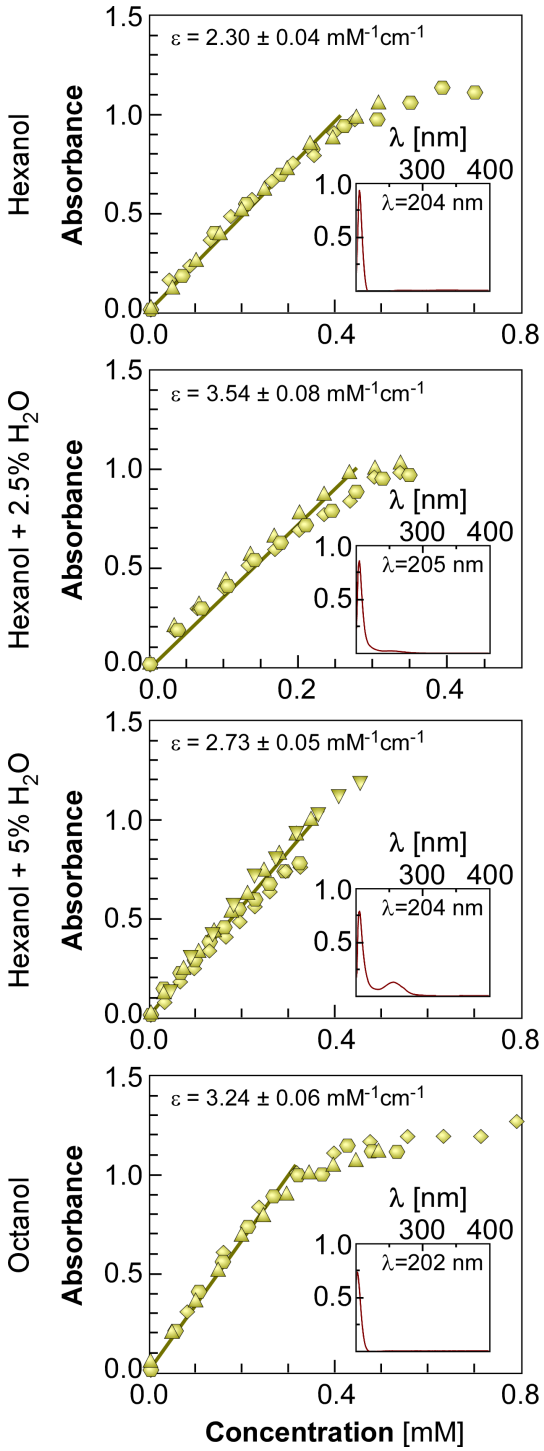

Figure 74: Extinction coefficients of cholesterol in hexanol and octanol based solvents. Insets are spectra of cholesterol in the designated solvent.

Table 9: Extinction coefficients of cholesterol in various solvents

Solvent	ε [$mM^{-1}cm^{-1}$]	λ [nm]
Methanol	4.11 ± 0.08	201
Ethanol	3.36 ± 0.06	202
Ethanol + 5% H_2O	4.10 ± 0.04	202
Ethanol + 7.5% H_2O	4.6 ± 0.2	201
Ethanol + 10% H_2O	5.10 ± 0.09	201
Butanol	2.87 ± 0.05	204
Butanol + 2.5% H_2O	3.03 ± 0.05	204
Butanol + 5% H_2O	3.56 ± 0.08	203
Butanol + 7.5% H_2O	3.81 ± 0.07	203
Hexanol	2.30 ± 0.04	205
Hexanol + 2.5% H_2O	3.54 ± 0.08	204
Hexanol + 5% H_2O	2.73 ± 0.05	205
Octanol	3.24 ± 0.06	202

7.1.3 Measuring Cholesterol Solubility

After determining the extinction coefficients, the solubility of cholesterol in each solvent could be measured. In 20 mL glass vials with septum caps, excess cholesterol powder was added to 3-5 mL of solvent. For each solvent, three separate vials were prepared to ensure reproducibility. All of the vials were stored in the dark at 25°C. The only exceptions were for ethanol with 5% H_2O, ethanol with 7.5% H_2O and ethanol with 10% H_2O where a temperature dependence of solubility was observed. For those systems, three vials were made for each separate temperature. After one week of equilibration, every vial was examined to ensure powder was still present. If all of the solid cholesterol had dissolved, more powder was added to each vial. After two weeks and three weeks of isolation, 0.2 mL of solution was filtered through a 0.2 μm PTFE filter. The filtered solutions were diluted to acceptable concentration for UV-Vis spectrophotometry (absorbance less than 1.0 and greater than 0.5) and the absorbance spectra were measured. All dilutions used filtered solvent and the spectra were blanked with filtered solvents. The solubility was tabulated for each solvent at all temperatures. In Figure 75,

cholesterol solubility is compared between all solvents at 25°C from the Beer-Lambert Law method.

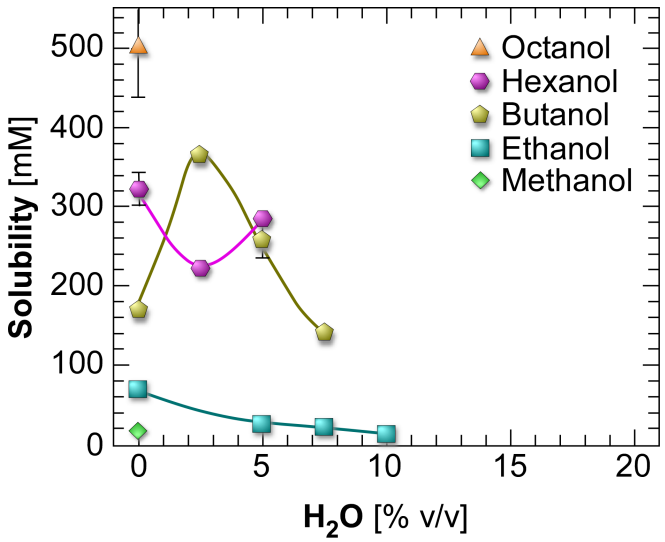

Figure 75: Solubility of cholesterol in various solvents (alcohols) with varying percentages of water determined using the extinction coefficients and the Beer-Lambert Law.

The second method for determining the solubility of cholesterol is monitoring the dissolution of cholesterol over time. A known mass of cholesterol was placed in a 20 mL glass vial with a septum cap with a specific volume that will not cause full dissolution of the solid powder. Every three or four days, the vial was examined to see if full dissolution had transpired. If solid remained, a small amount of solvent was added to the vial. If it appeared as though all the cholesterol had dissolved, the vial was observed underneath an inverted microscope to ensure full dissolution. More solvent was added to each vial until full dissolution occurred. This process lasted for over 30 days for some solvent systems. At this time, the solubility was calculated by the known mass of cholesterol at the beginning of the experiment compared to the total volume of solvent necessary for dissolution. Errors for this method arise due to dissolution at a lower volume than the increment addition. Only one vial was prepared and monitored for each solvent at 25°C.

The results could be reproducible, but they were not performed at this time. In Figure 76, the solubility of cholesterol from the dissolution method can be viewed.

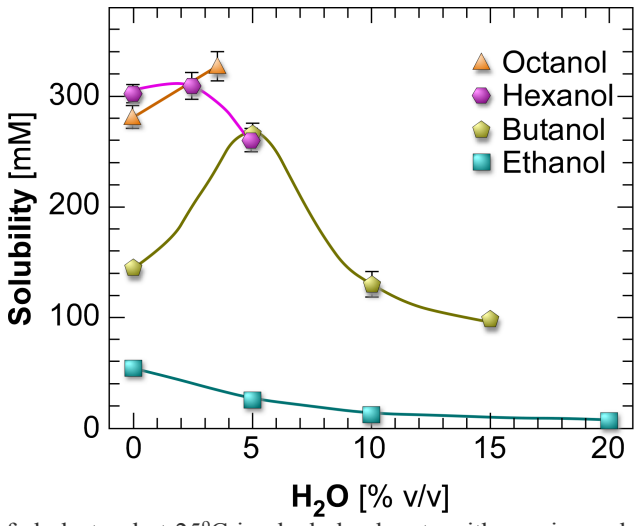

Figure 76: Solubility of cholesterol at 25°C in alcohol solvents with varying volume percentages of water determined by monitoring the dissolution of cholesterol powder over time.

When comparing the solubilities measured between the two methods, the values tend to be similar with a few exceptions in hexanol and octanol solvents. Notably, the solubility of cholesterol in octanol appears higher with the extinction coefficient method than with the dissolution method. Hofmann and coworkers observed a maximum solubility of cholesterol in pure alcohol solvents at approximately 7-carbon chain length. I observe a downward trend after an increase in the solubility using the dissolution method, but discern only an increasing trend with the extinction coefficient procedure. This could be due to the limited samples when performing dissolution or high solubility of cholesterol in octanol. It is possible to identify the same maximum at the 7-carbon chain length if the solvents are extended to odd chain length alcohols and longer chain lengths. If we assume this trend occurs in this system, the solubility present in phospholipids characteristic of gallstones and atherosclerosis would be similar to the solubility observed with ethanol.

For hexanol, the solubility of cholesterol with 2.5% water dissolved varies between the two methods as they show opposite trends. To verify if these values are reproducibly detected, the solubility of cholesterol in hexanol with 1.25% and 3.75% water could be found using extinction coefficients or dissolution. For the dissolution method, more trials could be performed to duplicate the previous experiments.

The solubility of cholesterol in the gallbladder ranges from 5-50 mM. The only alcohol with corresponding solubility to the values in the body is ethanol; therefore, I selected ethanol for all subsequent studies.

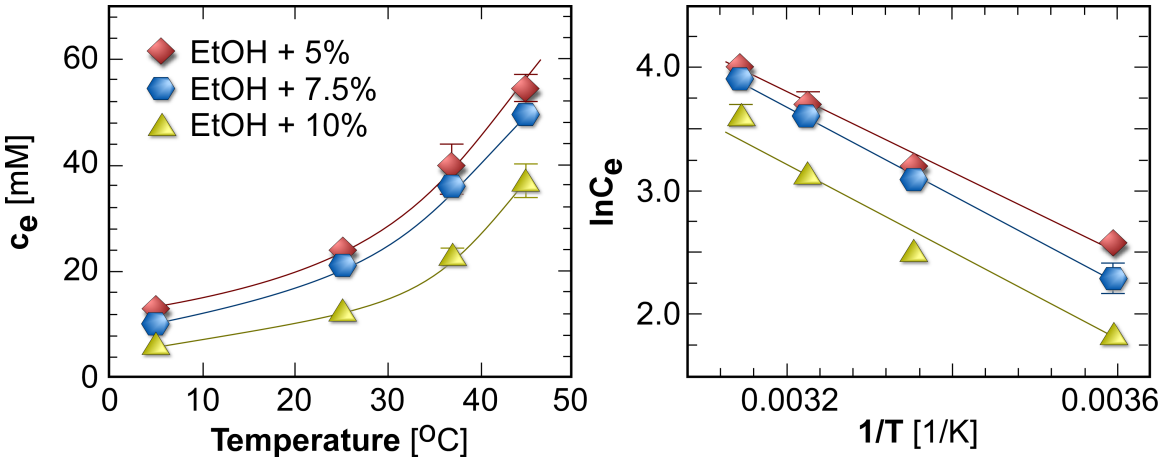

Figure 77: Temperature dependence of the solubility of cholesterol in ethanol with varying percentages of water dissolved in the solvent.

The effect of temperature on the solubility of cholesterol was evaluated in ethanol containing 5, 7.5 and 10% water as shown in Figure 77. For all three systems, the solubility increases as temperature increases. If the solubility is converted using the van't Hoff equation (Equation 9), the enthalpies and entropies of crystallization of cholesterol can be assessed. These values are listed in Table 10. As the volume percentage of water dissolved in ethanol increases, the enthalpy of crystallization decreases. However, the errors of these values show some overlap (particularly at higher water content). Overall,

these values can be utilized to assess if crystallization of cholesterol is governed by thermodynamics.

Table 10: Thermodynamics of crystallization of cholesterol

Solvent	ΔH [kJ mol^{-1}]	ΔS [J $mol^{-1}K^{-1}$]
EtOH + 5% H_2O	-26 ± 2	115 ± 7
EtOH + 7.5% H_2O	-30 ± 1	126 ± 4
EtOH + 10% H_2O	-32 ± 4	115 ± 7

The gallbladder and blood contain both aqueous and organic media. If the solubility of cholesterol in water is compared to the solubility in ethanol, the difference is more than five orders of magnitude as shown in Figure 78. The putative low solubility in water demonstrates the difficulties with crystallization in an aqueous environment. The degree of supersaturation that can be achieved is limited, thus hindering crystallization. The high solubility of cholesterol in ethanol enables a supersaturation to be achieved easily with rapid crystallization.

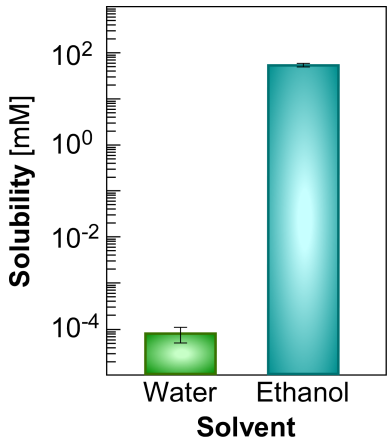

Figure 78: Comparison of the solubility of cholesterol at 25°C in water versus ethanol.

Chapter 8: Bulk Crystallization & AFM Studies

Initially, I wanted to survey the differences between crystals grown in a purely aqueous medium to an organic medium. The only growth procedures in an aqueous solution in the literature contain some amount of lipid or organic solution. Therefore, I had to use an approach to dissolve a sufficient quantity of cholesterol to create a supersaturated solution for growth.

8.1 Purely Aqueous Environment

Using a phosphate buffer at pH 5.6, a 1.2 mM solution of cholesterol was made in a 10 mL round bottom flask. The solid did not dissolve as expected; therefore, the solution was refluxed at 125^{o}C (oil bath temperature) for 2 hours. The temperature was decreased by 5^{o}C every hour until the temperature was 100^{o}C. The solution was refluxed for another hour before the solution was filtered through a 0.45 μm Supor filter paper with a 47 mm diameter. The filter paper was rinsed with deionized water and placed in a glass petri dish in a 37^{o}C oven to dry.

The time for reflux was adjusted to allow for longer crystallization time. The heating bath was initially set at 125^{o}C for 17 hours and subsequently lower by 5^{o}C every 2 hours until reaching 100^{o}C. The flask remained in the oil bath for another 13 hours before filtration. The crystals produced from this method can be seen in Figure 79. Few crystals were found on the filter paper and uniformity of crystal morphology could not be detected. This finding reinforces the requirement of an organic medium for crystallization of cholesterol in the body. There was insufficient powder to perform XRD and determine which polymorph of cholesterol crystallized from the aqueous solution.

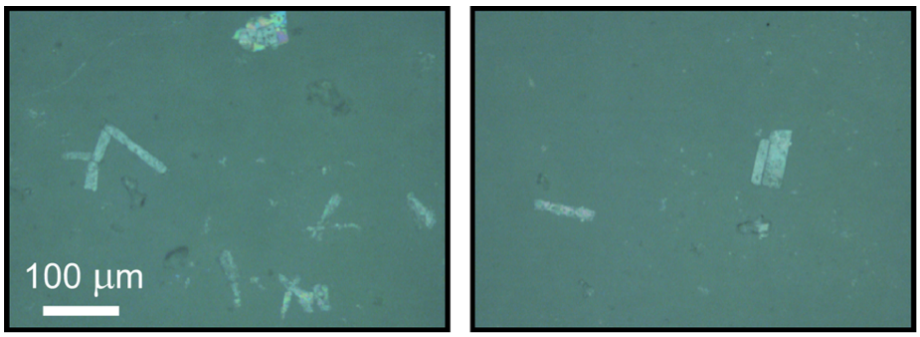

Figure 79: Cholesterol crystals grown from a phosphate buffer, pH 5.6, at reflux with a slow cooling rate.

8.2 Ethanol Solvents

Several methods have been previously described to grow cholesterol monohydrate crystals in ethanol with 5% water with timescales ranging from only a few hours to weeks. One protocol requires a special crystallization cell with a controlled heated water bath to slowly lower the temperature while another protocol allows slow evaporation to change the supersaturation in solution. Using this knowledge, I could begin to develop similar procedures to grow cholesterol crystals.

Initially, I dissolved cholesterol powder in 4 mL of an organic solvent in a 20 mL glass vial with a septum cap. The vial was sealed with a layer of parafilm and placed in a 60^{o}C oven to fully dissolve the solid. Depending on the concentration of cholesterol, the amount of time the vials spent in the oven ranged from 1.5-12 hours to allow full dissolution. The vials were removed and stored at 25^{o}C in the dark. After 24 hours, the vials were filtered through a 0.45 µm Supor filter paper with a 47 mm diameter. The filtration system was cleaned thoroughly and rinsed with ethanol to ensure no water was present during separation. If any water is present, the solution will precipitate cholesterol instantaneously. The filter papers were placed into plastic petri dishes to dry at 23^{o}C. Examples of cholesterol crystals grown with this method are shown in Figure 80.

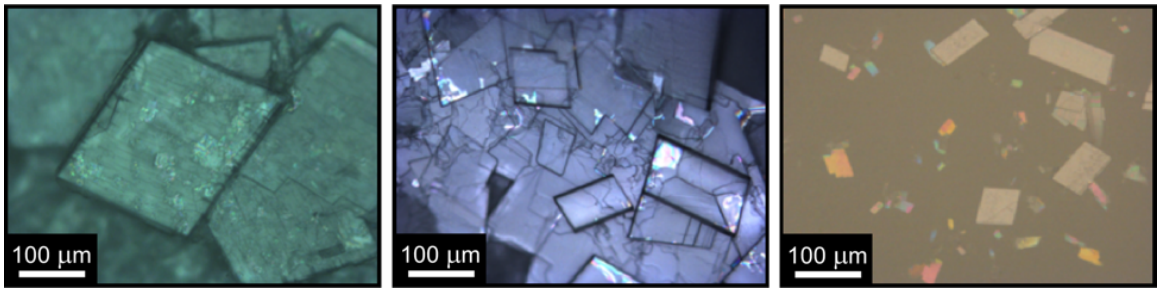

Figure 80: Optical microscopy images of cholesterol crystals grown from (left to right) 64.1 mM in ethanol, 30.0 mM in ethanol with 5% water, and 15.0 mM in ethanol with 10% water.

This method readily produces cholesterol crystals, but control over the polydispersity is limited as sizes vary greatly. To circumvent this problem, I examined the effect of crystallization time, supersaturation, isolation techniques and cooling rate after characterization of the crystal structure to determine which polymorph of cholesterol crystallizes.

To characterize the crystals, I made large batches of crystals with supersaturation ratios (C / C_e) between 1.5 and 2. After filtration and drying, I crushed the crystals into a fine powder with a mortar and pestle. Using XRD (Siemens D5000 X-ray Diffractometer with a CuKα radiation source [40 kV, 30 mA, 1.54 Å]), the crystal structure of samples grown from each solvent could be determined. The effects of drying on the structure of the crystals were observed. At various hour intervals of drying at room temperature, the recovered solid could be crushed into a powder. One powder sample was also dried at an elevated temperature of 37^{o}C to check for any structural transformation. In Figure 81, the XRD patterns are compared for different drying times for as synthesized crystals prepared from ethanol with 5% water growth solutions.

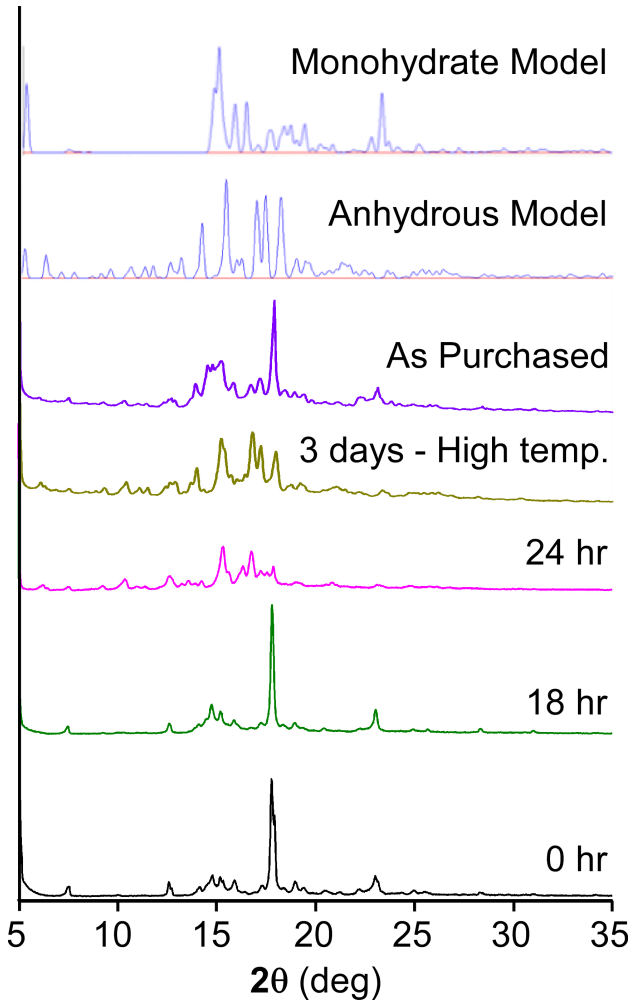

Figure 81: XRD patterns of cholesterol crystals grown from ethanol with 5% water after varying drying times with model patterns produced from Diamond. At 0 hours, the crystals are hydrated, but after 3 days at 37°C, the crystals are fully anhydrous.

As water evaporates from the crystals, there are distinct changes in Bragg peaks(i.e., some peaks disappear and new peaks arise, indicating a change in the crystalline structure). The hydrated crystal XRD pattern resembles the monohydrate model with d-spacings of the crystals matching the models (Figure 82). When fully dry, the crystals are anhydrous cholesterol, which matches previous literature stating water exits the crystal structure. When examining the crystals under an optical microscope for long periods of time, the surface slowly shifts from transparent to opaque. This emphasizes how storage and longevity of crystals will impact future experiments.

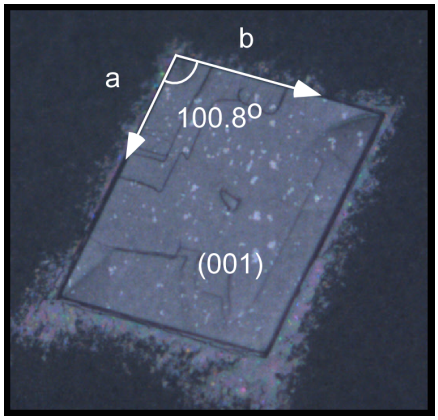

Figure 82: Cholesterol crystal grown in ethanol with 5% water exhibiting dihedral angles characteristic of cholesterol monohydrate.

Similar XRD experiments were performed for cholesterol crystals prepared from ethanol with 10% water growth solutions. The results are shown in Figure 83. The patterns are consistent with those from ethanol with 5% water in Figure 81. The 5% difference in water dissolved in ethanol has no apparent effect on the type of cholesterol crystallized from solution.

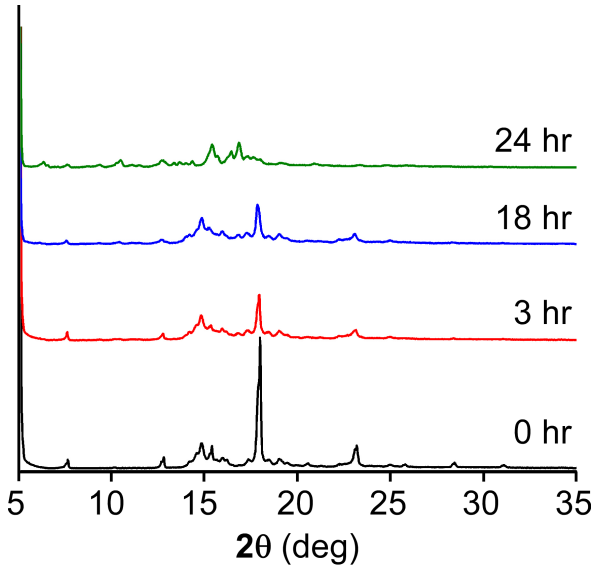

Figure 83: XRD patterns of cholesterol crystals grown from ethanol with 10% water after varying drying times.

8.2.1 Effects of Growth Conditions in Ethanol with 5% H_2O

The growth of crystals can be controlled by a variety of factors. To produce uniform (i.e., low polydisperse size) crystals, I methodically adjusted the crystallization time, supersaturation and rate of cooling individually. Initially, I examined how the length of crystallization time affects the crystals (see Figure 84). The length of time is measured as time after removal from the oven to cause supersaturation until the solution is filtered. At time zero there are no crystals as expected but the length of time for crystallization of a 29.7 mM cholesterol in ethanol with 5% water did not provide uniform crystals. There was also lack of reproducibility between samples prepared under the same conditions.

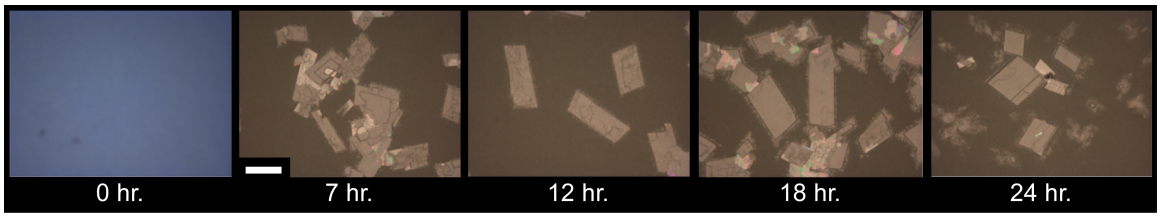

Figure 84: Effect of crystallization time for 29.7 mM cholesterol growth solution over the course of 24 hours. Scale bar is 100 μm.

Next, I adjusted the degree of supersaturation of the growth solution with a constant growth time of 24 hours (Figure 85). The growth solution concentrations ranged from 23.9 to 31.3 mM cholesterol. If the supersaturation is too high, the filter paper is completely covered with crystals, which are indistinguishable from each other in optical micrographs. With these conditions, reproducibility does not occur and the sizes of crystals vary from tens of microns up to a few millimeters.

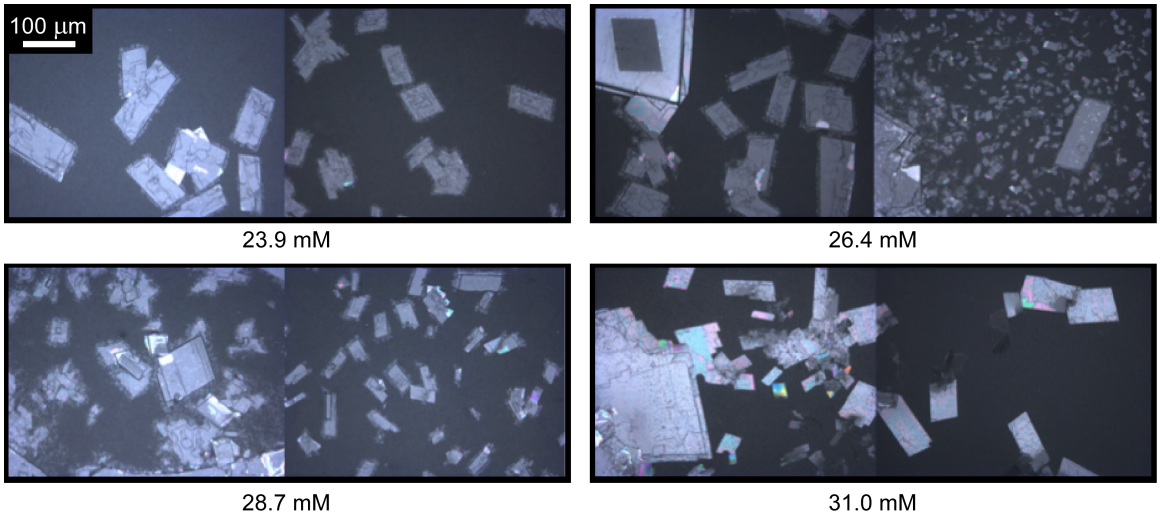

Figure 85: Optical micrographs of cholesterol crystals grown from varying degrees of supersaturations in ethanol with 5% water.

The driving force of crystallization is supersaturation, and adjusting the rate of cooling can decrease or increase supersaturation. With a lower cooling rate, the net change in supersaturation is slower enabling the growth rate of crystals to be more easily controlled. For the next set of experiments, the glass vials were placed in a water bath circulator after dissolution in the oven. The initial temperature was 50^{o}C with incremental decreases in temperature over 8 hours. Every hour, the temperature was lowered by 5^{o}C until reaching 35^{o}C. Then, the temperature was reduced by 2^{o}C every hour until reaching 25^{o}C where the vials were then transported to the 25^{o}C drawer outside of the water bath circulator. The solutions were allowed to crystallize for another 19 hours at 25^{o}C before filtration. The crystals produced with this method at varying supersaturation can be viewed in Figure 86. Under these conditions, few crystals appear at concentrations less than 25 mM cholesterol (each with indistinct morphologies). However, above 27 mM cholesterol, low polydisperse (uniform) crystals can be seen. Therefore, this method seems to be effective at creating crystals with a low polydispersity. In this method, the

vials are agitated (in the water bath) as the water circulates, causing discrepancies between sample batches.

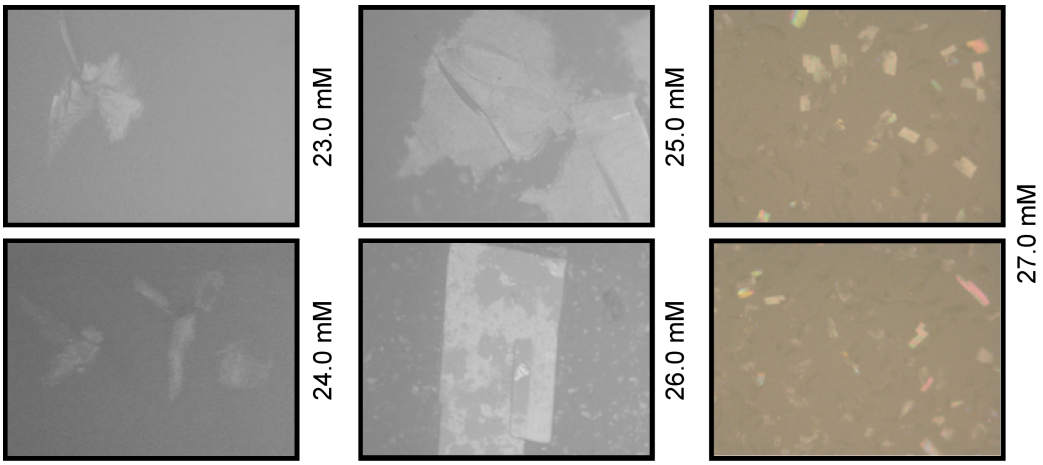

Figure 86: Cholesterol crystals produced using a slower cooling rate in a water bath circulator with several growth concentrations.

To decrease agitation, the type of water bath was switched to a simple setup as shown in Figure 87. The temperature of the heated water bath was measured with a mercury thermometer during the experiment. After removal from the oven following dissolution, the temperature of the water bath was maintained at 55°C for one hour. The temperature of the water bath is lowered every hour by 6–7°C until approximately 29°C. For at least three hours, this temperature is maintained then changed to 23°C. Solutions were filtered after another 16 hours of crystallization.

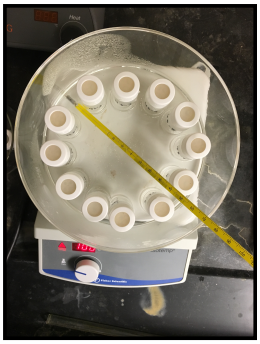

Figure 87: Setup of the water bath with vials used to produce cholesterol crystals with limited agitation and a slow cooling rate.

In Figure 88, the cholesterol crystals produced with limited agitation and a slower cooling rate can be seen. For these samples, lower supersaturation results in reduced polydispersity and larger crystals compared to those produced at high supersaturation. As the concentration of cholesterol increases, the number of distinguishable single crystals decreases. However, the number of crystals present on the filter paper increases as the supersaturation increases. With this method, the reproducibility between samples is improved and outlier crystals of larger size are observed less frequently at higher cholesterol concentrations.

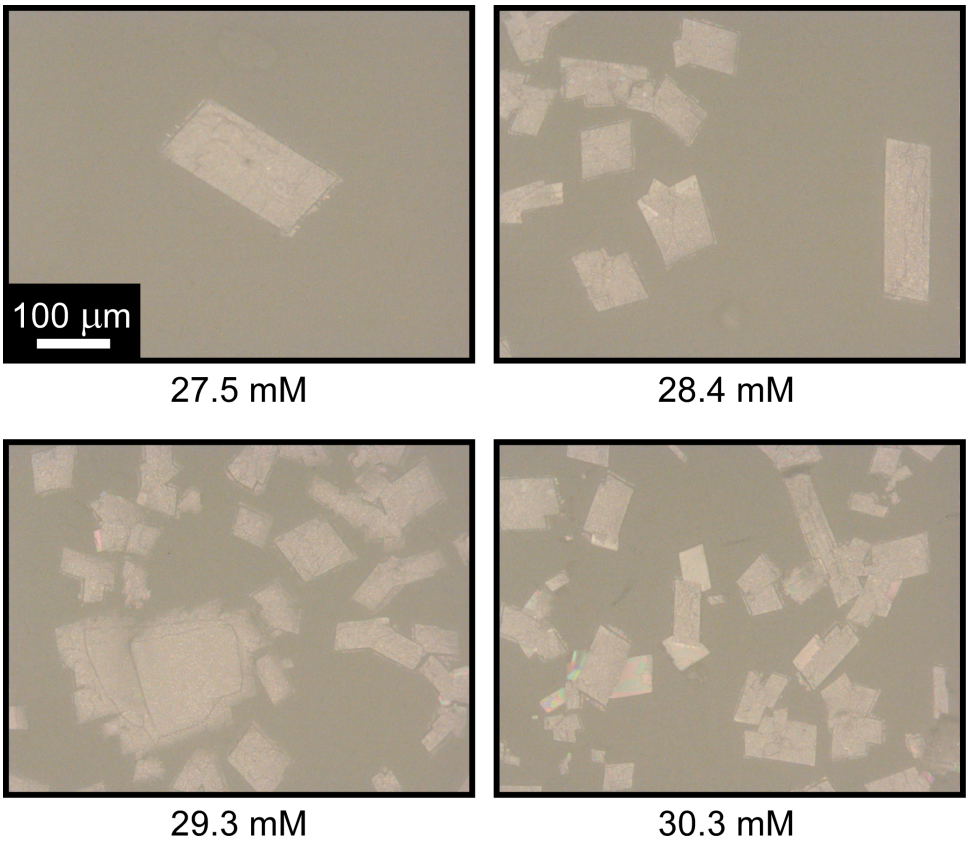

Figure 88: Microscope images of cholesterol crystals grown using a water bath with limited agitation and a slow cooling rate.

In summary, this method proves to be useful for further studies of bulk crystallization and *in situ* AFM measurements. The supersaturation of the solution,

cooling rate temperatures, and time of cooling can be adjusted to yield crystals with desirable features depending on what is vital for the experiment.

8.3 AFM Surface Studies

To begin AFM surface studies, the crystals produced with the bulk crystallization methods needed to be mounted on metal AFM specimen disks. Jennifer Swift and coworkers working with cholesterol monohydrate utilized epoxy to attach large crystals for *in situ* AFM dissolution studies.[226] For my studies, I attempted to use a variety of epoxies as well as directly attach the crystals to glass.

Cholesterol monohydrate crystals do not adhere to the surface of glass coverslips during growth. The glass coverslip's surface is hydrophilic while the crystals are hydrophobic, which prevents attachment. To bypass this, I functionalized the surface of glass coverslips with (7-octan-1-yl) trimethoxysilane. After silanization, water droplets placed on the surface of the coverslips did not spread across the glass (contrary to the non-functionalized surface). However, cholesterol crystals did not grow on the surface of silanized glass coverslips regularly and required higher supersaturation growth solutions. More crystals formed in solution instead of on the glass. If a crystal attached to the surface, it could not be used for *in situ* AFM as crystals immediately detached in growth solutions.

Before trying to press crystals into epoxy on AFM disks, I tested each epoxy's compatibility with ethanol. In almost all of the epoxies, swelling prevented further usage. However, Norland Optical Adhesive 81 (ultraviolet cure glue) was not impacted by the presence of ethanol and was used for AFM studies.

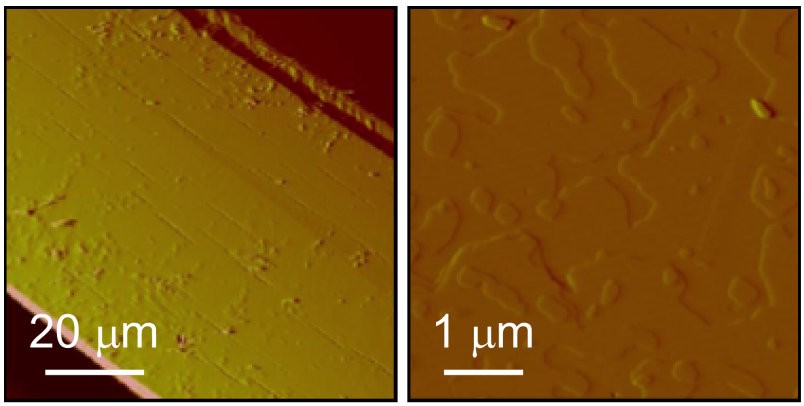

Figure 89: AFM images of cholesterol monohydrate crystals.

In Figure 89, the surface of a cholesterol monohydrate crystal in air can be viewed. I used a Multimode atomic force microscope (Nanoscope IV) from Digital Instruments. AFM images were captured in tapping mode using Olympus TR800PSA probes (Silicon nitride, Cr–Au coated, with spring constant 0.15 N/m). The resonance frequency for tapping mode would fall into two ranges for imaging in solution: 100-130 kHz and 340-370 kHz. I collected images in height and amplitude modes with 256 scan lines per image. Cholesterol monohydrate crystals are soft and easily altered by contact mode imaging with the AFM tip. The surface can be etched away with a single pass across the imaging area. As a result, contact mode imaging could not be used for any experiments; only tapping mode would not impact the surface features.

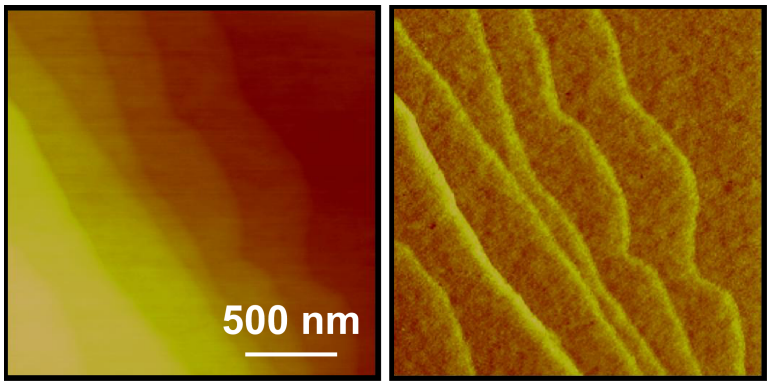

Figure 90: Flattened AFM height image depicting layers on the surface of a cholesterol monohydrate crystal on the left. The right image is the amplitude mode of the same surface.

In tapping mode, the surface of the crystals could be analyzed and imaged as shown in Figure 90. With height images, the step heights can be measured to determine if the crystal structure matches the unit cell of cholesterol monohydrate. In Figure 91, the frequency of step heights can be seen. This histogram illustrates how the step heights roughly correlate to expected step values of half step, step and step bunches of cholesterol monohydrate crystals in the c-direction (3.4 nm).

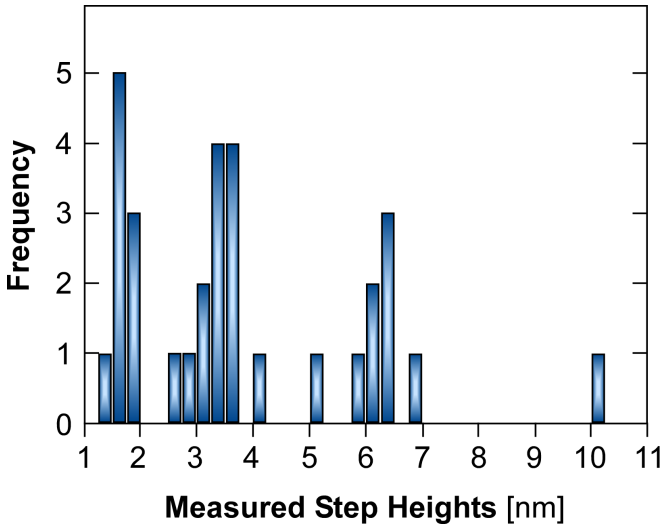

Figure 91: Histogram of measured step heights from cholesterol crystals from flattened AFM height images.

Half step values occur due to the packing of cholesterol monohydrate structures. In the c-direction, two cholesterol molecules are stacked linearly as demonstrated in Figure 92. The determination of the growth mechanism of cholesterol monohydrate would likely provide insight as to how molecules incorporate into the crystalline structure. If single monomers are added (i.e., classical crystallization), the steps will propagate as half step heights. In contrast, dimers or oligomers could bind to surface sites causing the crystal to grow nonclassically.

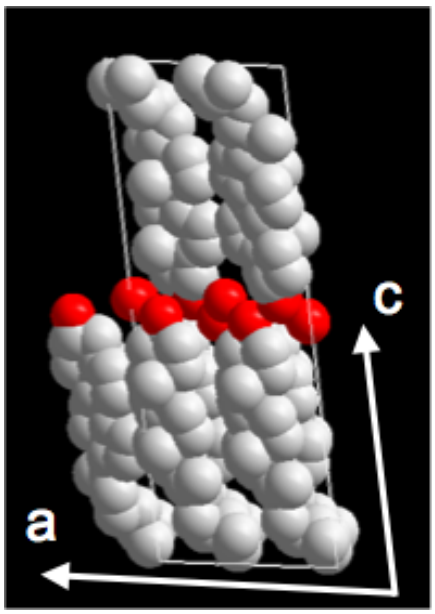

Figure 92: Model of unit cell of cholesterol monohydrate. C-direction is upward illustrating how cholesterol molecules stack with hydrogen bonding.

For *in situ* AFM studies, the method of mounting crystals to the AFM disk has a huge impact on whether dynamic surface events will occur. If the glue is not tacky enough, any crystals mounted in the glue will detach as soon as the growth solution is pushed into the AFM liquid cell. Pressing the crystals into glue that is excessively tacky will not allow any solution to have an effect on the crystals. For example, pure ethanol was used to dissolve the crystals as the solubility of cholesterol is double in this solvent compared to ethanol with 5% water. However, the crystal will not indicate any signs of dissolution or change in the surface whatsoever. Therefore, the optimal method for crystal attachment is as follows. Norland Optical Adhesive is spread across the surface of a metal AFM specimen disk with either a razor blade or square glass coverslip. The glue is cured under a UV lamp for 1.5 minutes. From mildly dry to fully dried filter papers, cholesterol crystals are removed with tweezers (note that they tend to stick to the tweezers when gripping the crystals) and placed in the middle of the glue on the AFM puck. The only force pressing the crystals into the glue is the weight of the crystal itself.

With this method, small crystals (ca. 1 mm) do not attach to the tweezers and can only be removed from the filter paper with scraping which destroys the crystals. With wet filter papers, the crystals stick to the filter paper and do not come off without manual force causing crystals to break apart. After crystal placement in the glue, the specimens are cured under the UV lamp for another 10 minutes before removal and use for *in situ* AFM.

I have prepared growth (supersaturated) and dissolution (undersaturated) solutions for *in situ* AFM by creating solutions with specific concentrations according to the methods described for bulk crystallization. After removal from the oven, the concentration can be verified using UV-Vis spectrophotometry. The range of concentrations useful for imaging will be narrow due to the high solubility and fast growth of the crystals. While I have been unable to uncover the growth mechanism of cholesterol monohydrate in a mixed aqueous-organic environment of ethanol with 5% water at this point in time, I have provided a base platform of knowledge for someone to take over this project.

8.4 Effects of Bile Salts

Simultaneously while trying to uncover the growth mechanism of cholesterol monohydrate, I wanted to visualize the effects of potential inhibitors present in the body on the bulk crystallization of cholesterol. Previous studies have found that several bile salts, aspirin, osteopontin, and caffeine to inhibit cholesterol crystallization.[227-230] There are numerous bile salts and I selected five different molecules (Figure 93) to test for inhibition: chenodeoxycholic acid, cholic acid, lithocholic acid, deoxycholic acid and ursodeoxycholic acid. When performing bulk crystallization, stock solutions of bile salts

dissolved in ethanol with 5% water were used to help dissolve cholesterol instead of pure solvent.

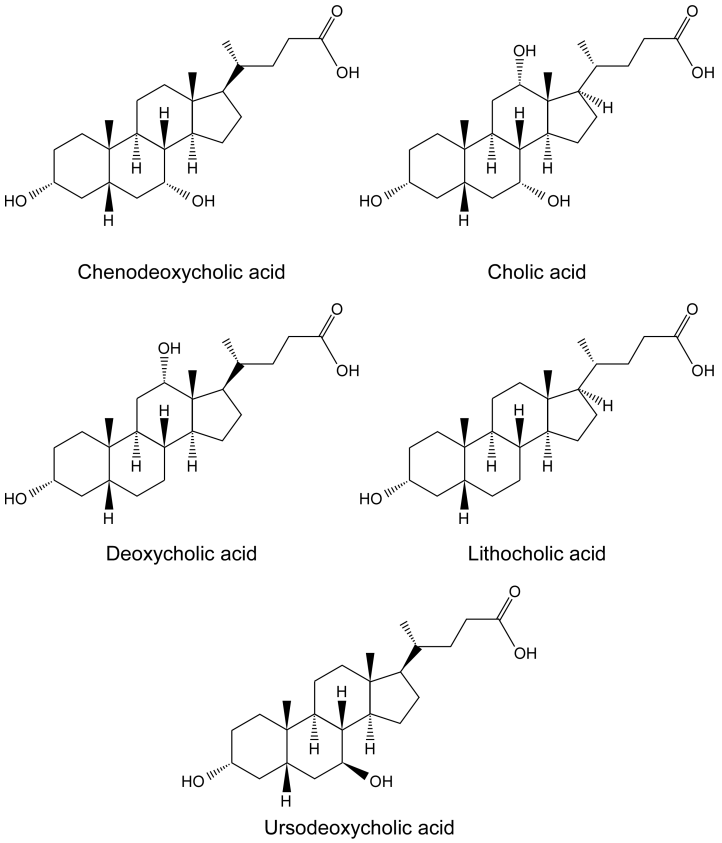

Figure 93: Five bile salt structures selected to test as potential inhibitors of crystallization.

Initial studies using 10 mM bile salt and 27.5 mM cholesterol concentration reveal effects only for lithocholic acid and ursodeoxycholic acid. Both bile salts show a decrease in the number of crystals present on the filter indicating an effect on nucleation. However, these bile salts can cause changes in the solubility of cholesterol, which may be the cause of the decrease in crystal number. More studies must be performed with these bile salts and other potential inhibitors to determine the efficacy and potency along with how these potentially act as inhibitors with *in situ* AFM surface studies.

Chapter 9: Summary of the Cholesterol Project and Direction for the Future

Overall, I have examined the solution properties of cholesterol in a variety of alcohol solvents with increasing water content. Solubility increases with higher chain length alcohols, reaching a potential maximum at 7-carbon chain length. The alcohol with a solubility range comparable to the conditions for gallstones and atherosclerosis is ethanol. As the amount of water dissolved in the alcohol increases, the solubility of cholesterol decreases. For butanol, we observed an initial increase at low water content and then a subsequent decrease at higher water content. If the solubility of cholesterol in pure water is compared to that in pure ethanol or a lipid environment, we observe a five order of magnitude difference. This result is similar to differences in hematin solubility in aqueous and organic media.

Cholesterol crystals were grown in bulk under a variety of conditions to determine which crystal polymorph was formed, the effects on polydispersity of crystals, and optimal growth conditions. Water is capable of evaporating from the crystal structure of cholesterol, highlighting the importance of selecting a method of drying. The rate of cooling is the most influential factor in determining how polydisperse the crystals produced will be. Initial perspectives of bile salts as inhibitors of crystallization indicate chenodeoxycholic acid and ursodeoxycholic acid affect nucleation and/or the solubility of cholesterol.

Preliminary efforts aimed to uncover the mechanism of crystallization of cholesterol monohydrate. The basal surface of cholesterol crystals was examined by AFM where steps in the c-direction with heights characteristic of cholesterol monohydrate were observed. The process for working with soft cholesterol crystals and

mounting them on AFM specimen disks has been determined along with the range of cholesterol concentrations leading to surface growth. Overall, I have provided a generalized platform for studying the growth of cholesterol crystals.

References:

1 Selvam, R. & Kalaiselvi, P. Oxalate binding proteins in calcium oxalate nephrolithiasis. *Urological Research* **31**, 242-256, (2003).

2 Asplin, J. R. Hyperoxaluric calcium nephrolithiasis. *Endocrinology and Metabolism Clinics of North America* **31**, 927-949 (2002).

3 Sedaghat, A. & Grundy, S. M. Cholesterol Crystals and the Formation of Cholesterol Gallstones. *New England Journal of Medicine* **302**, 1274-1277, (1980).

4 Admirand, W. H. & Small, D. M. The physicochemical basis of cholesterol gallstone formation in man. *Journal of Clinical Investigation* **47**, 1043-1052 (1968).

5 Lim, R. S., Suhalim, J. L., Miyazaki-Anzai, S., Miyazaki, M., Levi, M., Potma, E. O. & Tromberg, B. J. Identification of cholesterol crystals in plaques of atherosclerotic mice using hyperspectral CARS imaging. *Journal of Lipid Research* **52**, (2011).

6 Grebe, A. & Latz, E. Cholesterol Crystals and Inflammation. *Current Rheumatology Reports* **15**, 1-7, (2013).

7 Francis, S. E., Sullivan, D. J. & Goldberg, D. E. Hemoglobin metabolism in the malaria parasite Plasmodium falciparum. *Annual Review of Microbiology* **51**, 97-123 (1997).

8 Pagola, S., Stephens, P. W., Bohle, D. S., Kosar, A. D. & Madsen, S. K. The structure of malaria pigment b-haematin. *Nature* **404**, 307-310 (2000).

9 De Yoreo, J. J., Gilbert, P. U., Sommerdijk, N. A., Penn, R. L., Whitelam, S., Joester, D., Zhang, H., Rimer, J. D., Navrotsky, A. & Banfield, J. F. Crystallization by particle attachment in synthetic, biogenic, and geologic environments. *Science* **349**, aaa6760 (2015).

10 Markov, I. V. *Crystal growth for beginners: fundamentals of nucleation, crystal growth and epitaxy*. (World Scientific, 2003).

11 Burton, W.-K., Cabrera, N. & Frank, F. The growth of crystals and the equilibrium structure of their surfaces. *Philosophical Transactions of the Royal Society of London A: Mathematical, Physical and Engineering Sciences* **243**, 299-358 (1951).

12 Olafson, K. N., Li, R., Alamani, B. G. & Rimer, J. D. Engineering Crystal Modifiers: Bridging Classical and Nonclassical Crystallization. *Chemistry of Materials*, (2016).

13 Chernov, A. A. *Modern Crystallography III, Crystal Growth*. (Springer, 1984).

14 Vekilov, P., Kuznetsov, Y. G. & Chernov, A. Interstep interaction in solution growth;(101) ADP face. *Journal of Crystal Growth* **121**, 643-655 (1992).

15 Vekilov, P. G. What determines the rate of growth of crystals from solution? *Crystal Growth and Design* **7**, 2796-2810 (2007).

16 Olafson, K. N., Ketchum, M. A., Rimer, J. D. & Vekilov, P. G. Molecular Mechanisms of Hematin Crystallization from Organic Solvent. *Crystal Growth & Design* **15**, 5535-5542, (2015).

17 Sazaki, G., Zepeda, S., Nakatsubo, S., Yokoyama, E. & Furukawa, Y. Elementary steps at the surface of ice crystals visualized by advanced optical microscopy. *Proceedings of the National Academy of Sciences* **107**, 19702-19707 (2010).

18 Murshed, M. & McKee, M. D. Molecular determinants of extracellular matrix mineralization in bone and blood vessels. *Current Opinion in Nephrology and Hypertension* **19**, 359-365 (2010).

19 Shi, J. & Wang, X. Functional semiconductor nanowires via vapor deposition. *Journal of Vacuum Science & Technology B* **29**, 060801 (2011).

20 Rimer, J. D., An, Z., Zhu, Z., Lee, M. H., Goldfarb, D. S., Wesson, J. A. & Ward, M. D. Crystal growth inhibitors for the prevention of L-cystine kidney stones through molecular design. *Science* **330**, 337-341 (2010).

21 Chung, J., Granja, I., Taylor, M. G., Mpourmpakis, G., Asplin, J. R. & Rimer, J. D. Molecular modifiers reveal a mechanism of pathological crystal growth inhibition. *Nature*, 1-5 (2016).

22 Teng, H. H., Dove, P. M. & De Yoreo, J. J. Kinetics of calcite growth: surface processes and relationships to macroscopic rate laws. *Geochimica et Cosmochimica Acta* **64**, 2255-2266 (2000).

23 Reviakine, I., Georgiou, D. K. & Vekilov, P. G. Capillarity effects on crystallization kinetics: insulin. *Journal of the American Chemical Society* **125**, 11684-11693 (2003).

24 Yucelen, G. I., Kang, D.-Y., Guerrero-Ferreira, R. C., Wright, E. R., Beckham, H. W. & Nair, S. Shaping single-walled metal oxide nanotubes from precursors of controlled curvature. *Nano Letters* **12**, 827-832 (2012).

25 Gower, L. B. & Odom, D. J. Deposition of calcium carbonate films by a polymer-induced liquid-precursor (PILP) process. *Journal of Crystal Growth* **210**, 719-734 (2000).

26 Gong, Y. U., Killian, C. E., Olson, I. C., Appathurai, N. P., Amasino, A. L., Martin, M. C., Holt, L. J., Wilt, F. H. & Gilbert, P. Phase transitions in biogenic amorphous calcium carbonate. *Proceedings of the National Academy of Sciences* **109**, 6088-6093 (2012).

27 Lupulescu, A. I. & Rimer, J. D. In situ imaging of silicalite-1 surface growth reveals the mechanism of crystallization. *Science* **344**, 729-732 (2014).

28 Ren, N., Subotić, B., Bronić, J., Tang, Y., Dutour Sikirić, M., Mišić, T., Svetličić, V., Bosnar, S. & Antonić Jelić, T. Unusual pathway of crystallization of zeolite ZSM-5 in a heterogeneous system: phenomenology and starting considerations. *Chemistry of Materials* **24**, 1726-1737 (2012).

29 Kumar, M., Luo, H., Román-Leshkov, Y. & Rimer, J. D. SSZ-13 crystallization by particle attachment and deterministic pathways to crystal size control. *Journal of the American Chemical Society* **137**, 13007-13017 (2015).

30 Qiu, S., Wierzbicki, A., Orme, C., Cody, A., Hoyer, J., Nancollas, G., Zepeda, S. & De Yoreo, J. Molecular modulation of calcium oxalate crystallization by osteopontin and citrate. *Proceedings of the National Academy of Sciences* **101**, 1811-1815 (2004).

31 Risthaus, P., Bosbach, D., Becker, U. & Putnis, A. Barite scale formation and dissolution at high ionic strength studied with atomic force microscopy. *Colloids and Surfaces A: Physicochemical and Engineering Aspects* **191**, 201-214 (2001).

32 Andersson, M., Dobberschütz, S., Sand, K., Tobler, D., De Yoreo, J. & Stipp, S. A Microkinetic Model of Calcite Step Growth. *Angewandte Chemie* **128**, 11252-11256 (2016).

33 Estroff, L. A. Introduction: biomineralization. *Chemical Reviews* **108**, 4329-4331 (2008).

34 Aizenberg, J., Albeck, S., Weiner, S. & Addadi, L. Crystal-protein interactions studied by overgrowth of calcite on biogenic skeletal elements. *Journal of Crystal Growth* **142**, 156-164 (1994).

35 Leed, A., DuBay, K., Ursos, L. M. B., Sears, D., de Dios, A. C. & Roepe, P. D. Solution Structures of Antimalarial Drug−Heme Complexes†. *Biochemistry* **41**, 10245-10255, (2002).

36 Schaber, S. D., Gerogiorgis, D. I., Ramachandran, R., Evans, J. M., Barton, P. I. & Trout, B. L. Economic analysis of integrated continuous and batch pharmaceutical manufacturing: a case study. *Industrial & Engineering Chemistry Research* **50**, 10083-10092 (2011).

37 Durbin, S. D., Carlson, W. E. & Saros, M. In situ studies of protein crystal growth by atomic force microscopy. *Journal of Physics D: Applied Physics* **26**, B128 (1993).

38 Kumar, M., Li, R. & Rimer, J. D. Assembly and Evolution of Amorphous Precursors in Zeolite L Crystallization. *Chemistry of Materials* **28**, 1714-1727 (2016).

39 Greenwood, B. Progress in malaria control in endemic areas. *Travel Medicine and Infectious Disease* **6**, 173-176, (2008).

40 WHO. World Malaria Report 2013. *World Health Organization, Geneva* (2013.).

41 Florens, L., Washburn, M. P., Raine, J. D., Anthony, R. M., Grainger, M., Haynes, J. D., Moch, J. K., Muster, N., Sacci, J. B., Tabb, D. L., Witney, A. A., Wolters, D., Wu, Y., Gardner, M. J., Holder, A. A., Sinden, R. E., Yates, J. R. & Carucci, D. J. A proteomic view of the Plasmodium falciparum life cycle. *Nature* **419**, 520-526, (2002).

42 Garnham, P., Wernsdorfer, W. & McGregor, I. Malaria parasites of man: life-cycles and morphology (excluding ultrastructure). *Malaria: principles and practice of malariology. Volume 1.*, 61-96 (1988).

43 Cowman, A. F. & Crabb, B. S. Invasion of Red Blood Cells by Malaria Parasites. *Cell* **124**, 755-766, (2006).

44 Miller, L. H., Baruch, D. I., Marsh, K. & Doumbo, O. K. The pathogenic basis of malaria. *Nature* **415**, 673-679 (2002).

45 Pisciotta, J. M., Coppens, I., Tripathi, A. K., Scholl, P. F., Shuman, J., Bajad, S., Shulaev, V. & Sullivan, D. J., Jr. The role of neutral lipid nanospheres in Plasmodium falciparum haem crystallization. *Biochemical Journal* **402**, 197-204, (2007).

46 Sullivan, D. Theories on malaria pigment formation and quinoline action. *International Journal for Parasitology* **32**, 1645-1653 (2002).

47 Haynes, R. K., Cheu, K.-W., Li, K.-Y., Tang, M. M.-K., Wong, H.-N., Chen, M.-J., Guo, Z.-F., Guo, Z.-H., Coghi, P. & Monti, D. A Partial Convergence in Action of Methylene Blue and Artemisinins: Antagonism with Chloroquine, a Reversal with Verapamil, and an Insight into the Antimalarial Activity of

Chloroquine. *ChemMedChem* **6**, 1603-1615, doi:10.1002/cmdc.201100184 (2011).

48 Aweeka, F. T. & German, P. I. Clinical pharmacology of artemisinin-based combination therapies. *Clinical Pharmacokinetics* **47**, 91+ (2008).

49 Sanchez, C. P., Dave, A., Stein, W. D. & Lanzer, M. Transporters as mediators of drug resistance in Plasmodium falciparum. *International Journal for Parasitology* **40**, 1109-1118, (2010).

50 Ridley, R. G. Medical need, scientific opportunity and the drive for antimalarial drugs. *Nature* **415**, 686-693 (2002).

51 Phyo, A. P., Nkhoma, S., Stepniewska, K., Ashley, E. A., Nair, S., McGready, R., ler Moo, C., Al-Saai, S., Dondorp, A. M., Lwin, K. M., Singhasivanon, P., Day, N. P. J., White, N. J., Anderson, T. J. C. & Nosten, F. Emergence of artemisinin-resistant malaria on the western border of Thailand: a longitudinal study. *Lancet* **379**, 1960-1966, (2012).

52 Kappe, S. H., Vaughan, A. M., Boddey, J. A. & Cowman, A. F. That was then but this is now: malaria research in the time of an eradication agenda. *Science* **328**, 862-866, (2010).

53 Chatterjee, S., Tanabe, K. & Nodiff, E. A. In search of next generation antimalarials. *Bioorganic & Medicinal Chemistry Letters* **24**, 4106-4109 (2014).

54 Ketchum, M. A., Olafson, K. N., Petrova, E. V., Rimer, J. D. & Vekilov, P. G. Hematin crystallization from aqueous and organic solvents. *Journal of Chemical Physics* **139**, (2013).

55 Chong, C. R., Chen, X., Shi, L., Liu, J. O. & Sullivan, D. J. A clinical drug library screen identifies astemizole as an antimalarial agent. *Nature Chemical Biology* **2**, 415-416, (2006).

56 Johnston, D. E. & Kaplan, M. M. Pathogenesis and treatment of gallstones. *New England Journal of Medicine* **328**, 412-421 (1993).

57 LaMont, J. & Carey, M. Cholesterol gallstone formation. 2. Pathobiology and pathomechanics. *Progress in liver diseases* **10**, 165 (1992).

58 Everhart, J. E., Khare, M., Hill, M. & Maurer, K. R. Prevalence and ethnic differences in gallbladder disease in the United States. *Gastroenterology* **117**, 632-639 (1999).

59 Sandler, R. S., Everhart, J. E., Donowitz, M., Adams, E., Cronin, K., Goodman, C., Gemmen, E., Shah, S., Avdic, A. & Rubin, R. The burden of selected digestive diseases in the United States. *Gastroenterology* **122**, 1500-1511 (2002).

60 Kalser, S. NATIONAL-INSTITUTES-OF-HEALTH CONSENSUS DEVELOPMENT CONFERENCE STATEMENT ON GALLSTONES AND LAPAROSCOPIC CHOLECYSTECTOMY. *American Journal of Surgery* **165**, 390-398 (1993).

61 DABNEY, W. O. ART. XI-The Use of Choleate of Soda to prevent the formation of Gall-Stones. *The American Journal of the Medical Sciences* **142**, 410-412 (1876).

62 Rewbridge, A. G. The disappearance of gallstone shadows following the prolonged administration of bile salts. *Surgery* **1**, 62 (1937).

63 Sauerbruch, T., Delius, M., Paumgartner, G., Holl, J., Wess, O., Weber, W., Hepp, W. & Brendel, W. Fragmentation of gallstones by extracorporeal shock waves. *New England Journal of Medicine* **314**, 818-822 (1986).

64 Mouret, P. Celioscopic surgery. Evolution or revolution? *Chirurgie; mémoires de l'Académie de chirurgie* **116**, 829 (1990).

65 Danzinger, R. G., Hofmann, A. F., Schoenfield, L. J. & Thistle, J. L. Dissolution of cholesterol gallstones by chenodeoxycholic acid. *New England Journal of Medicine* **286**, 1-8 (1972).

66 Makino, I., Shinozaki, K., Yoshino, K. & Nakagawa, S. Dissolution of cholesterol gallstones by long-term administration of ursodeoxycholic acid. *Nihon Shokakibyo Gakkai zasshi= The Japanese journal of gastro-enterology* **72**, 690 (1975).

67 Libby, P., Ridker, P. M. & Maseri, A. Inflammation and atherosclerosis. *Circulation* **105**, 1135-1143 (2002).

68 Rocha, V. Z. & Libby, P. Obesity, inflammation, and atherosclerosis. *Nature Reviews Cardiology* **6**, 399-409 (2009).

69 Libby, P., Okamoto, Y., Rocha, V. Z. & Folco, E. Inflammation in atherosclerosis: transition from theory to practice. *Circulation Journal* **74**, 213-220 (2010).

70 Lloyd-Jones, D., Adams, R., Carnethon, M., De Simone, G., Ferguson, T. B., Flegal, K., Ford, E., Furie, K., Go, A. & Greenlund, K. Heart disease and stroke statistics—2009 update a report from the American Heart Association Statistics

Committee and Stroke Statistics Subcommittee. *Circulation* **119**, e21-e181 (2009).

71 Heidenreich, P. A., Trogdon, J. G., Khavjou, O. A., Butler, J., Dracup, K., Ezekowitz, M. D., Finkelstein, E. A., Hong, Y., Johnston, S. C. & Khera, A. Forecasting the future of cardiovascular disease in the United States a policy statement from the American heart association. *Circulation* **123**, 933-944 (2011).

72 Endo, A. A historical perspective on the discovery of statins. *Proceedings of the Japan Academy, Series B* **86**, 484-493 (2010).

73 Hirsch, A. T., Hartman, L., Town, R. J. & Virnig, B. A. National health care costs of peripheral arterial disease in the Medicare population. *Vascular Medicine* **13**, 209-215 (2008).

74 Davidson, M. H. Overview of prevention and treatment of atherosclerosis with lipid-altering therapy for pharmacy directors. *The American journal of managed care* **13**, S260-269 (2007).

75 Portincasa, P., Moschetta, A., Mazzone, A., Palasciano, G., Svelto, M. & Calamita, G. Water handling and aquaporins in bile formation: recent advances and research trends. *Journal of hepatology* **39**, 864-874 (2003).

76 Saad, H. Y. & Higuchi, W. I. Water solubility of cholesterol. *Journal of pharmaceutical sciences* **54**, 1205-1206 (1965).

77 Marieb, E. N. & Hoehn, K. *Human anatomy & physiology*. (Pearson Education, 2007).

78 Power, H. J. History of malaria. *eLS* (2001).

79 Greenwood, B. M., Fidock, D. A., Kyle, D. E., Kappe, S. H., Alonso, P. L., Collins, F. H. & Duffy, P. E. Malaria: progress, perils, and prospects for eradication. *The Journal of clinical investigation* **118**, 1266-1276 (2008).

80 Dondorp, A. M., Kager, P. A., Vreeken, J. & White, N. J. Abnormal Blood Flow and Red Blood Cell Deformability in Severe Malaria. *Parasitology Today* **16**, 228-232, (2000).

81 Idro, R., Marsh, K., John, C. C. & Newton, C. R. Cerebral malaria: mechanisms of brain injury and strategies for improved neurocognitive outcome. *Pediatric Research* **68**, 267-274 (2010).

82 Wongsrichanalai, C., Barcus, M. J., Muth, S., Sutamihardja, A. & Wernsdorfer, W. H. A review of malaria diagnostic tools: microscopy and rapid diagnostic test (RDT). *The American Journal of Tropical Medicine and Hygiene* **77**, 119-127 (2007).

83 Moody, A. Rapid diagnostic tests for malaria parasites. *Clinical Microbiology Reviews* **15**, 66-78 (2002).

84 Cooke, A. H., Moody, A., Lemon, K., Chiodini, P. & Horton, J. Use of the fluorochrome benzothiocarboxypurine in malaria diagnosis. *Transactions of the Royal Society of Tropical Medicine and Hygiene* **86**, 378 (1992).

85 Peyron, F., Martet, G. & Vigier, J. Dipstick antigen-capture assay for malaria detection. *The Lancet* **343**, 1502-1503 (1994).

86 Singh, N., Valecha, N. & Sharma, V. Malaria diagnosis by field workers using an immunochromatographic test. *Transactions of the Royal Society of Tropical Medicine and Hygiene* **91**, 396-397 (1997).

87 Piper, R., Vanderjagt, D., Holbrook, J. & Makler, M. Malaria lactate dehydrogenase: target for diagnosis and drug development. *Annals of Tropical Medicine and Parasitology* **90**, 433 (1996).

88 Rock, E., Marsh, K., Saul, A., Wellems, T., Taylor, D. W., Maloy, W. & Howard, R. Comparative analysis of the Plasmodium falciparum histidine-rich proteins HRP-I, HRP-II and HRP-III in malaria parasites of diverse origin. *Parasitology* **95**, 209-227 (1987).

89 Makler, M., Piper, R. & Milhous, W. Lactate dehydrogenase and the diagnosis of malaria. *Parasitology Today* **14**, 376-377 (1998).

90 Meier, B., Döbeli, H. & Certa, U. Stage-specific expression of aldolase isoenzymes in the rodent malaria parasite Plasmodium berghei. *Molecular and Biochemical Parasitology* **52**, 15-27 (1992).

91 Wyler, D. J. Malaria—resurgence, resistance, and research. *New England Journal of Medicine* **308**, 875-878 (1983).

92 Zucker, J. R. Changing patterns of autochthonous malaria transmission in the United States: a review of recent outbreaks. *Emerging Infectious Diseases* **2**, 37 (1996).

93 Kager, P. Malaria control: constraints and opportunities. *Tropical Medicine and International Health* **7**, 1042-1046 (2002).

94 Wallace, D. The history of antimalarials. *Lupus* **5**, S2-S3 (1996).

95 Achan, J., Talisuna, A. O., Erhart, A., Yeka, A., Tibenderana, J. K., Baliraine, F. N., Rosenthal, P. J. & D'Alessandro, U. Quinine, an old anti-malarial drug in a modern world: role in the treatment of malaria. *Malaria Journal* **10**, 1 (2011).

96 Rosenthal, P. J. *Antimalarial chemotherapy: mechanisms of action, resistance, and new directions in drug discovery*. (Springer Science & Business Media, 2001).

97 Salako, L. & Sowunmi, A. Disposition of quinine in plasma, red blood cells and saliva after oral and intravenous administration to healthy adult Africans. *European Journal of Clinical Pharmacology* **42**, 171-174 (1992).

98 Wellems, T. E. & Plowe, C. V. Chloroquine-resistant malaria. *Journal of Infectious Diseases* **184**, 770-776 (2001).

99 Klayman, D. L. Qinghaosu (artemisinin): an antimalarial drug from China. *Science* **228**, 1049-1055 (1985).

100 Meshnick, S. R. Artemisinin: mechanisms of action, resistance and toxicity. *International Journal for Parasitology* **32**, 1655-1660, (2002).

101 Targett, G., Drakeley, C., Jawara, M., von Seidlein, L., Coleman, R., Deen, J., Pinder, M., Doherty, T., Sutherland, C. & Walraven, G. Artesunate reduces but does not prevent posttreatment transmission of Plasmodium falciparum to Anopheles gambiae. *Journal of Infectious Diseases* **183**, 1254-1259 (2001).

102 Brossi, A., Venugopalan, B., Dominguez Gerpe, L., Yeh, H., Flippen-Anderson, J., Buchs, P., Luo, X., Milhous, W. & Peters, W. Arteether, a new antimalarial drug: synthesis and antimalarial properties. *Journal of Medicinal Chemistry* **31**, 645-650 (1988).

103 Antimalarials, C. Chemical studies on qinghaosu (artemisinine). *J. Tradit. Chin. Med* **2**, 3-8 (1972).

104 Halliwell, B. & Gutteridge, J. in *Free radicals in biology and medicine* 351-425 (Oxford University Press Oxford, 1999).

105 Krungkrai, S. R. & Yuthavong, Y. The antimalarial action on Plasmodium falciparum of qinghaosu and artesunate in combination with agents which modulate oxidant stress. *Transactions of the Royal Society of Tropical Medicine and Hygiene* **81**, 710-714 (1987).

106 Pandey, A. V., Tekwani, B. L., Singh, R. L. & Chauhan, V. S. Artemisinin, an endoperoxide antimalarial, disrupts the hemoglobin catabolism and heme detoxification systems in malarial parasite. *Journal of Biological Chemistry* **274**, 19383-19388 (1999).

107 White, N. Assessment of the pharmacodynamic properties of antimalarial drugs in vivo. *Antimicrobial Agents and Chemotherapy* **41**, 1413 (1997).

108 Meshnick, S. R., Thomas, A., Ranz, A., Xu, C.-M. & Pan, H.-Z. Artemisinin (qinghaosu): the role of intracellular hemin in its mechanism of antimalarial action. *Molecular and Biochemical Parasitology* **49**, 181-189 (1991).

109 Phyo, A. P., Nkhoma, S., Stepniewska, K., Ashley, E. A., Nair, S., McGready, R., ler Moo, C., Al-Saai, S., Dondorp, A. M. & Lwin, K. M. Emergence of artemisinin-resistant malaria on the western border of Thailand: a longitudinal study. *The Lancet* **379**, 1960-1966 (2012).

110 Dondorp, A. M., Nosten, F., Yi, P., Das, D., Phyo, A. P., Tarning, J., Lwin, K. M., Ariey, F., Hanpithakpong, W. & Lee, S. J. Artemisinin resistance in Plasmodium falciparum malaria. *New England Journal of Medicine* **361**, 455-467 (2009).

111 Noedl, H., Se, Y., Schaecher, K., Smith, B. L., Socheat, D. & Fukuda, M. M. Evidence of artemisinin-resistant malaria in western Cambodia. *New England Journal of Medicine* **359**, (2008).

112 Ashley, E. A., Dhorda, M., Fairhurst, R. M., Amaratunga, C., Lim, P., Suon, S., Sreng, S., Anderson, J. M., Mao, S. & Sam, B. Spread of artemisinin resistance in Plasmodium falciparum malaria. *New England Journal of Medicine* **371**, 411-423 (2014).

113 Takala-Harrison, S., Jacob, C. G., Arze, C., Cummings, M. P., Silva, J. C., Dondorp, A. M., Fukuda, M. M., Hien, T. T., Mayxay, M. & Noedl, H. Independent emergence of artemisinin resistance mutations among Plasmodium falciparum in Southeast Asia. *Journal of Infectious Diseases* **211**, 670-679 (2015).

114 D'alessandro, U. & Buttiens, H. History and importance of antimalarial drug resistance. *Tropical Medicine and International Health* **6**, 845-848 (2001).

115 Olliaro, P., Nevill, C., LeBras, J., Ringwald, P., Mussano, P., Garner, P. & Brasseur, P. Systematic review of amodiaquine treatment in uncomplicated malaria. *The Lancet* **348**, 1196-1201 (1996).

116 Wongsrichanalai, C., Pickard, A. L., Wernsdorfer, W. H. & Meshnick, S. R. Epidemiology of drug-resistant malaria. *The Lancet infectious diseases* **2**, 209-218 (2002).

117 Chen, M. M., Shi, L. & Sullivan, D. J. Haemoproteus and Schistosoma synthesize heme polymers similar

to Plasmodium hemozoin and b-hematin. *Molecular and Biochemical Parasitology* **113**, 1-8 (2001).

118 Weissbuch, I. & Leiserowitz, L. Interplay Between Malaria, Crystalline Hemozoin Formation, and Antimalarial Drug Action and Design. *Chemical Reviews* **108**, 4899-4914, (2008).

119 Slater, A. F. G., Swiggard, W. J., Orton, B. R., Flitter, W. D., Goldberg, D. E., Cerami, A. & Henderson, G. B. An iron-carboxylate bond links the heme units of malaria pigment. *Proceedings of the National Academy of Science* **88**, 325-329 (1991).

120 Adams, P. A., Berman, P. A. M., Egan, T. J., Marsh, P. J. & Silver, J. The iron environment in heme and heme-antimalarial complexes of pharmacological interest. *Journal of Inorganic Biochemistry* **63**, 69-77, (1996).

121 Egan, T. J., Mavuso, W. W. & Ncokazi, K. K. The Mechanism of β-Hematin Formation in Acetate Solution. Parallels between Hemozoin Formation and Biomineralization Processes†. *Biochemistry* **40**, 204-213, (2000).

122 Egan, T. J. Haemozoin formation. *Molecular and Biochemical Parasitology* **157**, 127-136, (2008).

123 Ambele, M. A., Sewell, B. T., Cummings, F. R., Smith, P. J. & Egan, T. J. Synthetic Hemozoin (β-Hematin) Crystals Nucleate at the Surface of Neutral Lipid Droplets that Control Their Sizes. *Crystal Growth & Design* **13**, 4442-4452, (2013).

124 Gildenhuys, J., Roex, T. l., Egan, T. J. & de Villiers, K. A. The Single Crystal X-ray Structure of β-Hematin DMSO Solvate Grown in the Presence of Chloroquine, a β-Hematin Growth-Rate Inhibitor. *Journal of the American Chemical Society* **135**, 1037-1047, (2012).

125 Pisciotta, J. M. & Sullivan, D. Hemozoin: oil versus water. *Parasitology International* **57**, 89-96, (2008).

126 Kapishnikov, S., Weiner, A., Shimoni, E., Guttmann, P., Schneider, G., Dahan-Pasternak, N., Dzikowski, R., Leiserowitz, L. & Elbauma, M. Oriented nucleation of hemozoin at the digestive vacuole membrane in Plasmodium falciparum. *Proceedings of the National Academy of Science* **109**, 11188-11193, (2012).

127 Egan, T. J., Chen, J. Y. J., de Villiers, K. A., Mabotha, T. E., Naidoo, K. J., Ncokazi, K. K., Langford, S. J., McNaughton, D., Pandiancherri, S. & Wood, B. R. Haemozoin (β-haematin) biomineralization occurs by self-assembly near the lipid/water interface. *FEBS Letters* **580**, 5105-5110, (2006).

128 Berlin, E. & Sainz, E. Acyl chain interactions and the modulation of phase changes in glycerolipids. *Biochimica et Biophysica Acta (BBA) - Biomembranes* **855**, 1-7, (1986).

129 Hoang, A. N., Sandlin, R. D., Omar, A., Egan, T. J. & Wright, D. W. The Neutral Lipid Composition Present in the Digestive Vacuole of Plasmodium falciparum Concentrates Heme and Mediates β-Hematin Formation with an Unusually Low Activation Energy. *Biochemistry* **49**, 10107-10116, (2010).

130 Hayward, R., Saliba, K. J. & Kirk, K. The pH of the digestive vacuole of Plasmodium falciparum is not associated with chloroquine resistance. *Journal of Cell Science* **119**, 1016-1025, (2006).

131 Gligorijevic, B., McAllister, R., Urbach, J. S. & Roepe, P. D. Spinning Disk Confocal Microscopy of Live, Intraerythrocytic Malarial Parasites. 1.

Quantification of Hemozoin Development for Drug Sensitive versus Resistant Malaria. *Biochemistry* **45**, 12400-12410, (2006).

132 Šegatin, N. & Klofutar, C. Thermodynamics of the Solubility of Water in 1-Hexanol, 1-Octanol, 1-Decanol, and Cyclohexanol. *Monatshefte für Chemie/Chemical Monthly* **135**, 241-248, (2003).

133 Pagola, S., Stephens, P. W., Bohle, D. S., Kosar, A. D. & Madsen, S. K. The structure of malaria pigment β-haematin. *Nature* **404** 307-310 (2000).

134 Olafson, K. N., Ketchum, M. A., Rimer, J. D. & Vekilov, P. G. Mechanisms of hematin crystallization and inhibition by the antimalarial drug chloroquine. *Proceedings of the National Academy of Sciences* **112**, 4946-4951, (2015).

135 Ncokazi, K. K. & Egan, T. J. A colorimetric high-throughput β-hematin inhibition screening assay for use in the search for antimalarial compounds. *Analytical Biochemistry* **338**, 306-319, (2005).

136 Marques, H. M., Munro, O. Q. & Crawcour, M. L. Coordination of N-donor ligands by hematohemin. *Inorganica Chimica Acta* **196**, 221-229, (1992).

137 Chong, C. R. & Sullivan Jr, D. J. Inhibition of heme crystal growth by antimalarials and other compounds: implications for drug discovery. *Biochemical Pharmacology* **66**, 2201-2212, (2003).

138 Egan, T. J., Ross, D. C. & Adams, P. A. Quinoline anti-malarial drugs inhibit spontaneous formation of β-haematin (malaria pigment). *FEBS Letters* **352**, 54-57, (1994).

139 Farmanesh, S., Ramamoorthy, S., Chung, J., Asplin, J. R., Karande, P. & Rimer, J. D. Specificity of Growth Inhibitors and their Cooperative Effects in Calcium

Oxalate Monohydrate Crystallization. *Journal of the American Chemical Society* **136**, 367-376, (2014).

140 Farmanesh, S., Chung, J., Sosa, R. D., Kwak, J. H., Karande, P. & Rimer, J. D. Natural Promoters of Calcium Oxalate Monohydrate Crystallization. *Journal of the American Chemical Society* **136**, 12648-12657, (2014).

141 Pillay, S. N., Asplin, J. R. & Coe, F. L. Evidence that calgranulin is produced by kidney cells and is an inhibitor of calcium oxalate crystallization. *American Journal of Physiology - Renal Physiology* **275**, F255-F261 (1998).

142 Muñoz, J. A. & Valiente, M. Effects of trace metals on the inhibition of calcium oxalate crystallization. *Urological Research* **33**, 267-272, (2005).

143 Gunthorpe, M. E., Sikes, C. S. & Wheeler, A. P. Promotion and Inhibition of Calcium Carbonate Crystallization In Vitro by Matrix Protein From Blue Crab Exoskeleton. *The Biological Bulletin* **179**, 191-200 (1990).

144 O'Neill, P. M., Barton, V. E. & Ward, S. A. The Molecular Mechanism of Action of Artemisinin—The Debate Continues. *Molecules* **15**, (2010).

145 Fu, G., Qiu, S. R., Orme, C. A., Morse, D. E. & De Yoreo, J. J. Acceleration of calcite kinetics by abalone nacre proteins. *Advanced Materials* **17**, 2678-2683 (2005).

146 Elhadj, S., De Yoreo, J., Hoyer, J. & Dove, P. Role of molecular charge and hydrophilicity in regulating the kinetics of crystal growth. *Proceedings of the National Academy of Sciences* **103**, 19237-19242 (2006).

147 Petsev, D. N., Chen, K., Gliko, O. & Vekilov, P. G. Diffusion-limited kinetics of the solution-solid phase transition of molecular substances. *Proc. Natl. Acad. Sci. USA* **100**, 792-796 (2003).

148 Vekilov, P. G. What Is the Molecular-Level Role of the Solution Components in Protein Crystallization? *Cryst. Growth Des.* **7**, 2239-2246 (2007).

149 Madsen, H. E. L. Influence of foreign metal ions on crystal growth and morphology of brushite (CaHPO 4, 2H 2 O) and its transformation to octacalcium phosphate and apatite. *Journal of Crystal Growth* **310**, 2602-2612 (2008).

150 Wasylenki, L. E., Dove, P. M., Wilson, D. S. & De Yoreo, J. J. Nanoscale effects of strontium on calcite growth: An in situ AFM study in the absence of vital effects. *Geochimica et Cosmochimica Acta* **69**, 3017-3027 (2005).

151 Hawley, S. R., Bray, P. G., Mungthin, M., Atkinson, J. D., O'Neill, P. M. & Ward, S. A. Relationship between Antimalarial Drug Activity, Accumulation, and Inhibition of Heme Polymerization in Plasmodium falciparum In Vitro. *Antimicrobial Agents and Chemotherapy* **42**, 682-686 (1998).

152 Dorn, A., Vippagunta, S. R., Matile, H., Jaquet, C., Vennerstrom, J. L. & Ridley, R. G. An Assessment of Drug-Haematin Binding as a Mechanism for Inhibition of Haematin Polymerisation by Quinoline Antimalarials. *Biochemical Pharmacology* **55**, 727-736, (1998).

153 Elueze, E. I., Croft, S. L. & Warhurst, D. C. Activity of pyronaridine and mepacrine against twelve strains of Plasmodium falciparum in vitro. *Journal of Antimicrobial Chemotherapy* **37**, 511-518, (1996).

154 Pradines, B., Spiegel, A., Rogier, C., Tall, A., Mosnier, J., Fusai, T., Trape, J. F. & Parzy, D. Antibiotics for prophylaxis of Plasmodium falciparum infections: in vitro activity of doxycycline against Senegalese isolates. *The American Journal of Tropical Medicine and Hygiene* **62**, 82-85 (2000).

155 Vippagunta, S. R., Dorn, A., Bubendorf, A., Ridley, R. G. & Vennerstrom, J. L. Deferoxamine: Stimulation of hematin polymerization and antagonism of its inhibition by chloroquine. *Biochemical Pharmacology* **58**, 817-824, (1999).

156 Pradines, B., Briolant, S., Henry, M., Oeuvray, C., Baret, E., Amalvict, R., Didillon, E. & Rogier, C. Absence of association between pyronaridine in vitro responses and polymorphisms in genes involved in quinoline resistance in Plasmodium falciparum. *Malaria Journal* **9**, 1-7, (2010).

157 Wongsrichanalai, C., The Dung, N., Nguyen Trung, T., Wimonwattrawatee, T., Sookto, P., Gray Heppner, D. & Kawamoto, F. In vitro susceptibility of Plasmodium falciparum isolates in Vietnam to artemisinin derivatives and other antimalarials. *Acta Tropica* **63**, 151-158, (1997).

158 Dorn, A., Vippagunta, S. R., Matile, H., Bubendorf, A., Vennerstrom, J. L. & Ridley, R. G. A Comparison and Analysis of Several Ways to Promote Haematin (Haem) Polymerisation and an Assessment of Its Initiation In Vitro. *Biochemical Pharmacology* **55**, 737-747, (1998).

159 Basco, L. K., Gillotin, C., Gimenez, F., Farinotti, R. & Le Bras, J. In vitro activity of the enantiomers of mefloquine, halofantrine and enpiroline against Plasmodium falciparum. *British Journal of Clinical Pharmacology* **33**, 517-520, (1992).

160 Phyo, A. P., Nkhoma, S., Stepniewska, K., Ashley, E. A., Nair, S., McGready, R., ler Moo, C., Al-Saai, S., Dondorp, A. M., Lwin, K. M., Singhasivanon, P., Day, N. P. J., White, N. J., Anderson, T. J. C. & Nosten, F. Emergence of artemisinin-resistant malaria on the western border of Thailand: a longitudinal study. *The Lancet* **379**, 1960-1966 (2012).

161 Mberu, E. K., Mosobo, M. K., Nzila, A. M., Kokwaro, G. O., Sibley, C. H. & Watkins, W. M. The changing in vitro susceptibility pattern to pyrimethamine/sulfadoxine in Plasmodium falciparum field isolates from Kilifi, Kenya. *The American Journal of Tropical Medicine and Hygiene* **62**, 396-401 (2000).

162 Gordon‐Taylor, G. On gall‐stones and their sufferers. *British Journal of Surgery* **25**, 241-251 (1937).

163 Shehadi, W. The biliary system through the ages. *International surgery* **64**, 63 (1979).

164 Thompson, R. C., Allam, A. H., Lombardi, G. P., Wann, L. S., Sutherland, M. L., Sutherland, J. D., Soliman, M. A.-T., Frohlich, B., Mininberg, D. T. & Monge, J. M. Atherosclerosis across 4000 years of human history: the Horus study of four ancient populations. *The Lancet* **381**, 1211-1222 (2013).

165 Thudichum, J. L. W. *A treatise on gall-stones: their chemistry, pathology, and treatment*. (J. Churchill, 1863).

166 Choban, P. S. Gallstones. *Medical Update for Psychiatrists* **1**, 61-63 (1996).

167 Lamont, J. T., Smith, B. F. & Moore, J. R. Role of gallbladder mucin in pathophysiology of gallstones. *Hepatology* **4** (1984).

168 Portincasa, P., Moschetta, A. & Palasciano, G. Cholesterol gallstone disease. *The Lancet* **368**, 230-239 (2006).

169 Trotman, B. Pigment gallstone disease. *Gastroenterology Clinics of North America* **20**, 111-126 (1991).

170 Trotman, B. W., Ostrow, J. D., Soloway, R. D., Cheong, E. B. & Longyear, R. B. Pigment vs cholesterol cholelithiasis: comparison of stone and bile composition. *The American journal of digestive Diseases* **19**, 585-590 (1974).

171 Wang, D. & Carey, M. Characterization of crystallization pathways during cholesterol precipitation from human gallbladder biles: identical pathways to corresponding model biles with three predominating sequences. *Journal of Lipid Research* **37**, 2539-2549 (1996).

172 Wang, D. & Carey, M. Complete mapping of crystallization pathways during cholesterol precipitation from model bile: influence of physical-chemical variables of pathophysiologic relevance and identification of a stable liquid crystalline state in cold, dilute and hydrophilic bile salt-containing systems. *Journal of Lipid Research* **37**, 606-630 (1996).

173 Konikoff, F. M., Danino, D., Weihs, D., Rubin, M. & Talmon, Y. Microstructural evolution of lipid aggregates in nucleating model and human biles visualized by cryogenic transmission electron microscopy. *Hepatology* **31**, 261-268 (2000).

174 Ko, C. W., Sekijima, J. H. & Lee, S. P. Biliary sludge. *Annals of internal medicine* **130**, 301-311 (1999).

175 van den Berg, A. A., van Buul, J. D., Ostrow, J. D. & Groen, A. K. Measurement of cholesterol gallstone growth in vitro. *Journal of Lipid Research* **41**, 189-194 (2000).

176 Cabral, D. & Small, D. Physical chemistry of bile: Handbook of Physiology. *American Physiology Society, Bethesda, USA* (1989).

177 French, E. & Robb, W. Biliary and renal colic. *British medical journal* **2**, 135 (1963).

178 THISTLE, J. L., CLEARY, P. A., LACHIN, J. M., TYOR, M. P. & HERSH, T. The natural history of cholelithiasis: the National Cooperative Gallstone Study. *Annals of internal medicine* **101**, 171-175 (1984).

179 Leopold, G. R., Amberg, J., Gosink, B. B. & Mittelstaedt, C. Gray Scale Ultrasonic Cholecystography: A Comparison with Conventional Radiographic Techniques 1. *Radiology* **121**, 445-448 (1976).

180 Kalimi, R., Gecelter, G. R., Caplin, D., Brickman, M., Tronco, G. T., Love, C., Yao, J., Simms, H. H. & Marini, C. P. Diagnosis of acute cholecystitis: sensitivity of sonography, cholescintigraphy, and combined sonography-cholescintigraphy. *Journal of the American College of Surgeons* **193**, 609-613 (2001).

181 Sivak, M. V. Endoscopic management of bile duct stones. *The American Journal of Surgery* **158**, 228-240 (1989).

182 Ransohoff, D. F. & Gracie, W. A. Treatment of gallstones. *Annals of internal medicine* **119**, 606-619 (1993).

183 Langenbuch, C. Ein fall von exstirpation der gallenblase wegen chronischer cholelithiasis. *Klin Wochenschr* **19**, 725 (1882).

184 Magnuson, T. H., Lillemoe, K. D. & Pitt, H. A. How many Americans will be eligible for biliary lithotripsy? *Archives of surgery* **124**, 1195-1200 (1989).

185 Allen, M. J., Borody, T. J., Bugliosi, T. F., May, G. R., LaRusso, N. F. & Thistle, J. L. Rapid dissolution of gallstones by methyl tert-butyl ether: preliminary observations. *New England Journal of Medicine* **312**, 217-220 (1985).

186 Thistle, J. L., May, G. R., Bender, C. E., Williams, H. J., LeRoy, A. J., Nelson, P. E., Peine, C. J., Petersen, B. T. & McCullough, J. E. Dissolution of cholesterol gallbladder stones by methyl tert-butyl ether administered by percutaneous transhepatic catheter. *New England Journal of Medicine* **320**, 633-639 (1989).

187 VanSonnenberg, E., Hofmann, A., Neoptolemus, J., Wittich, G., Princenthal, R. & Willson, S. Gallstone dissolution with methyl-tert-butyl ether via percutaneous cholecystostomy: success and caveats. *American Journal of Roentgenology* **146**, 865-867 (1986).

188 Villanova, N., Bazzoli, F., Taroni, F., Frabboni, R., Mazzella, G., Festi, D., Barbara, L. & Roda, E. Gallstone recurrence after successful oral bile acid treatment: A 12-year follow-up study and evaluation of long-term postdissolution treatment. *Gastroenterology* **97**, 726-731 (1989).

189 Sackmann, M., Niller, H., Klueppelberg, U., Von Ritter, C., Pauletzki, J., Holl, J., Berr, F., Neubrand, M., Sauerbruch, T. & Paumgartner, G. Gallstone recurrence after shock-wave therapy. *GASTROENTEROLOGY-BALTIMORE THEN PHILADELPHIA*- **106**, 225-225 (1994).

190 Blum, C. A. & Adams, D. B. Who did the first laparoscopic cholecystectomy? *Journal of minimal access surgery* **7**, 165 (2011).

191 Polychronidis, A., Laftsidis, P., Bounovas, A. & Simopoulos, C. Twenty years of laparoscopic cholecystectomy: Philippe Mouret-March 17, 1987. *JOURNAL-SOCIETY OF LAPAROENDOSCOPIC SURGEONS* **12**, 109 (2008).

192 Heaton, K., Braddon, F., Mountford, R., Hughes, A. & Emmett, P. Symptomatic and silent gall stones in the community. *Gut* **32**, 316-320 (1991).

193 Attili, A. 225-231 (Raven Press, New York).

194 Bennion, L. J. & Grundy, S. M. Risk factors for the development of cholelithiasis in man. *New England Journal of Medicine* **299**, 1161-1167 (1978).

195 Liddle, R. A., Goldstein, R. B. & Saxton, J. Gallstone formation during weight-reduction dieting. *Archives of internal medicine* **149**, 1750-1753 (1989).

196 Attili, A., Capocaccia, R., Carulli, N., Festi, D., Roda, E., Barbara, L., Capocaccia, L., Menotti, A., Okolicsanyi, L. & Ricci, G. Factors associated with gallstone disease in the MICOL experience. *Hepatology* **26**, 809-818 (1997).

197 Shaffer, E. A. Epidemiology and risk factors for gallstone disease: has the paradigm changed in the 21st century? *Current gastroenterology reports* **7**, 132-140 (2005).

198 Lloyd-Jones, D., Adams, R. J., Brown, T. M., Carnethon, M., Dai, S., De Simone, G., Ferguson, T. B., Ford, E., Furie, K. & Gillespie, C. Heart disease and stroke statistics—2010 update A report from the American Heart Association. *Circulation* **121**, e46-e215 (2010).

199 Badimón, L., Vilahur, G. & Padró, T. Lipoproteínas, plaquetas y aterotrombosis. *Revista española de cardiología* **62**, 1161-1178 (2009).

200 Linton, M. F. & Fazio, S. Macrophages, inflammation, and atherosclerosis. *International Journal of Obesity & Related Metabolic Disorders* **27** (2003).

201 Insull, W. The pathology of atherosclerosis: plaque development and plaque responses to medical treatment. *The American journal of medicine* **122**, S3-S14 (2009).

202 Falk, E. Pathogenesis of atherosclerosis. *Journal of the American College of Cardiology* **47**, C7-C12 (2006).

203 Virmani, R., Kolodgie, F. D., Burke, A. P., Finn, A. V., Gold, H. K., Tulenko, T. N., Wrenn, S. P. & Narula, J. Atherosclerotic plaque progression and vulnerability to rupture angiogenesis as a source of intraplaque hemorrhage. *Arteriosclerosis, thrombosis, and vascular biology* **25**, 2054-2061 (2005).

204 Falk, E. Plaque rupture with severe pre-existing stenosis precipitating coronary thrombosis. Characteristics of coronary atherosclerotic plaques underlying fatal occlusive thrombi. *British heart journal* **50**, 127-134 (1983).

205 Stang, P., Carson, A., Rose, K., Mo, J., Ephross, S., Shahar, E. & Szklo, M. Headache, cerebrovascular symptoms, and stroke The Atherosclerosis Risk in Communities Study. *Neurology* **64**, 1573-1577 (2005).

206 Ross, R. & Glomset, J. A. The pathogenesis of atherosclerosis. *New England Journal of Medicine* **295**, 369-377 (1976).

207 Ibañez, B., Badimon, J. J. & Garcia, M. J. Diagnosis of atherosclerosis by imaging. *The American journal of medicine* **122**, S15-S25 (2009).

208 Teramoto, T., Sasaki, J., Ishibashi, S., Birou, S., Daida, H., Dohi, S., Egusa, G., Hiro, T., Hirobe, K. & Iida, M. Diagnosis of atherosclerosis. *Journal of atherosclerosis and thrombosis* **21**, 296-298 (2014).

209 Guardado, J. H., Vinhas, H., Martins, C., Pereira, E. & Pereira, H. Grave vasoespasmo coronário. *Revista Portuguesa de Cardiologia* **31**, 597-601 (2012).

210 McGill Jr, H. C. in *The Thrombotic Process in Atherogenesis* 273-280 (Springer, 1978).

211 Fruchart, J.-C., Nierman, M. C., Stroes, E. S., Kastelein, J. J. & Duriez, P. New risk factors for atherosclerosis and patient risk assessment. *Circulation* **109**, III-15-III-19 (2004).

212 Tobert, J. A. Lovastatin and beyond: the history of the HMG-CoA reductase inhibitors. *Nature Reviews Drug Discovery* **2**, 517-526 (2003).

213 Faxon, D. P., Weber, V. J., Haudenschild, C., Gottsman, S. B., McGovern, W. A. & Ryan, T. J. Acute effects of transluminal angioplasty in three experimental models of atherosclerosis. *Arteriosclerosis, thrombosis, and vascular biology* **2**, 125-133 (1982).

214 Craven, B. M. Crystal structure of cholesterol monohydrate. (1976).

215 Loomis, C. R., Shipley, G. G. & Small, D. M. The phase behavior of hydrated cholesterol. *Journal of Lipid Research* **20**, 525-535 (1979).

216 Shieh, H., Hoard, L. & Nordman, C. Crystal structure of anhydrous cholesterol. (1977).

217 Cooper, R. A., Leslie, M. H., Fischkoff, S., Shinitzky, M. & Shattil, S. J. Factors influencing the lipid composition and fluidity of red cell membranes in vitro:

production of red cells possessing more than two cholesterols per phospholipid. *Biochemistry* **17**, 327-331, (1978).

218 Finean, J. B. Cholesterol: lecithin association at molecular ratios of up to 2 : 1. *Chemistry and physics of lipids* **14**, 313-320, (1975).

219 Yeagle, P. L., Hutton, W. C., Huang, C.-H. & Martin, R. B. Headgroup conformation and lipid--cholesterol association in phosphatidylcholine vesicles: a 31P (1H) nuclear Overhauser effect study. *Proceedings of the National Academy of Sciences* **72**, 3477-3481 (1975).

220 Gilbert, D. B. & Reynolds, J. A. Thermodynamic equilibria of cholesterol-detergent-water. *Biochemistry* **15**, 71-74, (1976).

221 Wintersteiner, O. & Bergström, S. The products formed by the action of oxygen on colloidal solutions of cholesterol. *Journal of Biological Chemistry* **137**, 785-786 (1941).

222 Van Lier, J. E. & Smith, L. L. Sterol metabolism. VII. Autoxidation of cholesterol via hydroperoxide intermediates. *The Journal of organic chemistry* **35**, 2627-2632 (1970).

223 Garti, N., Karpuj, L. & Sarig, S. Correlation between crystal habit and the composition of solvated and nonsolvated cholesterol crystals. *Journal of Lipid Research* **22**, 785-791 (1981).

224 Varsano, N., Fargion, I., Wolf, S. G., Leiserowitz, L. & Addadi, L. Formation of 3D Cholesterol Crystals from 2D Nucleation Sites in Lipid Bilayer Membranes: Implications for Atherosclerosis. *Journal of the American Chemical Society* **137**, 1601-1607, (2015).

225 Konikoff, F., Chung, D., Donovan, J., Small, D. & Carey, M. Filamentous, helical, and tubular microstructures during cholesterol crystallization from bile. Evidence that cholesterol does not nucleate classic monohydrate plates. *Journal of Clinical Investigation* **90**, 1155 (1992).

226 Abendan, R. S. & Swift, J. A. Surface Characterization of Cholesterol Monohydrate Single Crystals by Chemical Force Microscopy. *Langmuir* **18**, 4847-4853, (2002).

227 Yang, L., Chen, J. H., Cai, D., Wang, L. Y. & Zha, X. L. Osteopontin plays an anti‐nucleation role in cholesterol gallstone formation. *Hepatology Research* **41**, 437-445 (2011).

228 Busch, N., Lammert, F., Marschall, H.-U. & Matern, S. A new subgroup of lectin-bound biliary proteins binds to cholesterol crystals, modifies crystal morphology, and inhibits cholesterol crystallization. *Journal of Clinical Investigation* **96**, 3009 (1995).

229 Lu, J., Wu, D.-H. & Rohani, S. Influence of Ca 2+ on cholesterol crystallization from supersaturated model biles. *Fluid Phase Equilibria* **367**, 51-56 (2014).

230 Busch, N., Matiuck, N., Sahlin, S., Pillay, S. & Holzbach, R. T. Inhibition and promotion of cholesterol crystallization by protein fractions from normal human gallbladder bile. *Journal of Lipid Research* **32**, 695-702 (1991).